

# Fast fitting of neural ordinary differential equations by Bayesian neural gradient matching to infer ecological interactions from time series data

Willem Bonnaffé<sup>1,2</sup> & Tim Coulson<sup>2</sup>

1. Big Data Institute, University of Oxford, Old Road Campus, Oxford OX3 7LF
2. Department of Biology, University of Oxford, Zoology Research and Administration Building, 11a Mansfield Road, Oxford OX1 3SZ

**Emails:** willem.bonnaffe@nds.ox.ac.uk; tim.coulson@zoo.ox.ac.uk;

**Running title:** Fast NODEs to infer ecological interactions

**Keywords:** Artificial neural networks; Ecological dynamics; Ecological interactions; Geber method; Gradient matching; Neural ordinary differential equations; Microcosm; Ordinary differential equations; Prey-predator dynamics; Rotifer; Time series analysis;

**Specifications:** 257 words in abstract; 7861 words in text; 58 references; 6 figures; 2 tables

**Contact:** Willem Bonnaffé, 128 Southfield Park, Oxford, OX4 2BA, UK (w.bonnaffe@gmail.com)

**Statement of authorship:** Willem Bonnaffé designed the method, performed the analysis, wrote the manuscript; Tim Coulson led investigations, provided input for the manuscript, commented on the manuscript.

## **Abstract**

1. Inferring ecological interactions is hard because we often lack suitable parametric representations to portray them. Neural ordinary differential equations (NODEs) provide a way of estimating interactions nonparametrically from time series data. NODEs, however, are slow to fit, and inferred interactions have not been compared to the truth.

2. We provide a fast NODE fitting method, Bayesian neural gradient matching (BNGM), which relies on interpolating time series with neural networks, and fitting NODEs to the interpolated dynamics with Bayesian regularisation. We test the accuracy of the approach by inferring ecological interactions in time series generated by an ODE model with known interactions. We also infer interactions in experimentally replicated time series of a microcosm featuring an algae, flagellate, and rotifer population, as well as in the hare and lynx system.

3. Our BNGM approach allows us to cut down the fitting time of NODE systems to only a few seconds. The method provides accurate estimates of ecological interactions in the artificial system, as linear and nonlinear true interactions are estimated with minimal error. In the real systems, dynamics are driven by a mixture of linear and nonlinear ecological interactions, of which only the strongest are consistent across replicates.

4. Overall, NODEs alleviate the need for a mechanistic understanding of interactions, and BNGM alleviates the heavy computational cost. This is a crucial step availing quick NODE fitting, cross-validation, and uncertainty quantification, as well as more objective estimation of interactions, and complex context dependence, than parametric models.

# 1 Introduction

The concept of population is central in ecology (Berryman 2002). Ecologists have had a long-standing interest in finding laws that govern population dynamics, namely changes in the number of individuals in the populations (Lawton 1999; Turchin 1999). Population dynamics can be characterised by a logistic growth, or similar forms, limited by ecological interactions with other organisms, and by the state of the environment (Turchin 2001; Berryman 2003). Intra-specific interactions correspond to interactions between individuals of different sex, age or size classes, belonging to the same species (Turchin 2001). Inter-specific interactions are interactions between individuals from different species, be it competitors, preys, predators, or pathogens (Turchin 2001; Berryman 2003). These interactions can cause populations to have lagged effects impacting their own growth, often called feedback effects, mediated by their impact on the other populations they interact with (Berryman and Turchin 1997).

Characterising these interactions has been a longtime challenge. Ecologists started analysing time series data with parametric models (Royama 1984; Kendall et al. 1999; Ives et al. 2003; Gross, Ives, and Nordheim 2005), as time series of population counts are the most commonly collected long-term data in biology (Kendall et al. 1999). Initial analysis involved fitting simple auto-regressive linear models to time series of a single species, leading to contentious interpretations of interactions thereby inferred (e.g. Berryman and Turchin 1997). For instance, Royama et al. interpreted higher order lags as evidence of species interactions (Royama 1984), while Lande et al. interpreted them as age-structure signatures (Lande et al. 2002). Coulson et al. showed they can even be caused by

21 interactions between the sexes (Mysterud, Coulson, and Stenseth 2002). Jonzen et al. added doubt  
22 over interpreting lags by demonstrating that autocorrelation in environmental noise could prevent  
23 altogether the reliable estimation of lag effects in single species time series data (Jonzén et al.  
24 2002). More recent work has investigated time series of multiple species, environmental factors,  
25 and has mechanistically modelled various ecological interactions (e.g. Bruijning, Jongejans, and  
26 Turcotte 2019; Rosenbaum et al. 2019; Adams et al. 2020). In these models, ecological interactions  
27 are quantified explicitly by specific parameters, rather than phenomenologically with lags. This  
28 allowed for a more thorough quantification of interactions and comparison of alternative ecological  
29 interactions architectures.

30 However, ecologists still face two main obstacles when estimating ecological interactions from time  
31 series data. The first is that interactions are highly context-dependent, so that they change in time  
32 with the state of the ecosystem and of the environment (Song et al. 2020). Ecological interactions  
33 were traditionally considered linear or fixed, yet there is substantial evidence that this is not the  
34 case in nature (e.g. Bonsall, Meijden, and Crawley 2003; Gross, Ives, and Nordheim 2005; Kendall  
35 et al. 2005; Ushio et al. 2018; Bruijning, Jongejans, and Turcotte 2019; Rosenbaum et al. 2019;  
36 Bonnaffé et al. 2021). The effect of the population on itself depends on the density of individuals  
37 (e.g. Lingjaerde et al. 2001; Moe et al. 2005; Brook and Bradshaw 2006); while predation rates  
38 can depend on the density of the predator (Jost and Ellner 2000; Yoshida et al. 2003). Many  
39 vital rates underpinning ecological interactions are age- and size-dependent (Bonnaffé et al. 2018;  
40 Bonnaffé et al. 2021), and governed by environmental variables, such as temperature (Brown et al.

41 2004). Interactions also change following evolution of the traits that underpin them (Turchin 2003;  
42 Yoshida et al. 2003). This makes it virtually impossible to model the full complexity of ecological  
43 interactions (Lawton 1999; Kendall et al. 1999).

44 This leads to the second obstacle, known as structural sensitivity, namely sensitivity of the results  
45 to the structure of the model (Wood 2001; Adamson and Morozov 2013). Because of the com-  
46 plexity of the interactions, we often lack suitable mathematical representations to portray them  
47 (Jost and Ellner 2000; Wood 2001; Ellner, Seifu, and Smith 2002; Wu, Fukuhara, and Takeda  
48 2005). Parametric representations of the interactions are assumed *a priori*, which means that any  
49 interaction quantified is ultimately contingent on this arbitrary choice, and hence potentially bi-  
50 ased (Jost and Ellner 2000; Wood 2001; Ellner, Seifu, and Smith 2002; Wu, Fukuhara, and Takeda  
51 2005). Parametric inference of ecological interactions from time series data therefore only provides  
52 qualitative evidence, requiring further experimental verification and quantification (Kendall et al.  
53 1999).

54 Nonparametric modelling provides a powerful alternative that can help solve these problems (e.g.  
55 Jost and Ellner 2000; Wood 2001; Ellner, Seifu, and Smith 2002; Wu, Fukuhara, and Takeda 2005;  
56 Pasquali and Soresina 2018). Nonparametric forms give more freedom to researchers wishing  
57 to model population dynamics, and allow a test of whether the linear or linearised assumption of  
58 standard models is warranted. Interactions are quantified as the sensitivity of the nonparametric ap-  
59 proximation of the dynamics with respect to other state variables (Sugihara et al. 2012; Ushio et al.  
60 2018). Nonparametric models require minimal assumptions regarding the mathematical nature of

61 ecological interactions (Jost and Ellner 2000; Gross, Ives, and Nordheim 2005), and hence provide  
62 interaction estimates that are more robust to model structure (Wood 2001). In particular, arti-  
63 ficial neural networks (ANNs) offer a promising, yet underused, nonparametric alternative to linear  
64 functional forms. In previous work, we introduced a powerful framework, relying on neural ordi-  
65 nary differential equations (NODEs, Chen et al. 2019) to approximate the dynamics of populations  
66 nonparametrically, from which we derive ecological interactions (Bonnaffé, Sheldon, and Coulson  
67 2021). More specifically, the ANNs embedded in the ODEs learn nonparametrically the shape of  
68 the per capita growth rate of the populations and its dependence on the state variables of the system  
69 (Bonnaffé, Sheldon, and Coulson 2021). Combined with the Geber method (Hairston et al. 2005),  
70 we are able to estimate the direction, strength, and degree of nonlinearity of interactions.

71 One limitation of the approach lies in the computational cost of fitting the NODEs (Chen et al.  
72 2019; Bonnaffé, Sheldon, and Coulson 2021). This is due to the fact that NODEs, as with ODEs,  
73 need to be simulated over the entire range of the time series in order to compute the likelihood  
74 of the trajectories of the model. This can be avoided by using gradient matching, which requires  
75 interpolating the time series, and fitting the ODEs directly to the interpolated dynamics (Jost and  
76 Ellner 2000; Aarts and Veer 2001; Ellner, Seifu, and Smith 2002). Although a similar approach  
77 has been proposed (see Treven et al. 2021), there are no implementations of it to fitting NODEs,  
78 in spite of its great potential for cutting down computational costs. In addition, given the novelty  
79 of the framework, the accuracy and robustness of NODEs in estimating ecological interactions  
80 remain largely unexplored. Most of the work to date is concerned with the accuracy of the fitted

81 trajectories and of the forecasts (Mai, Shattuck, and O’Hern 2016; Treven et al. 2021; Frank 2022),  
82 while little attention has been given to the functional form of the processes that are producing  
83 the dynamics approximated by NODEs (but see Hu et al. 2020 for a step in this direction). It  
84 is important to understand to what extent the neural networks embedded within NODEs carry  
85 meaningful biological information (Novak and Stouffer 2021).

86 In this manuscript, we first introduce a novel fitting technique for NODEs, Bayesian neural gradient  
87 matching (BNGM). The method extends gradient matching by using neural networks to interpolate  
88 the time series data instead of splines (Ellner, Seifu, and Smith 2002), and Bayesian regularisa-  
89 tion to fit NODEs to the interpolated dynamics (Cawley and Talbot 2007). This cuts down the  
90 fitting time of NODEs to only a few seconds, compared to about 30 minutes in our previous work  
91 (Bonnaff , Sheldon, and Coulson 2021), allowing for efficient cross-validation, and uncertainty  
92 quantification. We then demonstrate that NODEs are highly accurate in recovering ecological in-  
93 teractions in an artificial three-species prey-predator system where truth is known. Finally, we  
94 conclude the work by characterising ecological interactions in three replicates of an experimental  
95 three-species prey-predator system with an algae, flagellate, and rotifer (Hiltunen et al. 2013), as  
96 well as in the classic hare and lynx time series (Odum and Barrett 1972). We find that only main  
97 interactions, between the algae and the rotifer, are conserved across the three replicates, and not  
98 the interactions of the flagellate with the other species. We also find that in most cases linear in-  
99 teractions are sufficient to explain the dynamics apart from nonlinearity in the effect of the prey on  
100 the top predator in both the rotifer and lynx.

## 101 **2 Material and Methods**

### 102 **2.1 Method overview**

103 We provide a nonparametric method for estimating ecological interactions from time series data of  
104 species density. We do this by approximating the dynamics of each species with neural ordinary  
105 differential equations (NODEs, Bonnaffé, Sheldon, and Coulson 2021). We then compute ecolog-  
106 ical interactions as the sensitivity of these dynamics to a change in the respective species densi-  
107 ties (Sugihara et al. 2012; Bonnaffé, Sheldon, and Coulson 2021). We provide a novel method,  
108 Bayesian neural gradient matching (BNGM), allowing us to fit NODE systems in a only a few  
109 seconds.

### 110 **2.2 Neural ordinary differential equation**

111 A NODE is a class of ordinary differential equation (ODE) that is partly or entirely defined as an ar-  
112 tificial neural network (ANN) (Chen et al. 2019). They are useful to infer dynamical processes non-  
113 parametrically from time series data (Bonnaffé, Sheldon, and Coulson 2021). We choose NODEs  
114 over standard statistical approaches because they offer two advantages. The first is that NODEs  
115 approximate the dynamics of populations nonparametrically. NODEs are therefore not subjected  
116 to incorrect model specifications (Jost and Ellner 2000; Adamson and Morozov 2013). This pro-  
117 vides a more objective estimation of the inter-dependences between state variables. The second  
118 advantage is that it is a dynamical systems approach. So that the approach includes lag effects  
119 through interacting state variables, not only direct effects between them.



120 We first consider a general NODE system,

$$\frac{dy_i}{dt} = f_p(y, \theta_i), \quad (1)$$

121 where  $dy_i/dt$  denotes the temporal change in the  $i^{th}$  variable of the system,  $y_i$ , as a function of the  
 122 other state variables  $y = \{y_1, y_2, \dots, y_I\}$ . The function  $f_p$  is a nonparametric function of the state  
 123 variables and its shape is controlled by the parameter vector  $\theta_i$ . In the context of NODEs,  $f_p$  is  
 124 an ANN. The most common class of ANN used in NODEs are single-layer fully connected feed-  
 125 forward ANNs (e.g. Wu, Fukuhara, and Takeda 2005), also referred to by single layer perceptrons  
 126 (SLPs, e.g. Bonnaff  , Sheldon, and Coulson 2021),

$$f_p(y, \theta_i) = f_\lambda \left( \theta_i^{(0)} + \sum_{j=1}^J \theta_{ij}^{(1)} f_\sigma \left( \theta_{ij}^{(2)} + \sum_{k=1}^K \theta_{ijk}^{(3)} y_k \right) \right), \quad (2)$$

127 which feature a single layer, containing  $J$  neurons, that maps the inputs, here the state variables  $y$ ,  
 128 to a single output, the dynamics of state variable  $i$ ,  $dy_i/dt$ . The parameter vector  $\theta_i$  contains the  
 129 weights  $\theta^{(l)}$  of the connections in the SLPs. SLPs can be viewed as weighted sums of activation  
 130 functions  $f_\sigma$ , which are usually chosen to be sigmoid functions  $f(x) = 1/(1 + \exp(-x))$ . The link  
 131 function  $f_\lambda$  allows to map the output of the network to a specific domain, for instance applying  
 132  $\tanh$  will constrain the dynamics between -1 and 1,  $dy_i/dt \in ]-1, 1[$ .

133 This general form can be changed to represent biological constraints on the state variables. In  
 134 particular for population dynamics, the state variables are strictly positive population densities,

135  $y_i = N_i \in \mathcal{R}^+$ . We could hence re-write equation (1) as,  $dN_i/dt = f_p(N, \theta_i)N_i$ , where the SLPs  
 136 approximate the per-capita growth rate of the populations. More details regarding these models  
 137 can be found in our previous work (Bonnaiffé, Sheldon, and Coulson 2021).

### 138 **2.3 Fitting NODEs by Bayesian neural gradient matching**

139 In this section, we describe how to estimate the parameters  $\theta$  of the NODE system given a set of  
 140 time series. Fitting NODEs can be highly computationally intensive, which hinders uncertainty  
 141 quantification, cross-validation, and model selection (Bonnaiffé, Sheldon, and Coulson 2021). We  
 142 solve this issue by introducing BNGM, a computationally efficient approach to fit NODEs. The ap-  
 143 proach involves two steps (Fig. 1). First, we interpolate the state variables and their dynamics with  
 144 neural networks (Fig. 1, red boxes). Second, we train each NODE to satisfy the interpolated state  
 145 and dynamics (Fig. 1, blue boxes). This bypasses the costly numerical integration of the NODE  
 146 system and provides a fully mathematically tractable expression for the posterior distribution of the  
 147 parameter vector  $\theta$ . We coin the term BNGM to emphasise two important refinements of the stan-  
 148 dard gradient matching algorithm (Ellner, Seifu, and Smith 2002). The first is that we use neural  
 149 networks as interpolation functions, and the second is that we use Bayesian regularisation to limit  
 150 overfitting and estimate uncertainty around parameters (Cawley and Talbot 2007).

#### 151 **Interpolating the time series**

152 The first step is to interpolate the time series and differentiate it with respect to time in order to ap-  
 153 proximate the state and dynamics of the variables. We perform the interpolation via nonparametric

154 regression of the interpolating functions on the time series data,

$$Y_{it} = \tilde{y}_i(t, \omega_i) + \varepsilon_{it}^{(o)}, \quad (3)$$

155 where  $Y_{it}$  is observed value of the state variable  $i$  at time  $t$ ,  $\tilde{y}_i(t, \omega_i)$  is the value predicted by the  
 156 interpolation function given the parameter vector  $\omega_i$ , and  $\varepsilon_{it}^{(o)}$  is the observation error between the  
 157 observation and prediction. The interpolation function is chosen to be a neural network,

$$\tilde{y}_i(t, \omega_i) = f_\lambda \left( \omega_i^{(0)} + \sum_{j=1}^J \omega_{ij}^{(1)} f_\sigma \left( \omega_{ij}^{(2)} + \omega_{ij}^{(3)} t \right) \right), \quad (4)$$

158 where the parameter vector  $\omega_i$  contains the weights  $\omega^{(l)}$  of the network. We can further differentiate  
 159 this expression with respect to time to obtain an interpolation of the dynamics of the state variables  
 160 (Fig. 1, red boxes),

$$\frac{\partial \tilde{y}_i}{\partial t}(t, \omega_i) = \sum_{j=1}^J \omega_{ij}^{(1)} \omega_{ij}^{(3)} \frac{\partial f_\sigma}{\partial t} \left( \omega_{ij}^{(2)} + \omega_{ij}^{(3)} t \right) \frac{\partial f_\lambda}{\partial t} \left( \omega_i^{(0)} + \sum_{k=1}^J \omega_{ik}^{(1)} f_\sigma \left( \omega_{ik}^{(2)} + \omega_{ik}^{(3)} t \right) \right). \quad (5)$$

## 161 **Fitting NODEs to the interpolated time series**

162 The second step is to train the NODE system (Eq. 1) to satisfy the interpolated dynamics. Thanks  
 163 to the interpolation step, this simply amounts to performing a nonparametric regression of each  
 164 NODE (Eq. 1) on the interpolated dynamics (Eq. 5),

$$\frac{\partial \tilde{y}_i}{\partial t}(t, \omega_i) = \frac{dy_i}{dt}(\tilde{y}, \theta_i) + \varepsilon_{it}^{(p)}, \quad (6)$$

where  $\varepsilon_{it}^{(p)}$  is the process error, namely the difference between the interpolated dynamics,  $\partial \tilde{y}_i / \partial t$  and the NODE,  $dy_i / dt$ , given the interpolated state variables  $\tilde{y} = \{\tilde{y}_1, \tilde{y}_2, \dots, \tilde{y}_I\}$  (Fig. 1, blue boxes).

### Bayesian regularisation

In the context of standard gradient matching, defining the observation model (Eq. 3) and process model (Eq. 6) would be sufficient to fit the NODE system (Eq. 1) to the time series via optimisation (Jost and Ellner 2000; Ellner, Seifu, and Smith 2002; Wu, Fukuhara, and Takeda 2005). We could find the parameter vector  $\omega_i$  and  $\theta_i$  that minimise the sum of squared observation and process errors,  $\varepsilon_{it}^{(o)}$  and  $\varepsilon_{it}^{(p)}$  (Eq. 3 and 6). However, this approach is prone to overfitting, and does not provide estimates of uncertainty around model predictions. To account for this, we introduce Bayesian regularisation, which allows us to control for overfitting by constraining parameters with prior distributions (Cawley and Talbot 2007), and to root our interpretation of uncertainty in a Bayesian framework.

First, we define a simple Bayesian model to fit the interpolation functions (Eq. 3) to the time series data. We assume normal distributions for the observation error,  $\varepsilon_{ij}^{(o)} \sim \mathcal{N}(0, \sigma_i)$ , and for the parameters,  $\omega_{ij} \sim \mathcal{N}(0, \gamma_{ij})$ . Here, we are only interested in interpolating the time series accurately, irrespective of the value of  $\sigma_i$  and  $\gamma_{ij}$ . Therefore, we use the approach developed by Cawley and

182 Talbot to average out the value of the parameters  $\sigma_i$  and  $\gamma_{ij}$  in the full posterior distribution (Caw-  
 183 ley and Talbot 2007), assuming gamma hyperpriors  $p(\xi) \propto \frac{1}{\xi} \exp\{-\xi\}$  for both parameters. This  
 184 yields the following expression for the log marginal posterior density of the parameters,

$$\log P(\omega_i | Y_i) \propto -\frac{J}{2} \log \left( 1 + \sum_{j=1}^J \left( \varepsilon_{ij}^{(o)} \right)^2 \right) - \frac{K}{2} \log \left( 1 + \sum_{k=1}^K \omega_{ik}^2 \right) \quad (7)$$

185 where  $P$  is the marginal posterior density,  $\omega_i = \{\omega_{i1}, \omega_{i2}, \dots, \omega_{iK}\}$  is the observation parameter  
 186 vector controlling the interpolation function,  $Y_i = \{Y_{i1}, Y_{i2}, \dots, Y_{iJ}\}$  corresponds to the sequence of  
 187 observations of state variable  $i$  at time step  $j$ ,  $J$  is the total number of time steps in the time series,  
 188  $\varepsilon_{ij}^{(o)}$  is the observation error at time step  $j$  between the interpolated and observed value of variable  
 189  $i$ ,  $K$  is the total number of parameters. More details on how to derive this expression can be found  
 190 in a supplementary file (Supplementary A).

191 Then, we define a simple Bayesian model to fit the NODEs to the interpolated dynamics, given the  
 192 interpolated states. We assume normal distributions for the observation error,  $\varepsilon_{ij}^{(p)} \sim \mathcal{N}(0, \sigma_i)$ , and  
 193 parameters,  $\theta_{ik} \sim \mathcal{N}(0, \delta_{ik})$ . This gives the following expression for the log posterior density of  
 194 the parameters given the interpolations,

$$\log p(\theta_i | \omega) \propto -\frac{1}{2} \sum_{j=1}^J \left( \frac{\varepsilon_{ij}^{(p)}}{\sigma_i} \right)^2 - \frac{1}{2} \sum_{k=1}^K \left( \frac{\theta_{ik}}{\delta_{ik}} \right)^2 \quad (8)$$

195 where  $\theta_i = \{\theta_{i1}, \theta_{i2}, \dots, \theta_{iK}\}$  are the NODE parameters of the  $i^{th}$  variable,  $\omega = \{\omega_1, \omega_2, \dots, \omega_I\}$  are  
 196 the interpolation parameters of each state variable,  $\varepsilon_{ij}^{(p)}$  is the process error of variable  $i$  at time

step  $j$  between the interpolated dynamics and NODE prediction,  $\sigma_i$  is the standard deviation of the likelihood,  $K$  is the total number of parameters,  $\delta_{ik}$  is the standard deviation of the prior distribution of parameter  $\theta_{ik}$ .

This approach allows us to limit overfitting by adjusting the constraint on the parameters, which is controlled by the standard deviation of the parameter prior distributions,  $\delta_{ik}$  (Cawley and Talbot 2007; Bonnaffé, Sheldon, and Coulson 2021). We could set small values of  $\delta$  to limit the degree of nonlinearity in the response, or to eliminate specific variables from the model by constraining their parameters to be close to zero. We identify the appropriate degree of constraint  $\delta_i$  on NODE parameters via cross-validation. We train the NODE model on the first half of the interpolated data and predict the remaining half. We repeat this process for increasing values of  $\delta_i$ , until we find the value that maximises the log likelihood of the test data.

## 2.4 Inference and uncertainty quantification

Finally, we estimate uncertainty in parameter values by anchored ensembling, which produces approximate Bayesian estimates of the posterior distribution of the parameters (Pearce et al. 2018). This involves sampling a parameter vector from the prior distributions,  $\theta_i \sim \mathcal{N}(0, \delta_i)$ , and then optimising the posterior distribution from this starting point,  $\theta_i^* = \underset{\theta_i}{\operatorname{argmax}} \log p(\theta_i | \omega)$ . By repeatedly taking samples, the sampled distribution  $\theta^*$  approaches the posterior distribution and provides estimates and error around the quantities that can be derived from the models. The expectation and uncertainty around derived quantities can then be obtained by computing the mean and variance of

216 the approximated posterior distributions. The great strength of this approach is that it is unlikely to  
 217 get stuck in local maxima hence providing a more robust optimisation of the posterior.

## 218 **2.5 Analysing NODEs**

219 In this study we are mainly interested in two outcomes of NODEs, namely inferring the direction  
 220 (or effect) and strength (or contribution) of interactions between the state variables (Bonnaiffé,  
 221 Sheldon, and Coulson 2021). We define the direction of the interaction between variable  $y_i$  and  $y_j$  as  
 222 the derivative of the dynamics of  $y_i$  with respect to  $y_j$ , and vice versa (Sugihara et al. 2012),

$$e_{ijt} = \frac{\partial}{\partial y_j} \frac{dy_i}{dt}. \quad (9)$$

223 Knowing the direction, however, is not sufficient to determine the importance of a variable for the  
 224 dynamics of another. Given the same effects, a variable that fluctuates a lot will have a greater  
 225 impact on the dynamics of a focal variable, compared to a variable that remains quasi-constant. We  
 226 hence compute the strength of the interaction by multiplying the dynamics of a variable  $y_j$  by its  
 227 effect on the focal variable  $y_i$ , also known as the Geber method (Hairston et al. 2005),

$$c_{ijt} = \frac{dy_j}{dt} \frac{\partial}{\partial y_j} \frac{dy_i}{dt}. \quad (10)$$

228 To summarise results across the entire time series we can compute the mean effects  $e_{ij}$  by av-  
 229 eraging  $e_{ijt}$  across all time steps,  $e_{ij} = 1/K \sum_k e_{ijk}$ , as well as the relative total contribution,  $c_{ij}$ ,  
 230 of a variable to the dynamics of another by computing the relative sum of square contributions,

231  $c_{ij} = \left( \sum_{jk} c_{ijk}^2 \right)^{-1} \sum_t c_{ijt}^2$ . By computing the direction and strength of interactions between all the  
 232 variables in the system we can build dynamically informed ecological interaction networks (e.g.  
 233 fig. 5). Other metrics can be computed by analysing the NODEs, such as equilibrium states, these  
 234 are discussed in our previous work (Bonnaiffé, Sheldon, and Coulson 2021).

## 235 **3 Case studies**

### 236 **3.1 Case study 1: artificial tri-trophic prey-predator oscillations**

237 In this first case study, we aim to demonstrate the accuracy of the NODE fitted by BNGM in  
 238 inferring nonlinear per-capita growth rates in a system where ground truth is known. Hence, we  
 239 simulate a set of time series from a tri-trophic ODE model with known equations and parameters,  
 240 and we compare the fitted NODEs to the actual ODEs.

#### 241 **System**

242 We consider a tri-trophic ODE system consisting of a prey, an intermediate predator, and a top  
 243 predator. The system is built on the real tri-trophic system featuring algae, flagellates, and rotifers,  
 244 considered in case study 2 (Hiltunen et al. 2013),

$$\begin{aligned}
 \frac{dG}{dt} &= \left( \alpha \left( 1 - \frac{G}{\kappa} \right) - \frac{\beta B}{1 + \delta G} - \frac{\gamma R}{1 + \delta G} \right) G \\
 \frac{dB}{dt} &= \left( \frac{\beta G}{1 + \delta G} - \phi R - \mu \right) B \\
 \frac{dR}{dt} &= \left( \frac{\gamma G}{1 + \delta G} + \phi B - \nu \right) R,
 \end{aligned} \tag{11}$$



where  $G$ ,  $B$ , and  $R$ , correspond to the prey, intermediate, and top predator population densities, respectively,  $\alpha$  is the prey intrinsic growth rate, limited by a carrying capacity  $\kappa$ ,  $\beta$  and  $\gamma$  are the predation rates by the intermediate and top predator,  $\delta$  is the saturation rate of prey predation, which emulates the capacity of the algae to display predator defense at higher algal density (Hiltunen et al. 2013),  $\phi$  is the predation rate of the intermediate predator by the top predator,  $\mu$  and  $\nu$  are the intrinsic mortality of the intermediate and top predator.

We simulate a case of invasion, by introducing the top predator at a low density, with a set of parameters that result in dampening prey-predator oscillations, namely  $\alpha = 1$ ,  $\beta = 2.5$ ,  $\gamma = 1.5$ ,  $\kappa = 3$ ,  $\delta = \phi = \mu = \nu = 1$ . We focus on the middle section of the time series,  $t \in [20, 50]$ , as in the initial section the top predator is rare, and in the later section populations have attained a fixed equilibrium point. The resulting time series are presented in figure 2.

## 256 **NODE model**

In order to nonparametrically learn the per-capita growth rate of each species, and to derive ecological interactions, we define a three-species NODE system,

$$\begin{aligned}\frac{dR}{dt} &= r_R(R, G, B, \beta_R)R \\ \frac{dG}{dt} &= r_G(R, G, B, \beta_G)G \\ \frac{dB}{dt} &= r_B(R, G, B, \beta_B)B,\end{aligned}\tag{12}$$

where the per-capita growth rates  $r_R$ ,  $r_G$ , and  $r_B$  are neural network functions of the density  $R$ ,  $G$ ,  $B$  of each species (function  $f_p$ , Eq. 2). We choose a combination of linear and exponential activation

261 functions  $f_{\sigma, j \leq J/2}(x) = x$ , and  $f_{\sigma, j > J/2}(x) = \exp(x)$ . This allows us to progressively switch from a  
 262 simple linear model to a nonlinear model by releasing the constraint on the exponential section of  
 263 the neural network during cross-validation. The number of units in the hidden layer  $J$  is chosen to  
 264 be 10, as this is a commonly used number for systems of that size (e.g. Wu, Fukuhara, and Takeda  
 265 2005; Bonnaff  , Sheldon, and Coulson 2021).

## 266 **Time series interpolation**

267 We interpolate the time series using the neural network described in section 2.3 (Eq. 4). We set  
 268 the number of neurons in the network to  $J = 30$ . We use sinusoid activation functions,  $f_{\sigma}(x) =$   
 269  $\sin(x)$ , so that the weights  $\omega_{ij}^{(1)}$ ,  $\omega_{ij}^{(2)}$ , and  $\omega_{ij}^{(3)}$  control the amplitude, shift, and frequency of the  
 270 oscillations in the time series, respectively. Given that the population densities are strictly positive  
 271  $R, G, B \in \mathcal{R}^+$ , we use an exponential link function,  $f_{\lambda}(x) = \exp(x)$ . We then approximate the  
 272 marginal posterior distribution of the interpolation parameters, and thereby of interpolated states  
 273 and dynamics, by taking 100 samples from the log marginal posterior distribution (Eq. 7) via  
 274 anchored ensembling. In practice, the high number of parameters in the neural network equation  
 275 may impede the fit of the time series, especially for short time series. We found that dividing the  
 276 number of parameters  $K$  (Eq. 7) by the number of neurons in the network  $J$  (Eq. 2) yields consistent  
 277 fitting results. Interpolated states and dynamics are presented in figure 2.

## 278 **Fitting NODEs to the interpolated time series**

279 We fit the NODE system to the interpolated time series. In practice, we fit the NODE to the expect-  
 280 ation of the interpolated state and dynamics,  $E(\tilde{y}_i)$  and  $E(d\tilde{y}_i/dt)$ , by averaging over all sampled

281 interpolation parameters. An alternative approach could be to consider the interpolation that max-  
 282 imises the log marginal posterior density, but this may decrease repeatability due to the difficulty of  
 283 reliably identifying a global maximum. Averaging across multiple interpolations ensures an overall  
 284 smoother and robust interpolation. In addition, we standardise the response and explanatory vari-  
 285 ables with respect to their mean and standard deviation (i.e.  $Z = (Y - \mu)/\sigma$ ). This is to facilitate  
 286 the training of the NODE by equalizing the scale of the different parameters in the neural network.  
 287 Then, we identify the optimal regularisation parameter  $\delta$  (Eq. 8) by cross-validation. To do that,  
 288 we split the data in half, train NODEs on the first half, and calculate the log likelihood of the test  
 289 set for increasing values of  $\delta$ , from 0.05 (linear) to 0.5 (highly nonlinear), by increments of 0.05.  
 290 This allows us to identify the maximum degree of nonlinearity,  $\delta$ , in the per-capita growth rate that  
 291 ensures generalisability throughout the time series. Then, we approximate the posterior distribu-  
 292 tion of the NODE parameters by taking 30 samples from the posterior distribution (Eq. 8). Finally,  
 293 we perform model selection by removing variables that do not result in a significant decrease in  
 294 the log likelihood of the model (assessed by comparing log likelihood confidence intervals). We  
 295 ensure moderate temporal autocorrelation and normality by visualising the residuals of the models.  
 296 We also ensure results repeatability by running the entire fitting process a second time.

### 297 **Computing ecological interactions**

298 Finally, we analyse the shape of the per-capita growth rates to recover the interaction between the  
 299 three species in the system. In particular, we look at the effect and contribution of each species  
 300 to the dynamics of the others. The effect is computed as the sensitivity (i.e. the gradient) of the

301 per-capita growth rate of a given species with respect to the density of the other species (Sugihara  
302 et al. 2012; Bonnaiffé, Sheldon, and Coulson 2021). The contribution is computed following the  
303 Geber method (Hairston et al. 2005), which consists in multiplying the dynamics of a variable by  
304 its effects on the other variables. We further compute the importance of a species in driving the  
305 dynamics of another by computing its relative total contribution compared to other species. More  
306 details on how to compute these quantities can be found in section 2.5 and in our previous study  
307 (Bonnaiffé, Sheldon, and Coulson 2021).

## 308 **Benchmark**

309 In order to demonstrate the suitability of BNGM for fitting NODEs and inferring ecological in-  
310 teractions we compare our approach to three existing methods. For this purpose, we focus on the  
311 artificial time series, as this offers the possibility for comparing predictions to the truth, known  
312 from the equations that generated the time series.

313 We first consider standard NODEs as our BNGM approach seeks to alleviate the computational  
314 cost of fitting NODEs. As for the BNGM model, we define the per capita growth rate as an ANN  
315 with a single layer, 3 inputs, 10 hidden nodes, and exponential activation functions. We use a  
316 Bayesian model, assuming log normal distributions for species density, and uniform uninforma-  
317 tive prior distributions for the network parameters, initial densities, and likelihood variance. Our  
318 implementation of standard NODEs differs from our BNGM approach in three ways. First, the  
319 standard NODE ANN has 3 outputs instead of one, as variables are fitted jointly. Second, comput-  
320 ing the posterior density of the parameters requires to solve the NODE system with a numerical

ODE solver. Third, we do not constrain the parameters of the network given that the prohibitive fitting times prevent the tuning of the regularisation parameters.

We also consider a parametric ODE model, as this is the closest parametric alternative to NODEs to infer ecological interactions. This model only differs from the standard NODE model in that the per-capita growth rate is approximated by second order polynomial functions, instead of an ANN, which is a standard choice for inferring simple nonlinearities.

To ensure the most meaningful comparison, we implemented the NODEBNGM, standard NODEs, and parametric ODE, in base R, using BFGS for optimisation (optim function, R V4). We also followed the same fitting procedure by independently training 30 models on the train set (i.e. 2/3 of the time series) and predicting the test set (remaining third).

Finally, we implement convergent cross-mapping (CCM). This technique performs locally linear approximations of the state space of the system to estimate the sensitivity of the dynamics of a variable to a change in other variables. For this we use the package rEDM, and adapted the example code provided for the three species system. We train the CCM model on the train set and predict outcomes on the test set. We then retrieve s-map coefficients (i.e. the interactions) and approximate the per-capita growth using finite differences, given that the standard implementation of CCM does not provide estimates of the dynamics.

For all four methods, we compute the runtime as the average time required to train a single model. Using the best identified model, we then predict the growth rate and ecological effects for the entire time series, including the test set. We compute the accuracy of the predictions by computing the

mean sum of squared error of predictions versus the truth for both the per capita growth rate and ecological effects, on the train and test set. We also build the corresponding dynamical interaction networks, using the inferred mean effects and total contributions, and compare them to the true network of interactions.

## 3.2 Case study 2: real tri-trophic prey-predator oscillations

In this second case study, we want to assess the quality of the NODE analysis when performed on a real time series. We are further interested in comparing the direction and strength of uncovered ecological interactions across virtually identical replicated time series.

### System

We consider a three-species laboratory microcosm consisting of an algal prey (*Chlorella autrophica*), a flagellate intermediate predator (*Oxyrrhis marina*), and a rotifer top predator (*Brachionus plicatilis*). The algal prey is consumed by the intermediate and top predator, which also consumes the intermediate predator (Arndt 1993). The dynamics of this system, here the daily change in the density of each species, were recorded in three replicated time series experiments performed by Hiltunen and colleagues (Hiltunen et al. 2013). We use their time series because they describe a simple yet biologically realistic ecosystem, and because the quality of the replication of their microcosm reduces as much as possible observational and experimental error, and rules out environmental variation (Hiltunen et al. 2013). We digitised these time series by extracting by hand the coordinates of every points in the referential of the axis of the graph of the original study, and

360 analysed them.

### 361 **NODE analysis**

362 We apply the same analysis as performed on the artificial tri-trophic prey-predator oscillations. This  
363 allows us to recover a nonparametric approximation of the growth rate of each species, and then  
364 derive the direction and strength of the ecological interactions that underpin their dynamics. We  
365 present detailed results of the analysis of the first time series (Fig. 4), and a summary comparison of  
366 the three time series (Fig. 5). Complementary results, including cross-validation plots, and detailed  
367 results for the other two replicates can be found in the supplementary material (Supplementary B-  
368 E).

### 369 **3.3 Case study 3: real di-trophic prey-predator oscillations**

370 Finally, we infer ecological interactions by NODE BNGM in the hare-lynx system (Odum and Bar-  
371 rett 1972). This is to provide an example of a longer time series, and to offer a point of comparison  
372 with previous and future implementations of NODEs, which commonly use this time series (e.g.  
373 Bonnaffé, Sheldon, and Coulson 2021; Frank 2022).

#### 374 **System**

375 The system is described in details in our previous work (Bonnaffé, Sheldon, and Coulson 2021).  
376 The data consist in a 90-year long time series of counts of hare and lynx pelts collected by trappers  
377 in the Hudson bay area in Canada (Odum and Barrett 1972). The time series displays characteristic  
378 10-year long prey-predator oscillations.

## 379 **NODE analysis**

380 We apply the same analysis as previously described, to the exception that the NODE system only  
381 features two variables,  $H$  and  $L$ , instead of 3. Results are presented in figure 6.

## 382 **3.4 Case study 4: fish community from the Maizuru Bay**

### 383 **System**

384 Finally, we demonstrate the capacity of NODEs to analyse the drivers of the dynamics of a larger  
385 community by analysing the time series of the Maizuru bay community (Ushio et al. 2018). The  
386 dataset for this system consists of 12-year long time series of fortnight abundance estimates of the  
387 15 dominant species in the Maizuru bay, Japan. The data was collected every two weeks along  
388 three 200m long and 2m wide transects by underwater visual census conducted along the coast of  
389 the Maizuru fishery research station of Kyoto University from 2002 to 2014 (for more details see  
390 Ushio et al. 2018). Bottom sea temperature (at 10m depth) was also recorded on each census. The  
391 dataset contains 14 dominant species of fish, and 1 genus of Jelly fish. Only species with more than  
392 1000 sightings were included in the final dataset.

393 We focussed our analysis on the species with the least sparse records. We discarded the follow-  
394 ing species from our analysis *Engraulis japonicus*, *Plotosus lineatus*, *Chaenogobius gulosus*, and  
395 *Siganus fuscescens*. We also excluded periods which presented jelly fish blooms, as these were  
396 isolated events which could cause numerical errors in the estimation of the dynamics of species  
397 abundance. In total, we considered a time period of a hundred time steps from June 2004 to



398 August 2008, and 11 species out of 15, namely *Aurelia sp*, *Sebastes inermis*, *Trachurus japoni-*  
399 *cus*, *Girella punctata*, *Pseudolabrus sieboldi*, *Halichoeres poecilopterus*, *Halichoeres tenuispinnis*,  
400 *Pterogobius zonoleucus*, *Tridentiger trigonocephalus*, *Sphyraena pinguis*, and *Rudarius ercodes*.  
401 We included the sea bottom temperature (in degrees celsius) as an additional environmental vari-  
402 able.

### 403 **NODE analysis**

404 We then analysed this dataset following the approach described in the method section. We split  
405 the data into three thirds to create a training, validation, testing set (final third), and we followed  
406 procedure as described before to tune the regularisation parameters. The NODE system consisted  
407 of 11 ODEs, where the per-capita growth rate is determined with a single-layer ANNs with 12  
408 input nodes, 10 hidden nodes, exponential activation functions, and 1 output node. Due to the  
409 high dimensionality of the effects obtained (11 by 12), we only present mean effects and total  
410 contributions, obtained by taking the mean, and the mean squares, respectively, of the effects and  
411 contributions across the entire time series (Fig. ). The time series of effects and contributions are  
412 presented in greater details in the supplementary material (Fig. Sxxx-xxx).

## 413 **4 Results**

### 414 **4.1 Benchmark**

415 Figure 3 shows the performance of fitting NODEs by BNGM, compared to standard NODEs, para-  
416 metric ODEs, and convergent cross mapping. We find that fitting NODEs by BNGM provides the  
417 highest estimation accuracy for growth rates and ecological effects, both on the training and test  
418 set, as well as competitive runtimes of only a handful of seconds. Standard NODEs provide a sim-  
419 ilar estimation accuracy, but take over 15 minutes to train. CCM is the fastest technique, as results  
420 are obtained in under a second, but is relatively less accurate. Parametric ODEs are found to be  
421 both slower and less accurate.

422 In addition, we present a breakdown of the runtime of fitting NODEs by BNGM for each system  
423 in table 1. We find that it takes on average 5.35 minutes to fit NODEs by BNGM. This includes  
424 taking 390 samples, and thereby performing 390 full optimisations, of the posterior distribution  
425 of the interpolation and NODE parameters. This amounts to about 5.37 second to sample each  
426 variable of the NODE system once. This is a 335 fold improvement over our previous approach,  
427 which took on average 30 minutes (Bonnaffé, Sheldon, and Coulson 2021).

### 428 **4.2 Case study 1: artificial tri-trophic system**

429 We present the results of fitting NODEs by BNGM to the artificial tri-trophic time series in figure  
430 2 and 3. We find that both the interpolation of the state variables and dynamics are highly accurate  
431 (Fig. 2), given that they closely match the ground truth, known from the equations of the ODE

432 model that we used to generate the time series (Eq. 11). Similarly, we find that the NODE approx-  
 433 imation of the per-capita growth rate of each species also closely matches the ground truth (Fig. 3,  
 434 a., d., g.). We find negative nonlinear effects of the two predators on the growth rate of the algae  
 435 (Fig. 3, b., blue and purple lines). This nonlinear pattern is mirrored by the effect of the algae  
 436 on the growth rate of the predators (Fig. 3, e. and h., red line). The linear interaction between  
 437 the two predators is also well-recovered (Fig. 3, e., blue line, and h., purple line). We find that  
 438 removing the intra-specific dependence in the growth rate of the predators did not affect the fit of  
 439 the model (Fig. e., purple line, and h., blue line). The BNGM approach hence accurately recovers  
 440 the dynamical characteristics of the artificial system.

### 441 **4.3 Case study 2: real tri-trophic prey-predator oscillations**

442 We present the in-depth analysis of the drivers of the dynamics of the algae, flagellate, and rotifer  
 443 population in replicate A (Fig. 4). Cross-validation reveals that there is no support for nonlinear  
 444 effects in the growth rate of the algae and flagellate for replicate A (Fig. 4, a. and b., d. and e.).  
 445 We find negative linear intra-specific density dependence in algal growth (Fig. 4, b., red line), and  
 446 negative linear inter-specific effects of the two predators (purple and blue line). We find that the  
 447 growth rate of the flagellate is virtually solely driven by predation by the rotifer (Fig. 4, e. and  
 448 f., blue line). The rotifer population itself is driven by a positive nonlinear effect of both preys  
 449 (Fig. h., red and purple line). There is also evidence for positive nonlinear intra-specific density  
 450 dependence (Fig. h., blue line). Overall, comparing results across the three replicates reveals that  
 451 the effect of the rotifer population on the flagellate and algae, and the effect of the algae on the

rotifer, are the strongest and most consistent interactions (Fig. 5, table 2). The interactions of the flagellate with the algae, and its effect on the rotifer population varies substantially across replicates (Fig. 5, table 2). Interestingly, intra-specific density dependence in rotifer and algae is also found to be inconsistent across the three replicates.

#### 4.4 Case study 3: real di-trophic prey-predator oscillations

We present the analysis of the drivers of the hare-lynx population dynamics in figure 6. Cross-validation provides support for nonlinear effects in the per-capita growth rate of the hare and lynx. We find that the hare population growth rate is mostly determined by a nonlinear negative effect of the lynx population (Fig. 6, b. and c. blue line), and by weak nonlinear positive density dependence (red line). The lynx growth rate is determined by a positive nonlinear effect of the hare (Fig. 6, e. and f., red line), and to a lesser extent by negative nonlinear intra-specific density dependence (blue line).

#### 4.5 Case study 4: drivers of the Maizuru bay community dynamics

We show the results of the NODE analysis of the drivers of the dynamics Maizuru bay community in figure 8. Our main finding is that the chameleon goby (*Tridentiger trionocephalus*) has a strong negative effect on the 8 of the 11 dominant species of the community. We find that *E. ercodes* also has a strong negative impact on other species in the community, although relatively smaller than that of the chamelon goby. We find a positive effect of sea bottom temperature on the growth rate of the chameleon goby. Other effects are found to be mostly positive and have a

471 relatively smaller impact on community dynamics.

## 472 **5 Discussion**

473 Characterising ecological interactions from time series data is challenging. This is due to the fact  
474 that interactions can be highly context-dependent processes (Song and Saavedra 2021), making it  
475 difficult to identify parametric models that encapsulate their complexity (Wood 2001). Interactions  
476 estimated with parametric models are contingent on the parameterisation arbitrarily chosen by the  
477 observer, and hence risk being biased (Wood 2001; Adamson and Morozov 2013). We provide  
478 a novel method for estimating ecological interactions nonparametrically, by using neural ordinary  
479 differential equations (NODEs) fitted with Bayesian neural gradient matching (BNGM). First, we  
480 remove the cost of fitting NODEs by introducing BNGM, which allows for NODE fitting in only  
481 a few seconds. The method involves interpolating time series and dynamics with neural networks,  
482 and then fitting NODEs to interpolated dynamics with Bayesian regularisation. We further demon-  
483 strate that this approach is accurate, as NODEs approximate with minimal error the ecological  
484 interactions in artificial time series, where real interactions are known. Finally, we estimate the  
485 strength, direction, importance, and nonlinearity of ecological interactions in 4 time series from  
486 natural and experimental systems, showing variation in ecological interactions within and across  
487 the time series.

### 488 **Bayesian neural gradient matching**

489 The Bayesian neural gradient matching (BNGM) approach that we propose here extends stan-

490 dard gradient matching, by using artificial neural networks (ANNs) as interpolating functions, and  
491 Bayesian regularisation to control the nonlinearity of the processes (Cawley and Talbot 2007). This  
492 allows us to accurately fit NODEs within seconds, making it potentially the most efficient current  
493 fitting technique available (see also Treven et al. 2021). The use of ANNs as interpolating func-  
494 tions sets it apart from the initial approach of Ellner et al., who use splines to interpolate the time  
495 series before approximating the ODEs (Ellner, Seifu, and Smith 2002). ANNs are more general  
496 and flexible than splines, as well as being easier to manipulate given that they are defined contin-  
497 uously on the state space, which is especially useful when handling multiple interactions between  
498 variables. Our approach is related to that of Wu et al., who use ANNs to approximate both the  
499 states and ODEs of prey-predator systems (Wu, Fukuhara, and Takeda 2005), as well as that of  
500 Treven and colleagues, who developed the Gaussian process equivalent (Treven et al. 2021). In  
501 both approaches, they train the interpolation functions at the same time as the NODEs, in order  
502 to constrain the interpolation of trajectories such that they can be achieved by the NODE system,  
503 which thereby introduces dynamical coupling between state variables. One of the risks of dynam-  
504 ical coupling approaches is that misestimating one of the state variables of the model biases the  
505 estimation of the states and dynamics of other variables. To avoid this, we fit each interpolation  
506 and NODE independently to each time series. In addition, this makes it possible to parallelise  
507 the code, resulting in potentially even faster computation. Our approach removes the main limita-  
508 tion of using NODEs, allowing for quick and extensive model comparison, cross-validation, and  
509 uncertainty quantification around estimates.

## 510 **Accuracy of NODEs in estimating ecological interactions**

511 Our approach relies on approximating population dynamics with NODEs and then computing their  
512 sensitivity to a change in the density of the different populations in the system (Bonnaiffé, Shel-  
513 don, and Coulson 2021). We demonstrate that NODEs accurately recover the dynamics, strength,  
514 direction, and nonlinearity of ecological interactions in artificial tri-trophic prey-predator time se-  
515 ries, where truth is known. In particular, we find that the interactions between the algae and the  
516 two predators are nonlinear, and thereby oscillate throughout the time series, which is consistent  
517 with the model, that features a resistance to predation at high algal density. We also recover the  
518 linear interactions between the two predators, which shows that the NODEs are sensitive enough  
519 to discriminate between linear and nonlinear interactions within and across time series. To our  
520 knowledge, this is the first assessment of the accuracy of NODEs in recovering interactions be-  
521 tween variables from time series data, as most of the work focuses on assessing the accuracy of  
522 the fitting and forecasting of time series (e.g. Mai, Shattuck, and O’Hern 2016; Chen et al. 2019;  
523 Treven et al. 2021; Frank 2022).

## 524 **Comparison with existing methods**

525 We find that fitting NODEs by BNGM provides higher estimation accuracies of ecological interac-  
526 tions, and reduces substantially fitting times compared to standard NODEs and parametric ODEs.  
527 This difference is attributable to three factors. First, BNGM alleviates the need for solving nu-  
528 merically the NODE system, which makes it faster to evaluate the posterior distribution. Second,  
529 it allows for the calculation of analytical gradients of the posterior distribution, which greatly im-

530 prove the speed of the gradient descent optimisation algorithm. Finally, it makes it possible to fit  
531 each variables independently on each, which results in a simpler optimisation problem.

532 CCM remains faster than our approach in recovering estimates of ecological interactions, however  
533 it does so by sacrificing accuracy. A possible explanation for this comes from the fact that CCM  
534 computes the sensitivity of the total population growth rate, rather than the per-capita growth rate,  
535 which can change estimated effects. Additionally, CCM relies on piecewise linear reconstructions  
536 of the state space, whereas NODEs computes a global nonlinear approximation of the per-capita  
537 growth rate on the entire range covered by the data. We view the former as potentially more  
538 sensitive to local noise in the state space, compared to the latter, which uses all evidence available  
539 to inform local inference.

540 Our approach opens new possibilities for nonparametric inference of ecological interactions from  
541 time series data. In addition to the ease of use, the lower fitting times makes it possible to tackle  
542 larger systems and apply more thorough statistical treatments of the uncertainty of these models,  
543 for instance by performing MCMC sampling method.

#### 544 **Ecological interactions in real prey-predator systems**

545 We further tested NODEs in a real setting, by inferring ecological interactions across three repli-  
546 cated time series of an experimental tri-trophic system of algae, flagellate, and rotifer populations  
547 (Hiltunen et al. 2013). Our approach reveals that only stronger interactions, namely the negative  
548 effects of the rotifer top predator on the other species, and the positive effect of algae on the rotifer,  
549 are conserved across the three replicated time series. We also find evidence for nonlinearity in



550 the dynamics of the rotifer, as the positive effect of the algae on rotifer growth oscillates through-  
551 out the time series. This is consistent with the biology of the system, as the algae tends to form  
552 anti-predation clumps at higher density, which would dampen the positive effect of algal density on  
553 rotifer growth at high algal density (Yoshida et al. 2003; Hiltunen et al. 2013). We find it interesting  
554 that the weaker interactions with the flagellate predator are not consistent across time series, given  
555 the controlled laboratory conditions. This system is known to evolve rapidly, it is hence possible  
556 that fast evolution of the different populations from the onset of the time series may have driven  
557 the system onto different attractors (Yoshida et al. 2003; Yoshida et al. 2007; Hiltunen et al. 2013).  
558 Additionally, stochasticity in population dynamics may have a similar effect (Dallas et al. 2021).  
559 Disentangling these two sources of variation would require refining the modelling framework, for  
560 instance by explicitly including evolution in the model (e.g. with the Price equation, Ellner, Geber,  
561 and Hairston 2011), and by using neural stochastic differential equations (i.e. NSDEs, Rackauckas  
562 et al. 2019) fitted with a particle filter. While these would constitute interesting developments, our  
563 method is still a useful first step, identifying differences between the time series, and demonstrating  
564 a reasonable amount of deterministic consistency in the dynamics, judging by the cross-validation  
565 and fits.

566 We also analysed the hare-lynx time series (Odum and Barrett 1972), as it is a common benchmark  
567 in the field of time series analysis, and provides a comparison point with our previous implemen-  
568 tation of NODEs (Bonnaiffé, Sheldon, and Coulson 2021). As in our previous study, we found a  
569 predatory inter-specific interaction between lynx and hare, and negative intra-specific density de-

pendence in the lynx. Evidence for positive density dependence in the hare was more limited than previously found. We also found stronger evidence for nonlinearity, as intra- and inter-specific effects oscillated throughout the time series, as a result of density dependence. This difference with our previous study is due to the fact that our previous implementation of NODEs was based on simulating the full NODE system, and hence imposed dynamical coupling between the variables. This dynamical coupling comes at a cost, if one variable is not explained well by the model, it will bias the interactions and dynamics of other variables. Here, the time series of lynx and hare are analysed independently, each state variable is interpolated as closely as desired, its effects on the dynamics of other variables are hence even more robust to model misspecification than before.

Overall, our approach provides a novel and powerful way of estimating interactions nonparametrically from time series data. The benefit of using NODEs is that they make no assumptions about the nature of the ecological interactions that drive the dynamics of the species (Chen et al. 2019; Bonnaiffé, Sheldon, and Coulson 2021). Hence, we have a better chance at estimating the actual value of the interactions, knowing that it is not subjected to potential incorrect model specifications (Jost and Ellner 2000; Ellner, Seifu, and Smith 2002; Wu, Fukuhara, and Takeda 2005; Kendall et al. 2005; Adamson and Morozov 2013). This approach is similar to Sugihara’s maps (S-maps, Sugihara et al. 2012), which estimate interactions in time series by approximating the Jacobian matrix nonparametrically via locally linear approximations of the state space (Deyle et al. 2015). However, because S-maps are locally linear, they do not assume the existence of a latent trajectory generated by an overarching model. This creates two caveats, the first being that they are

590 more sensitive to noise in the time series (Cenci and Saavedra 2018), the second being that they  
591 have no theoretical grounding given that they are at heart linear functions defined piecewise on  
592 the state space. NODEs remain in essence deterministic ODE models, assuming an overarching  
593 model driving the populations through the entire state-space, which can hence incorporate para-  
594 metric assumptions regarding the driving processes (Bonnaffé, Sheldon, and Coulson 2021). For  
595 instance, we model the per capita growth rate of populations explicitly in NODEs, while S-maps  
596 approximate the population-level growth. Overall, this makes NODEs more suitable than S-maps  
597 for fitting noisy data or exploring theory by testing specific assumptions.

#### 598 **Maizuru bay community**

599 We applied our approach to analyse the drivers of the dynamics of 11 species in the Maizuru bay.  
600 We inferred 11 by 12 ecological interactions, and 11 dependencies on water temperature. We found  
601 that the chameleon hobby had a strong negative impact on the other species of the system, showing  
602 a strong competitive potential. This species is viewed as an aggressive competitor, and is con-  
603 sidered an invasive species posing a serious threat to other populations in places where it has been  
604 introduced. We also find a positive effect of temperature on the growth rate of the chameleon hobby,  
605 which suggests that warming could have indirect negative effects on many species on Maizuru bay  
606 by favouring the reproduction of the gobby.

607 Surprisingly, our results differ substantially from those obtained by Ushio et al. in their original  
608 analysis of the system with convergent cross mapping. This may be due to a multitude of factors.  
609 First, we considered a different set of species, as some of the time series that Ushio and colleagues

610 used were too sparse to be suitable for our analysis. Additionally, this difference may be explained  
611 by the disparity in the estimation accuracies revealed by our benchmark analysis, relating to fun-  
612 damental mathematical differences between the two approach, as discussed previously.

613 If nothing else, our analysis of the Maizuru community dynamics demonstrates the usefulness of  
614 our BNGM method for fitting NODEs to a larger more realistic system.

### 615 **Limits and prospects**

616 One of the main difficulty in quantifying ecological interactions is to identify potential context de-  
617 pendences on other state variables (Song and Saavedra 2021), for example, whether predation rates  
618 are affected by temperature. Our approach allows for the quantification of context dependence,  
619 which shows as nonlinear fluctuations of interactions throughout the time series. In the present  
620 work, we only report nonlinearity as evidence for context dependence in the interactions, but we  
621 do not attempt to understand what it is attributable to. For instance, we identify nonlinear density  
622 dependence in the effect of the algae on the rotifer, but we do not know whether this is due to a  
623 change in the effect with algae density or rotifer density, or both. In order to disentangle these  
624 higher order effects we could compute the Hessian of the system, namely the second order deriva-  
625 tive of the dynamics with respect to the different state variables. Though this procedure is simple  
626 mathematically, it would result in 27 second order effects to analyse for the simple 3 species system  
627 considered here. This type of analysis would get rapidly out of hand for larger systems. Further  
628 work should hence consider how to handle these higher order effects, as a way to unveil context  
629 dependence in ecological interactions.

630 One further issue is that some interactions may depend on variables that are not observed. For  
631 instance, some population dynamics are strongly determined by their demographic state (Lande et  
632 al. 2002; Coulson et al. 2004), which would call for time series of the relevant demographic stages.  
633 In the system considered here, the dynamics of algae in the rotifer system are most likely coupled  
634 with that of nitrogen, for which no time series was available (Hiltunen et al. 2013). Our method  
635 only accounts for observed variables, so that time series for all important variables are required,  
636 though unaccounted variables are captured to some extent by nonlinear fluctuations in interactions.  
637 One interesting prospect would hence be to incorporate unobserved/latent state variables into the  
638 NODE system (Dupont, Doucet, and Teh 2019; Zhang et al. 2019; Frank 2022). Careful thought  
639 has to be given here as whether to use an ODE or NODE for the latent states given that they are not  
640 constrained by observations.

641 A further question is whether we could use similar approaches to analyse systems larger than the  
642 ones considered on this study. In particular, microbial communities feature thousands of species,  
643 and hence potentially millions of interactions. This poses a real problem for inference as even the  
644 simplest linear model would contain millions of parameters, hence entering deep learning territory.  
645 We believe that our success there is more readily limited by the availability of time series suffi-  
646 ciently long to identify this many interactions, rather than by our models. A possible next step  
647 could be to address the capacity of deeper NODE models to estimate interactions in large artifi-  
648 cial communities, which could inform us on the relationship between model complexity and data  
649 requirements in terms of time series length and sampling frequency.

650 We consider NODEs, which are only defined along the time dimension. The framework could  
651 easily be extended to any other dimension by considering partial differential equations instead  
652 (Rackauckas et al. 2019). For instance, in a spatial ecology context we could model the dynamics  
653 of populations along two additional spatial dimensions. In an evolutionary context, we could model  
654 the dynamics of populations in phenotype space, by adding phenotypic traits as an additional di-  
655 mension. The BNGM method could be instrumental in fitting these models, which are notoriously  
656 expensive to stimulate.

## 657 **Conclusion**

658 We provide a method, BNGM, which allows for NODE fitting in a matter of seconds. This is  
659 a crucial step for efficient model selection and uncertainty quantification in NODEs. We also  
660 demonstrate that NODEs allow for accurate estimation of the direction, strength, and nonlinear-  
661 ity of ecological interactions, in a system where truth is known. Finally, we estimate ecological  
662 interactions in real prey predator systems, showing that system dynamics are driven by a mixture  
663 of linear and nonlinear interactions, of which only strong ones seem to be generalisable across  
664 time series. Our study allows for efficient NODE fitting, and confirms the power of NODEs in  
665 identifying dynamical coupling between populations.

## 666 **Acknowledgments**

667 We thank warmly the Ecological and Evolutionary Dynamics Lab and Sheldon Lab Group at the  
668 department of Zoology for their feedback and support. We thank Ben Sheldon for insightful sug-  
669 gestions on early versions of the work. The work was supported by the Oxford-Oxitec scholarship

670 and the NERC DTP.

## 671 **Data accessibility**

672 All data and code will be made fully available at <https://github.com/WillemBonnafe/NODER/BNGM>,  
673 as well as on <https://datadryad.org/stash/dataset/doi:xxx>.

## 674 **Statement of authorship**

675 Willem Bonnaff  designed the method, performed the analysis, wrote the manuscript; Tim Coulson  
676 led investigations, provided input for the manuscript, commented on the manuscript.

## 677 **References**

678 Aarts, L. P. and P. V. D. Veer (2001). “Neural network method for solving partial differential equa-  
679 tions”. In: *Neural Processing Letters* 14 (3), pp. 261–271.

680 Adams, M. P. et al. (Apr. 2020). “Informing management decisions for ecological networks, using  
681 dynamic models calibrated to noisy time-series data”. In: *Ecology Letters* 23 (4), pp. 607–619.

682 Adamson, M. W. and A. Y. Morozov (2013). “When can we trust our model predictions? Un-  
683 earthing structural sensitivity in biological systems”. In: *Proceedings of the Royal Society A: Mathematical, Physical and Engineering Sciences* 469 (2149), pp. 1–19.

685 Arndt, H. (1993). “Rotifers as predators on components of the microbial web (bacteria, heterotrophic  
686 flagellates, ciliates) - a review”. In: *Hydrobiologia* 255-256 (1), pp. 231–246.

687 Berryman, A. and P. Turchin (1997). “Detection of density dependence: comment”. In: *Ecology* 78  
688 (1), pp. 318–320.

689 Berryman, A. A. (2002). “Population: a central concept for ecology?” In: *Oikos* 97 (3), pp. 439–  
690 442.

691 Berryman, A. A. (2003). “On principles, laws and theory in population ecology”. In: *Oikos* 103  
692 (3), pp. 695–701.

693 Bonnaiffé, W., S. Legendre, A. Danet, and E. Edeline (2021). “Comparison of size-structured and  
694 species-level trophic networks reveals antagonistic effects of temperature on vertical trophic  
695 diversity at the population and species level”. In: *Oikos*, pp. 1–14.

696 Bonnaiffé, W., M. Martin, M. Mugabo, S. Meylan, and J. F. L. Galliard (Dec. 2018). “Ontogenetic  
697 trajectories of body coloration reveal its function as a multicomponent nonsenescent signal”. In:  
698 *Ecology and Evolution* 8 (24), pp. 12299–12307.

699 Bonnaiffé, W., B. C. Sheldon, and T. Coulson (2021). “Neural ordinary differential equations for  
700 ecological and evolutionary time series analysis”. In: *Methods in Ecology and Evolution* 2, pp. 1–  
701 46.

702 Bonsall, M. B., E. V. D. Meijden, and M. J. Crawley (2003). “Contrasting dynamics in the same  
703 plant-herbivore interaction”. In: *Proceedings of the National Academy of Sciences of the United*  
704 *States of America* 100 (25), pp. 14932–14936.

705 Brook, B. W. and C. J. A. Bradshaw (2006). “Strength of evidence for density dependence in  
706 abundance time series of 1198 species”. In: *Ecology* 87 (6), pp. 1445–1451.



707 Brown, J. H., J. F. Gillooly, A. P. Allen, V. M. Savage, and G. B. West (2004). “Toward a metabolic  
708 theory of ecology”. In: *Ecology* 85 (7), pp. 1771–1789.

709 Bruijning, M., E. Jongejans, and M. M. Turcotte (2019). “Demographic responses underlying eco-  
710 evolutionary dynamics as revealed with inverse modelling”. In: *Journal of Animal Ecology* 88  
711 (5), pp. 768–779.

712 Cawley, G. C. and N. L. C. Talbot (2007). “Preventing over-fitting during model selection via  
713 bayesian regularisation of the hyper-parameters”. In: *Journal of Machine Learning Research* 8,  
714 pp. 841–861.

715 Cenci, S. and S. Saavedra (Oct. 2018). “Uncertainty quantification of the effects of biotic interac-  
716 tions on community dynamics from nonlinear time-series data”. In: *Journal of the Royal Society*  
717 *Interface* 15 (147).

718 Chen, R. T. Q., Y. Rubanova, J. Bettencourt, and D. Duvenaud (2019). “Neural Ordinary Differen-  
719 tial Equations”. In: *arXiv*, pp. 1–19.

720 Coulson, T., F. Guinness, J. Pemberton, and T. Clutton-Brock (2004). “The demographic conse-  
721 quences of releasing a population of red deer from culling”. In: *Ecology* 85 (2), pp. 411–422.

722 Dallas, T., B. A. Melbourne, G. Legault, and A. Hastings (2021). “Initial abundance and stochas-  
723 ticity influence competitive outcome in communities”. In: *Journal of Animal Ecology*, pp. 1–  
724 26.

725 Deyle, E. R., R. M. May, S. B. Munch, and G. Sugihara (Jan. 2015). “Tracking and forecasting  
726 ecosystem interactions in real time”. In: *Proceedings of the Royal Society B: Biological Sciences*  
727 283, pp. 1–9.

728 Dupont, E., A. Doucet, and Y. W. Teh (2019). “Augmented Neural ODEs”. In: *arXiv*, pp. 1–11.

729 Ellner, S. P., M. A. Geber, and N. G. J. Hairston (2011). “Does rapid evolution matter? Measuring  
730 the rate of contemporary evolution and its impacts on ecological dynamics”. In: *Ecology Letters*  
731 14 (6), pp. 603–614.

732 Ellner, S. P., Y. Seifu, and R. H. Smith (2002). “Fitting Population Dynamic Models to Time-Series  
733 Data by Gradient Matching”. In: *Ecology* 83 (8), p. 2256.

734 Frank, S. A. (2022). “Automatic differentiation and the optimization of differential equation models  
735 in biology”. In: *arXiv*, pp. 1–10.

736 Gross, K., A. R. Ives, and E. V. Nordheim (2005). “Estimating fluctuating vital rates from time-  
737 series data: A case study of aphid biocontrol”. In: *Ecology* 86 (3), pp. 740–752.

738 Hairston, N. G. J., S. P. Ellner, M. A. Geber, T. Yoshida, and J. A. Fox (2005). “Rapid evolution  
739 and the convergence of ecological and evolutionary time”. In: *Ecology Letters* 8 (10), pp. 1114–  
740 1127.

741 Hiltunen, T., L. E. Jones, S. P. Ellner, and N. G. J. Hairston (2013). “Temporal dynamics of a simple  
742 community with intraguild predation: an experimental test”. In: *Ecology* 94 (4), pp. 773–779.

743 Hu, P., W. Yang, Y. Zhu, and L. Hong (2020). “Revealing hidden dynamics from time-series data  
744 by ODENet”. In: *arXiv*, pp. 1–17.

745 Ives, A. R., B. Dennis, K. L. Cottingham, and S. R. Carpenter (2003). “Estimating community  
746 stability and ecological interactions from time-series data”. In: *Ecological Monographs* 73 (2),  
747 pp. 301–330.

- 748 Jonzén, N., P. Lundberg, E. Ranta, and V. Kaitala (Feb. 2002). “The irreducible uncertainty of  
749 the demography - Environment interaction in ecology”. In: *Proceedings of the Royal Society B: Biological Sciences* 269 (1488), pp. 221–225.
- 751 Jost, C. and S. P. Ellner (2000). “Testing for predator dependence in predator-prey dynamics: A  
752 non-parametric approach”. In: *Proceedings of the Royal Society B: Biological Sciences* 267  
753 (1453), pp. 1611–1620.
- 754 Kendall, B. E. et al. (1999). “Why do populations cycle? A synthesis of statistical and mechanistic  
755 modeling approaches”. In: *Ecology* 80 (6), pp. 1789–1805.
- 756 Kendall, B. E. et al. (2005). “Population cycles in the pine looper moth: Dynamical tests of mech-  
757 anistic hypotheses”. In: *Ecological Monographs* 75 (2), pp. 259–276.
- 758 Lande, R, S Engen, B.-E Saether, F Filli, E Matthysen, and H Weimerskirch (2002). “Estimating  
759 Density Dependence from Population Time Series Using Demographic Theory and Life-History  
760 Data”. In: *American Naturalist* 159, pp. 321–337.
- 761 Lawton, J. H. (1999). “Are There General Laws in Ecology ?” In: *Oikos* 84 (2), pp. 177–192.
- 762 Lingjaerde, O. C. et al. (2001). “Exploring the density-dependent structure of blowfly populations  
763 by nonparametric additive modeling”. In: *Ecology* 82 (9), pp. 2645–2658.
- 764 Mai, M., M. D. Shattuck, and C. S. O’Hern (2016). “Reconstruction of Ordinary Differential Equations  
765 From Time Series Data”. In: *arXiv*, pp. 1–15.
- 766 Moe, S. J., A. B. Kristoffersen, R. H. Smith, and N. C. Stenseth (2005). “From patterns to processes  
767 and back: Analysing density-dependent responses to an abiotic stressor by statistical and

768 mechanistic modelling”. In: *Proceedings of the Royal Society B: Biological Sciences* 272 (1577),  
 769 pp. 2133–2142.

770 Mysterud, A., T. Coulson, and N. C. Stenseth (2002). “The role of males in the dynamics of ungu-  
 771 late populations”. In: *Journal of Animal Ecology* 71, pp. 907–915.

772 Novak, M. and D. B. Stouffer (Nov. 2021). “Geometric Complexity and the Information-Theoretic  
 773 Comparison of Functional-Response Models”. In: *Frontiers in Ecology and Evolution* 9.

774 Odum, E. P. and G. W. Barrett (1972). “Fundamentals of Ecology”. In: *The Journal of Wildlife*  
 775 *Management* 36 (4), p. 1372.

776 Pasquali, S. and C. Soresina (2018). “Estimation of the mortality rate functions from time series  
 777 field data in a stage-structured demographic model for *Lobesia botrana*”. In: *arXiv*, pp. 1–15.

778 Pearce, T., F. Leibfried, A. Brintrup, M. Zaki, and A. Neely (2018). “Uncertainty in Neural Net-  
 779 works: Approximately Bayesian Ensembling”. In: *arXiv*, pp. 1–10.

780 Rackauckas, C., M. Innes, Y. Ma, J. Bettencourt, L. White, and V. Dixit (Feb. 2019). “DiffEqFlux.jl  
 781 - A Julia Library for Neural Differential Equations”. In: *arXiv*, pp. 1–17.

782 Rosenbaum, B., M. Raatz, G. Weithoff, G. F. Fussmann, and U. Gaedke (2019). “Estimating param-  
 783 eters from multiple time series of population dynamics using bayesian inference”. In: *Frontiers*  
 784 *in Ecology and Evolution* 6 (234), pp. 1–14.

785 Royama, T (1984). “Population Dynamics of the Spruce Budworm *Choristoneura fumiferana*”. In:  
 786 *Ecological Monographs* 54 (4), pp. 429–462.

787 Song, C., S. V. Ahn, R. P. Rohr, and S. Saavedra (May 2020). “Towards a Probabilistic Under-  
788 standing About the Context-Dependency of Species Interactions”. In: *Trends in Ecology and*  
789 *Evolution* 35 (5), pp. 384–396.

790 Song, C. and S. Saavedra (July 2021). “Bridging parametric and nonparametric measures of species  
791 interactions unveils new insights of non-equilibrium dynamics”. In: *Oikos* 130 (7), pp. 1027–  
792 1034.

793 Sugihara, G. et al. (2012). “Detecting causality in complex ecosystems”. In: *Science* 338 (6106),  
794 pp. 496–500.

795 Treven, L., P. Wenk, F. Dörfler, and A. Krause (2021). “Distributional Gradient Matching for Learn-  
796 ing Uncertain Neural Dynamics Models”. In: *arXiv*, pp. 1–14.

797 Turchin, P. (1999). “Population Regulation: A Synthetic View”. In: *Oikos* 84 (1), pp. 153–159.

798 – (2001). “Does population ecology have general laws?” In: *Oikos* 94, pp. 17–26.

799 – (2003). “Evolution in population dynamics”. In: *Nature* 424, pp. 257–258.

800 Ushio, M. et al. (Feb. 2018). “Fluctuating interaction network and time-varying stability of a natural  
801 fish community”. In: *Nature* 554 (7692), pp. 360–363.

802 Wood, S. N. (2001). “Partially specified ecological models”. In: *Ecological Monographs* 71 (1),  
803 pp. 1–25.

804 Wu, J., M. Fukuhara, and T. Takeda (2005). “Parameter estimation of an ecological system by  
805 a neural network with residual minimization training”. In: *Ecological Modelling* 189 (3-4),  
806 pp. 289–304.

807 Yoshida, T., S. P. Ellner, L. E. Jones, B. J. M. Bohannan, R. E. Lenski, and N. G. J. Hairston (2007).  
808 “Cryptic population dynamics: Rapid evolution masks trophic interactions”. In: *PLoS Biology* 5  
809 (9), pp. 1868–1879.

810 Yoshida, T., L. E. Jones, S. P. Ellner, G. F. Fussmann, and N. G. J. Hairston (2003). “Rapid evo-  
811 lution drives ecological dynamics in a predator – prey system”. In: *Nature* 424 (July), pp. 303–  
812 306.

813 Zhang, H., X. Gao, J. Unterman, and T. Arodz (July 2019). “Approximation Capabilities of Neural  
814 ODEs and Invertible Residual Networks”. In: *arXiv*, pp. 1–11.

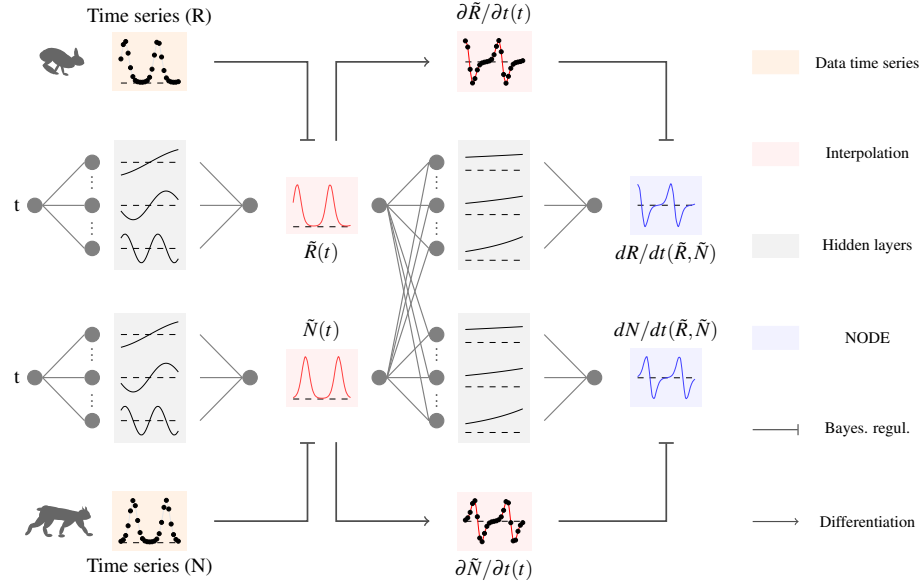


**Figure 1: Overview of fitting neural ordinary differential equations (NODE) by Bayesian neural gradient matching (BNGM).** In a first step we compute a continuous time approximation (interpolation) of each state variables, here the prey  $\tilde{R}(t)$  and predator density  $\tilde{N}(t)$  (red boxes). To do that we fit an ANN, that takes time as input, to each time series, via Bayesian regularisation. Interpolated dynamics of populations can then be computed by taking the derivative of the ANN with respect to time,  $\partial \tilde{R} / \partial t$  and  $\partial \tilde{N} / \partial t$ . In a second step, we fit each NODE,  $dR/dt$  and  $dN/dt$  (blue boxes), to the interpolated dynamics. To do that we fit an ANN, which takes as input the interpolated variables  $\tilde{R}(t)$  and  $\tilde{N}(t)$ , to the interpolated dynamics  $\partial \tilde{R} / \partial t$  and  $\partial \tilde{N} / \partial t$ , via Bayesian regularisation.

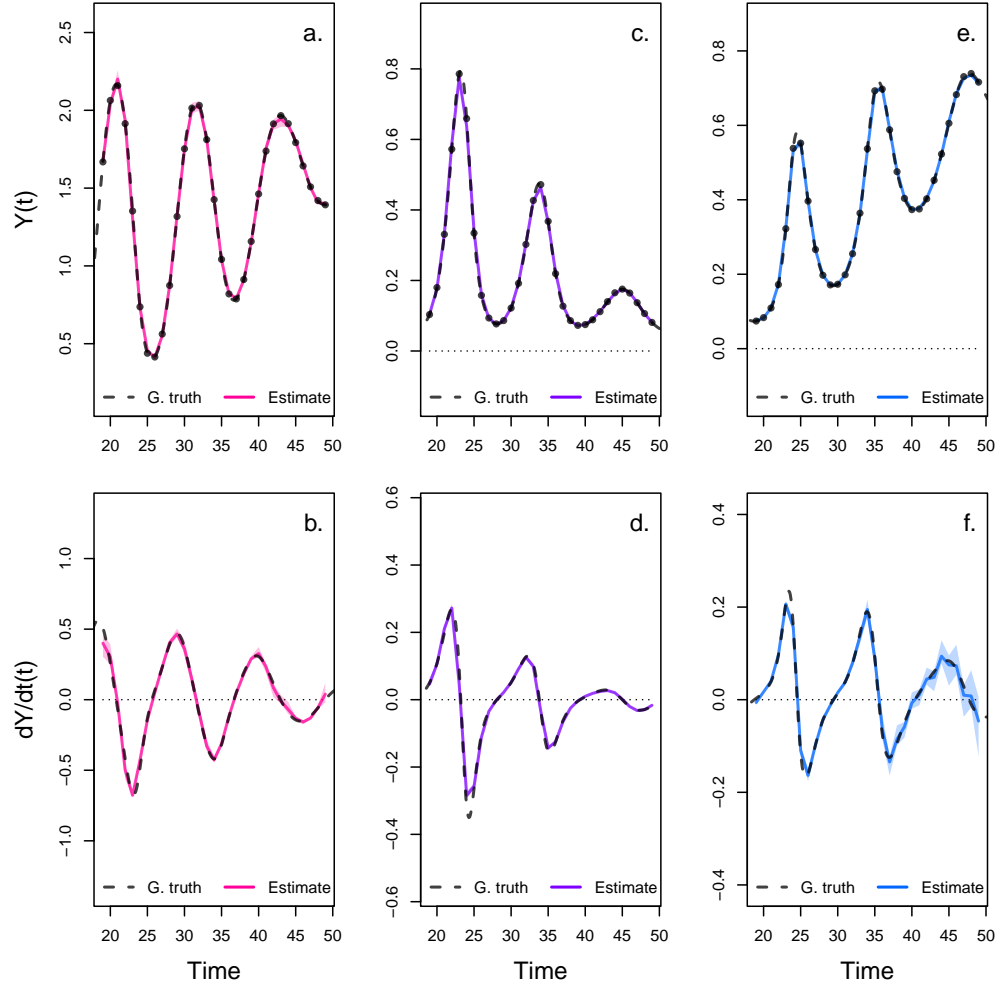


**Figure 2: Interpolated density and dynamics of prey, intermediate, and top predators in the artificial system.** This figure corresponds to the first step in the overview figure (Fig. 1). It shows the accuracy of the interpolated densities of prey (a.), intermediate (c.), and top predators (e.). We obtain interpolated densities by fitting observed densities (black dots) with ANNs that take time as input. The observed densities were obtained by sampling a tri-trophic prey-predator ODE model at regular time steps. We then derive interpolated dynamics (b., d., f.) by computing the temporal derivative of the interpolated densities with respect to time. In all graphs, the dashed line represents the ground truth, namely trajectories generated by the ODE model. The solid lines correspond to the interpolations. The shaded area shows the 90% confidence interval, obtained by approximately sampling the marginal posterior distributions.



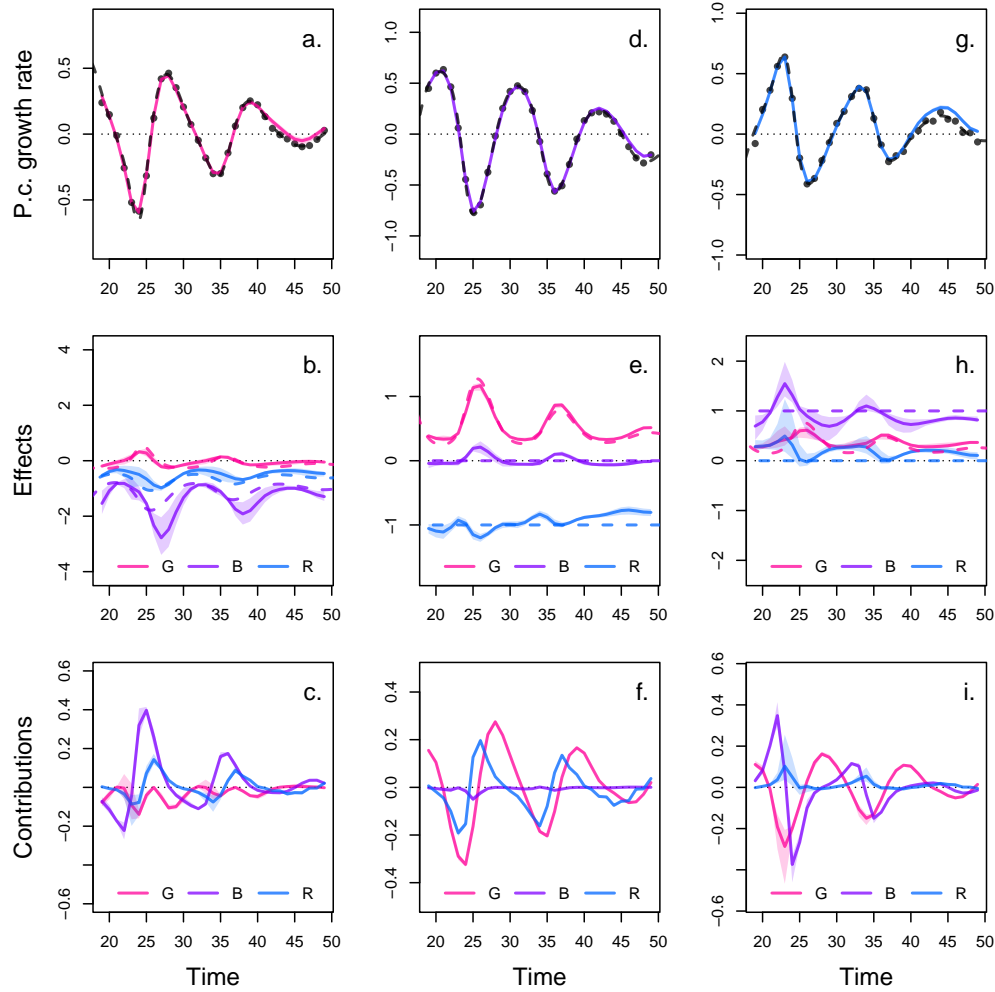


**Figure 3: Drivers of dynamics of prey, intermediate, and top predator in the artificial system.**

This figure corresponds to the second step in the overview figure (Fig. 1). It displays the NODE nonparametric approximations of the per-capita growth rate of prey (a., b., c.), intermediate (d., e., f.), and top predators (g., h., i.). We obtain the NODE approximations (a., d., g., solid line) by fitting the interpolated per-capita growth rates (black dots) with ANNs that take population densities as input. We then estimate the direction of ecological interactions (effects, b., e., h.) by computing the derivative of the NODE approximations with respect to each density. Finally, we compute the strength of ecological interactions (contributions, c., f., i.) by multiplying the interpolated dynamics of each population (fig. 1, b., d., f.) with its effects. Dashed lines correspond to ground truth, obtained from the original trajectories of the tri-trophic ODE model. The shaded area shows the 90% confidence interval, obtained by approximately sampling the posterior distributions.

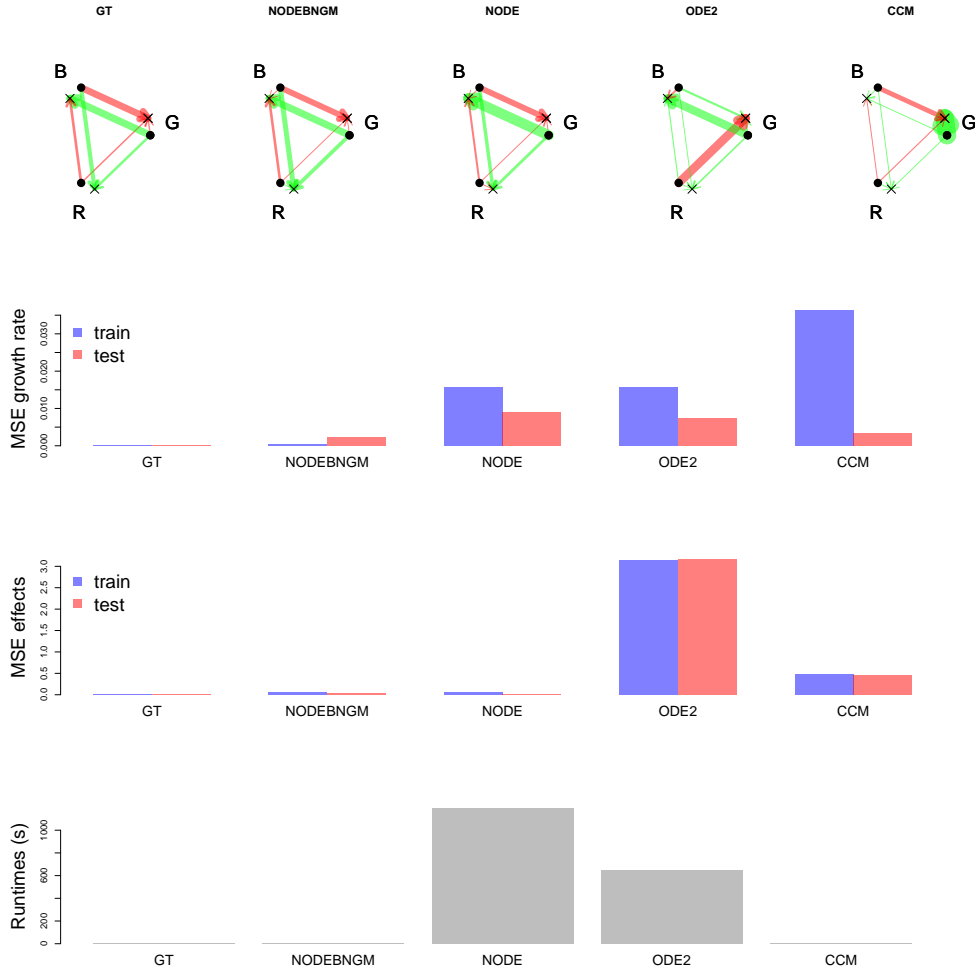


**Figure 4: Runtimes and accuracy of NODEs fitted by BNGM compared to standard NODEs, ODEs, and CCM. The NODEBNGM method (nonparametric) involves fitting a NODE system by Bayesian neural gradient matching (BNGM). The NODE method (nonparametric) involves fitting a NODE system with an ODE solver. The ODE2 method (parametric) involves fitting an ODE system with quadratic functions of species densities with an ODE solver. The CCM method (nonparametric) involves computing locally linear approximations of the state space. For each method, we trained 30 models on the two first thirds of the artificial time series where ground truth is known (Fig. xxx). We computed runtimes as the mean time (in seconds) required to train a single model. Using the best identified model, we predicted the growth rate and effects (i.e. growth rate density-dependence) on the train and test set. We computed accuracies as the mean squared error of predictions vs ground truth (known from the equations that generated the data) (see Fig. S5-7 for more details). At the top, we show the dynamical interaction network of the system predicted by the best models, where G, B, R correspond to the prey, intermediate and top predator, respectively, and green and red colours correspond to positive and negative interactions.**

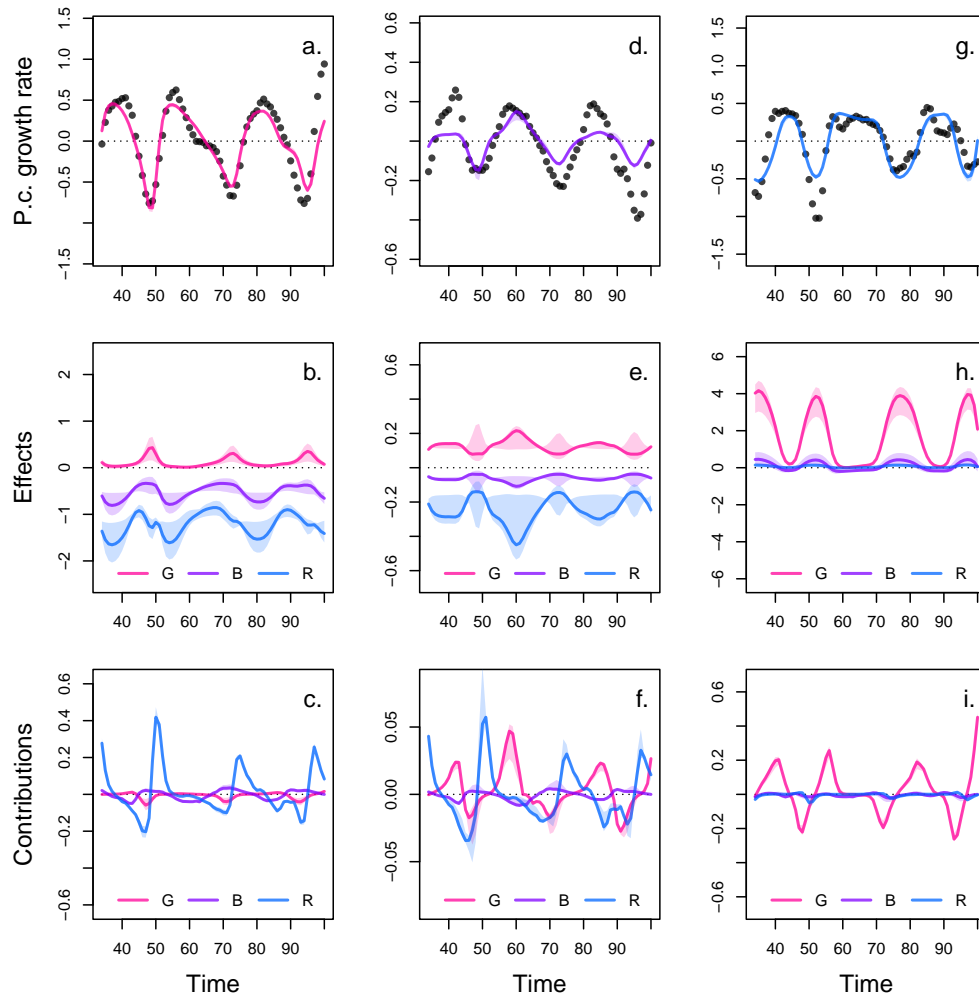


**Figure 5: Drivers of dynamics of algae, flagellate, and rotifer in replicate A.** This figure displays the NODE nonparametric approximations of the per-capita growth rate of algae (a., b., c.), flagellate (d., e., f.), and rotifer (g., h., i.). We obtain the NODE approximations (a., d., g., solid line) by fitting the interpolated per-capita growth rates (black dots) with ANNs that take population densities as input. We then estimate the direction of ecological interactions (effects, b., e., h.) by computing the derivative of the NODE approximations with respect to each density. Finally, we compute the strength of ecological interactions (contributions, c., f., i.) by multiplying the interpolated dynamics of each population with its effects. The shaded area shows the 90% confidence interval, obtained by approximately sampling the posterior distributions. The replicated time series were obtained by digitising the time series in Hiltunen et al. (2013).

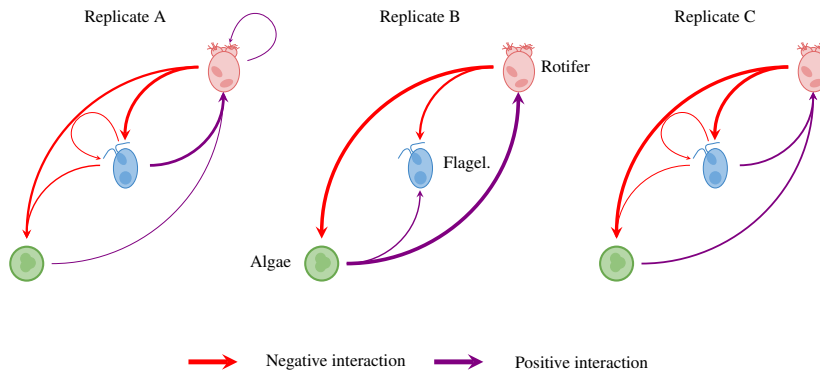


**Figure 6: Interaction networks inferred from 3 replicated time series of algae, flagellate, and rotifers.** This figure shows the direction and strength of ecological interactions inferred from 3 replicated sets of time series of algae, flagellate, and rotifer, using NODEs fitted by BNGM. The replicates B and C were analysed in the same way as replicate A (see fig. 4 for details). Red and purple arrows correspond to negative or positive mean effects. We estimated mean effects by averaging effects (i.e. derivative of NODE approximated per-capita growth rates with respect to each population density) across the time series. The width of the arrows is proportional to the relative strength of the ecological interaction. We compute the relative strength as the % of total contributions attributable to either algae, flagellate, or rotifer, obtained from summing the square of contributions of each species throughout the time series. For instance in replicate A, the relative strength of the effect of rotifer on algae is found by summing the square of the blue line in fig. 4 c., and comparing it to the sum of square of all contributions (Fig. 4 c., red, purple and blue lines). We provide the value of the mean effects and relative strengths in table 2. The replicated time series were obtained by digitising the time series in Hiltunen et al. (2013).

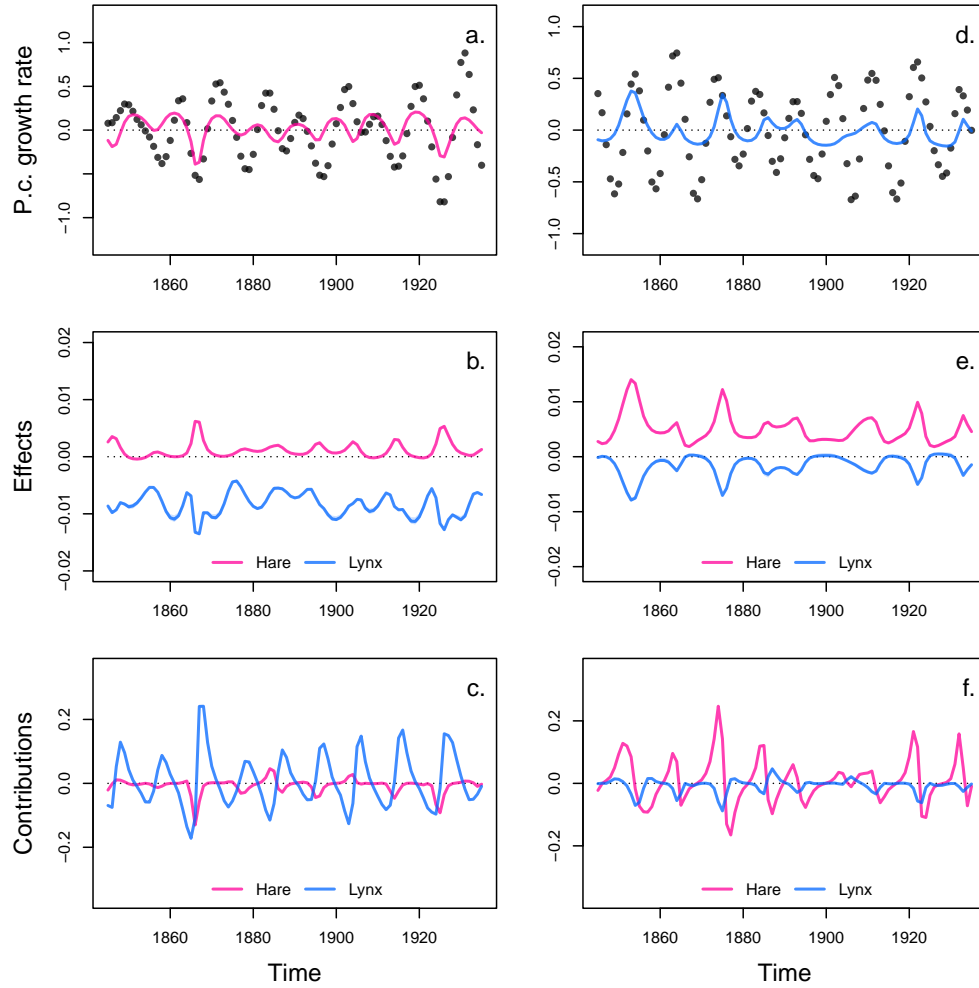


**Figure 7: Drivers of dynamics of hare and lynx in the Odum and Barrett pelt count time series.** This figure displays the NODE nonparametric approximations of the per-capita growth rate of hare (a., b., c.), and lynx (d., e., f.). We obtain the NODE approximations (a., d., solid line) by fitting the interpolated per-capita growth rates (black dots) with ANNs that take population densities as input. We then estimate the direction of ecological interactions (effects, b., e.) by computing the derivative of the NODE approximations with respect to each density. Finally, we compute the strength of ecological interactions (contributions, c., f.) by multiplying the interpolated dynamics of each population with its effects. The shaded area shows the 90% confidence interval, obtained by approximately sampling the posterior distributions.

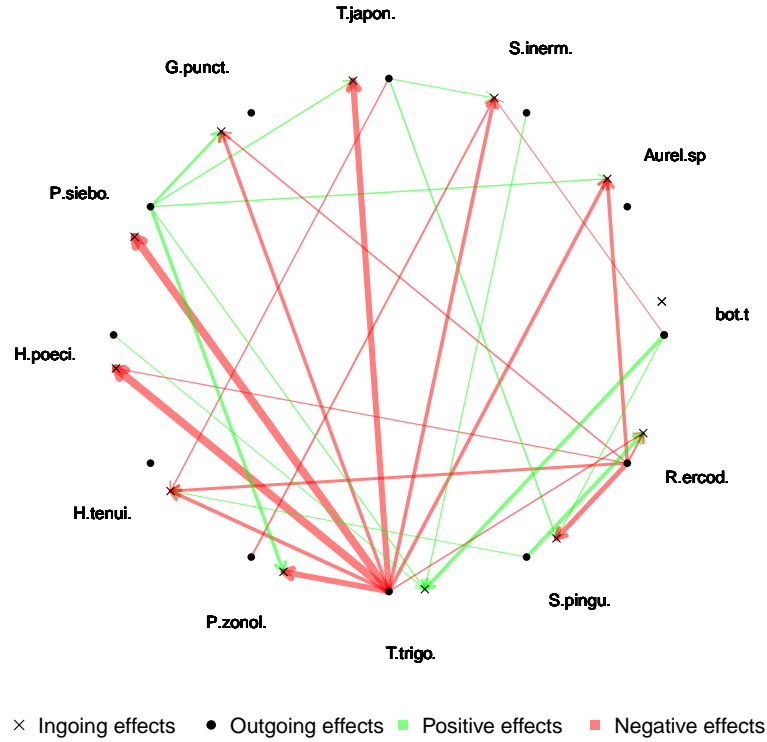


**Figure 8: Dynamical interaction network of the Maizuru bay community.** This figure summarises the results of the NODEBNGM analysis of the Maizuru bay community time series (Fig. 1). Bot.t corresponds to the water temperature. Species are referred to by their shortened acronym (see Fig. 1 for full names). Red and green arrows correspond to negative or positive mean effects, obtained by averaging the sensitivity of the growth rate of a species to the density of other species across the time series. The width of the arrows is proportional to the total contribution (in %) of species density to the growth rate of other species, obtained by averaging contributions across the time series.

**Table 1: Summary of model runtimes.** We measured the time required to perform 100 interpolations and 30 NODE fits to each variable in the systems. Replicate A, B, and C correspond to each replicated time series of the aglae, flagellate, and rotifer tri-trophic system (Hiltunen et al. 2013). The Hare-Lynx system correspond to the 90 years long time series of hare and lynx pelt counts (Odum and Barrett 1972). The number of time steps (N steps) is given for each time series. The total time per fit is obtain by dividing the total time in seconds by the number of fits (i.e. 130). It takes on average 5.35 minutes for the 130 NODE fits NODE, which amounts to 5.37 seconds per sample taken. This is 335 times faster than the 30 minutes fitting times obtained in a previous study (Bonnaffé, Sheldon, and Coulson 2021). These results were obtained on a macbook pro M1 MAX 2022, in base R (v4.0.2), with non-optimised code.

System	N var.	N steps	Interpolation		NODE fit		total	total p. fit
			N fits	time (s)	N fits	time (s)		
Replicate A	3	66	100	239.47	30	129.41	368.88	6.71
Replicate B	3	66	100	233.59	30	133.13	366.72	6.77
Replicate C	3	40	100	136.51	30	74.01	210.52	3.83
Hare-lynx	2	90	100	303.64	30	33.56	337.20	4.16

**Table 2: Comparison of the direction and strength of ecological interactions estimated by BNGM across 3 replicated tri-trophic microcosms.** Mean effects are obtained by averaging the effect of one species on the growth rate of another throughout the time series. The % of total contributions is obtained by summing the square of contributions of one species density to the growth of the other at each time step throughout the time series, then by computing the proportion of total change that it accounts for. The variables *G*, *B*, and *R* correspond to the population density of algae, flagellate, and rotifer respectively.  $r^2$  corresponds to the r squared of the NODE nonparametric approximation of the pre-capita growth rate of the three species.

		G	B	R
<hr/>				
<b>Replicate A</b>	$r^2$	0.3	0.47	0.94
<b>Mean effects</b>	on G	-0.61	-0.85	-1.41
	on B	0.00	0.08	-0.90
	on R	2.84	0.93	1.23
<b>% of total contributions</b>	to G	0.13	0.15	0.73
	to B	0.00	0.00	1.00
	to R	0.60	0.16	0.25
<hr/>				
<b>Replicate B</b>	$r^2$	0.65	0.85	0.47
<b>Mean effects</b>	on G	0.00	-0.56	-1.13
	on B	0.34	0.00	-0.58
	on R	0.87	0.00	0.19
<b>% of total contributions</b>	to G	0.00	0.06	0.94
	to B	0.23	0.00	0.77
	to R	0.95	0.00	0.05
<hr/>				
<b>Replicate C</b>	$r^2$	0.93	0.29	0.87
<b>Mean effects</b>	on G	-0.14	0.13	-2.31
	on B	-0.05	-0.09	-0.72
	on R	2.46	0.49	-0.09
<b>% of total contributions</b>	to G	0.02	0.02	0.96
	to B	0.00	0.01	0.99
	to R	0.79	0.18	0.03



## 815 **6 Supplementary**

### 816 **A Bayesian regularisation**

817 The fitting of the models is performed in a Bayesian framework, considering normal error structure  
818 for the residuals, and normal prior density distributions on the parameters

$$p(\theta|\mathcal{D}) \propto p(\mathcal{D}|\theta)p(\theta) \quad (13)$$

819 where  $\theta$  is the parameter vector of the model, and  $\mathcal{D}$  the evidence, namely the data that the model  
820 is fitted to. Assuming a normal likelihood for the residuals given the evidence we get

$$p(\mathcal{D}|\theta) = \prod_{i=1}^I \frac{1}{\sqrt{2\pi\sigma^2}} \exp \left\{ -\frac{e_i(\mathcal{D}, \theta)^2}{2\sigma^2} \right\} \quad (14)$$

821 where  $e_i(\mathcal{D}, \theta)$  are the residuals of the model given the parameters, and the evidence. In the case of  
822 the interpolation, the residuals correspond to the observation error  $\varepsilon^{(o)}$  (equation 3). In the case of  
823 the NODE approximation, they correspond to the process error  $\varepsilon^{(p)}$  (equation 7).  $I$  is the number  
824 of data points, either observations in the case of the interpolation, or interpolated points in the case  
825 of the NODE fitting.

826 The prior probability density functions for the parameters are given by

$$p(\theta) = \prod_{j=1}^J \frac{1}{\sqrt{2\pi\delta_j^2}} \exp \left\{ -\frac{\theta_j^2}{2\delta_j^2} \right\} \quad (15)$$

827 where  $J$  is the number of parameters in the models. The parameter  $\delta_j$  controls the dispersion of the  
828 priors, and thereby the complexity/level of constraint of the model.

829 Bayesian regularisation simply amounts to constraining the values of the parameters in the model  
830 to be close to a desired value. Usually, parameters are constrained by choosing normal priors  
831 centered about 0. In this case, the standard deviation of the normal priors governs the range of  
832 values that the parameters can take, and hence constrains more or less strongly the behaviour of the  
833 model (Cawley and Talbot 2007). There is no standard approach for choosing  $\delta$ . Low values of  
834 dispersion may increase constraint on parameters too drastically, which would lead to underfitting,  
835 and result in a reduction of the variance of parameter estimates and bias mean estimates towards  
836 0. In contrast, too high values of dispersion may lead to overfitting, by allowing for more complex  
837 shapes. To account for this, we optimise models on the second-level of inference. This means that  
838 we are finding the optimal value of  $\delta$ , in addition to optimising the model parameters.

839 In practice, choosing the level of constraint is difficult, Cawley and Talbot hence developed a  
840 criterion to perform model selection on the second level of inference. They proposed to optimise the  
841 marginal posterior distribution by averaging out the dispersion of the priors. With an appropriate  
842 choice of prior, the dispersion can be integrated out, leaving us with a formula for the posterior that  
843 only depends on the parameters of the model,

$$\log P(\theta|\mathcal{D}) \propto -\frac{I}{2} \log \left( \sum_{i=1}^I e_i(\mathcal{D}, \theta)^2 \right) - \frac{J}{2} \log \left( \sum_{j=1}^J \theta_j^2 \right) \quad (16)$$

844 where  $P(\theta|\mathcal{D})$  denotes the marginal posterior density,  $\mathcal{D}$  denotes the evidence,  $I$  and  $J$  denote  
845 the number of data points and parameters, respectively,  $e_i$  denote the residuals, and  $\theta$  denote the  
846 parameters of the model. The construction is elegant because it is not sensitive to the choice of  
847 prior hyperparameters, and simple as it amounts to optimising the log of the sum of squares, rather  
848 than the sum of squares (in the case of normal ordinary least square).

849 The issue with this formula is that the marginal posterior density is not finite when the parameters  
850 are 0, which leads to underfitting. In this paper we use a modified criterion, which corrects for that  
851 problem,

$$\log P(\theta|\mathcal{D}) \propto -\frac{I}{2} \log \left( 1 + \sum_{i=1}^I e_i(\mathcal{D}, \theta)^2 \right) - \frac{J}{2} \log \left( 1 + \sum_{j=1}^J \theta_j^2 \right) \quad (17)$$

852 where the marginal posterior density depends only on the residuals of the model when the parame-  
853 ters are equal to 0, and otherwise depends on both the parameters and the residuals. This construc-  
854 tion can be obtained simply by assuming a gamma prior for the parameters  $p(\xi) \propto \frac{1}{\xi} \exp\{-\xi\}$ ,  
855 where  $\xi$  is the regularisation parameter, instead of the improper Jeffreys' prior that Cawley and  
856 Talbot used in their original study, namely  $p(\xi) \propto \frac{1}{\xi}$ . The details of the integration of the posterior  
857 distribution over  $\xi$  can be found in Cawley and Talbot's original paper.

## B Complementary results benchmark analysis

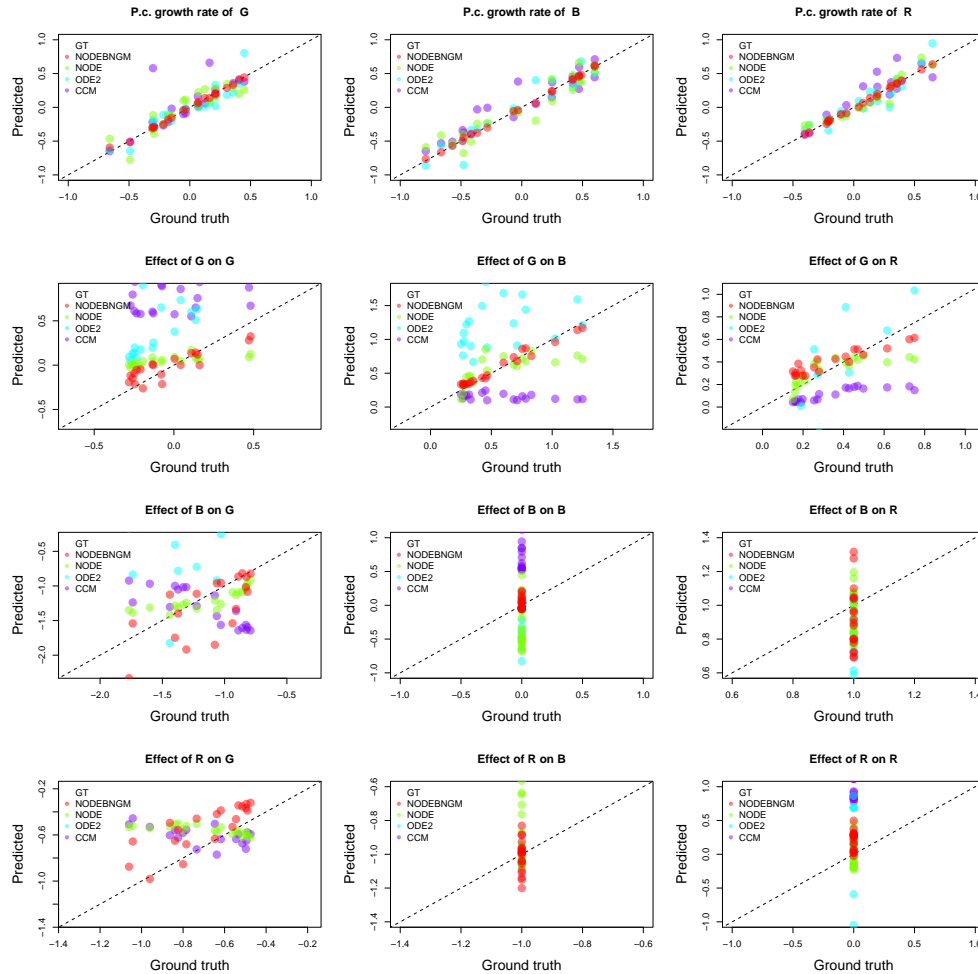


**Figure S1: Train set accuracy of predicted per-capita growth rates and effects estimated by NODEBNGM, standard NODEs, ODE2, and CCM.** The NODEBNGM method (nonparametric) involves fitting a NODE system by Bayesian neural gradient matching (BNGM). The NODE method (nonparametric) involves fitting a NODE system with an ODE solver. The ODE2 method (parametric) involves fitting an ODE system with quadratic functions of species densities with an ODE solver. The CCM method (nonparametric) involves computing locally linear approximations of the state space. For each method, we trained 30 models on the two first thirds of the artificial time series where ground truth is known (Fig. xxx). For each plot, the x-axis corresponds to the ground truth, known from the equations that generated the artificial time series, and the y-axis corresponds to the prediction of the best model. Effects are computed as the sensitivity (i.e. derivative) of the per-capita growth rate with respect to each species density G, B, and R, namely the prey, intermediate and top predator.

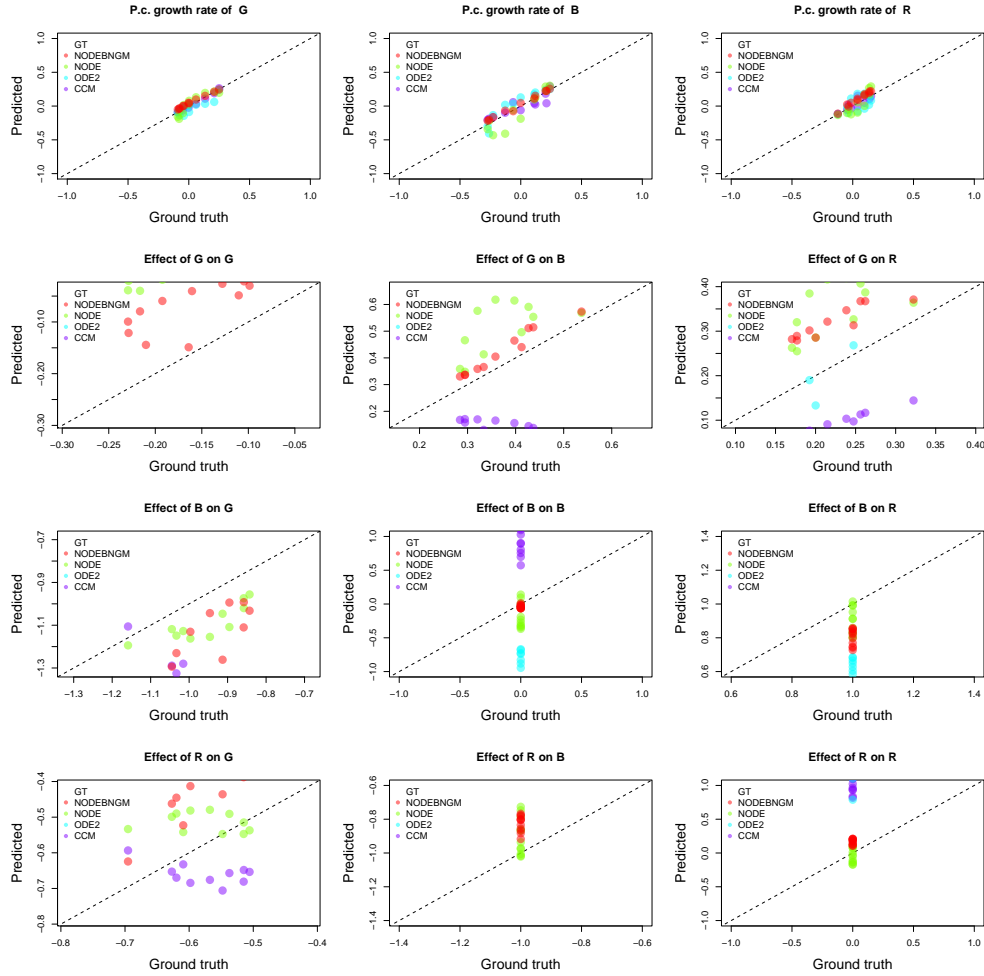


**Figure S2: Test set accuracy of predicted per-capita growth rates and effects estimated by NODEBNGM, standard NODEs, ODE2, and CCM.** The NODEBNGM method (nonparametric) involves fitting a NODE system by Bayesian neural gradient matching (BNGM). The NODE method (nonparametric) involves fitting a NODE system with an ODE solver. The ODE2 method (parametric) involves fitting an ODE system with quadratic functions of species densities with an ODE solver. The CCM method (nonparametric) involves computing locally linear approximations of the state space. For each method, we trained 30 models on the two first thirds of the artificial time series where ground truth is known (Fig. xxx). For each plot, the x-axis corresponds to the ground truth, known from the equations that generated the artificial time series, and the y-axis corresponds to the prediction of the best model. Effects are computed as the sensitivity (i.e. derivative) of the per-capita growth rate with respect to each species density G, B, and R, namely the prey, intermediate and top predator.

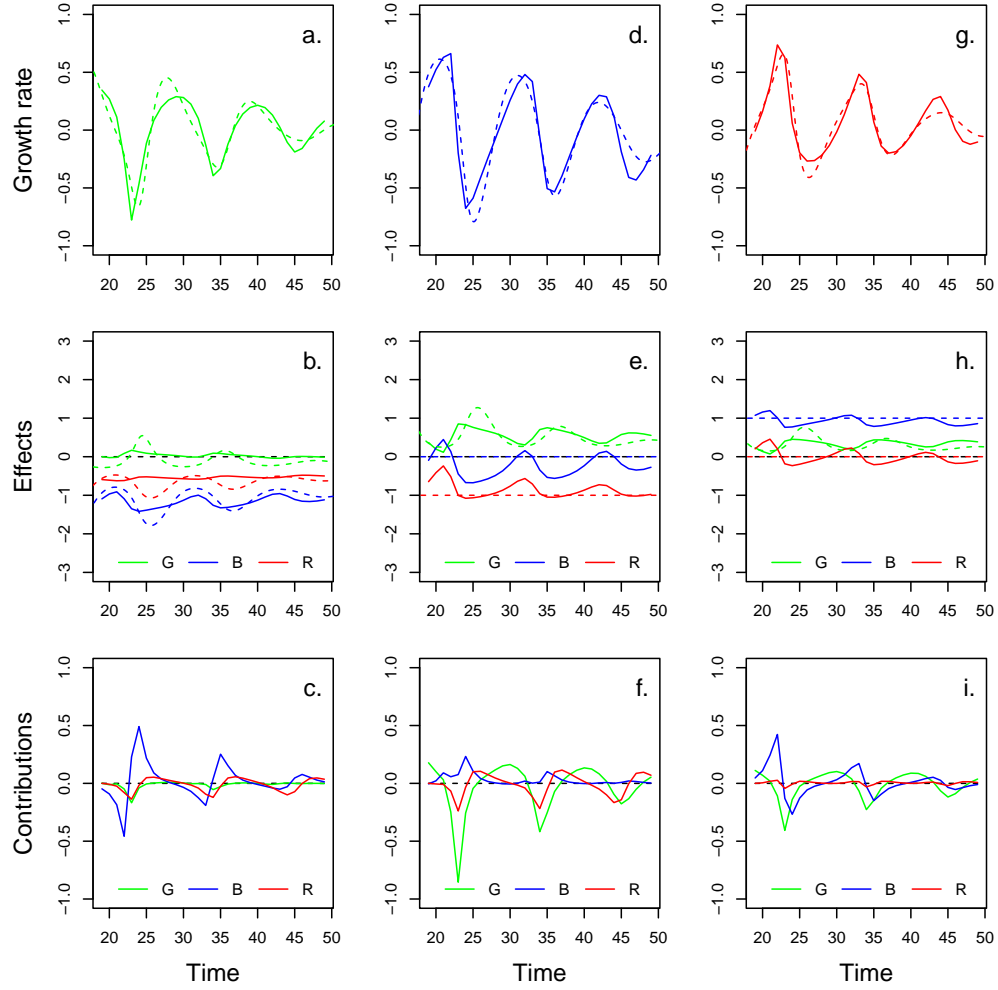


**Figure S3: Effects and contributions inferred by standard NODEs.** The standard NODE model nonparametrically approximates the per-capita growth rate of the 3 species with an ANN featuring a single layer, 3 input nodes, 10 hidden nodes, 3 outputs. 30 models are fitted to the two first third of the time series using BFGS and a runge-kutta ODE solver. The graphs present the predictions obtained for the model that maximises posterior density of the network parameters given the time series. We estimate the direction of ecological interactions (effects) by computing the derivative of the per-capita growth rate approximations with respect to each density. Finally, we compute the strength of ecological interactions (contributions) by multiplying the interpolated dynamics of each population with its effects.

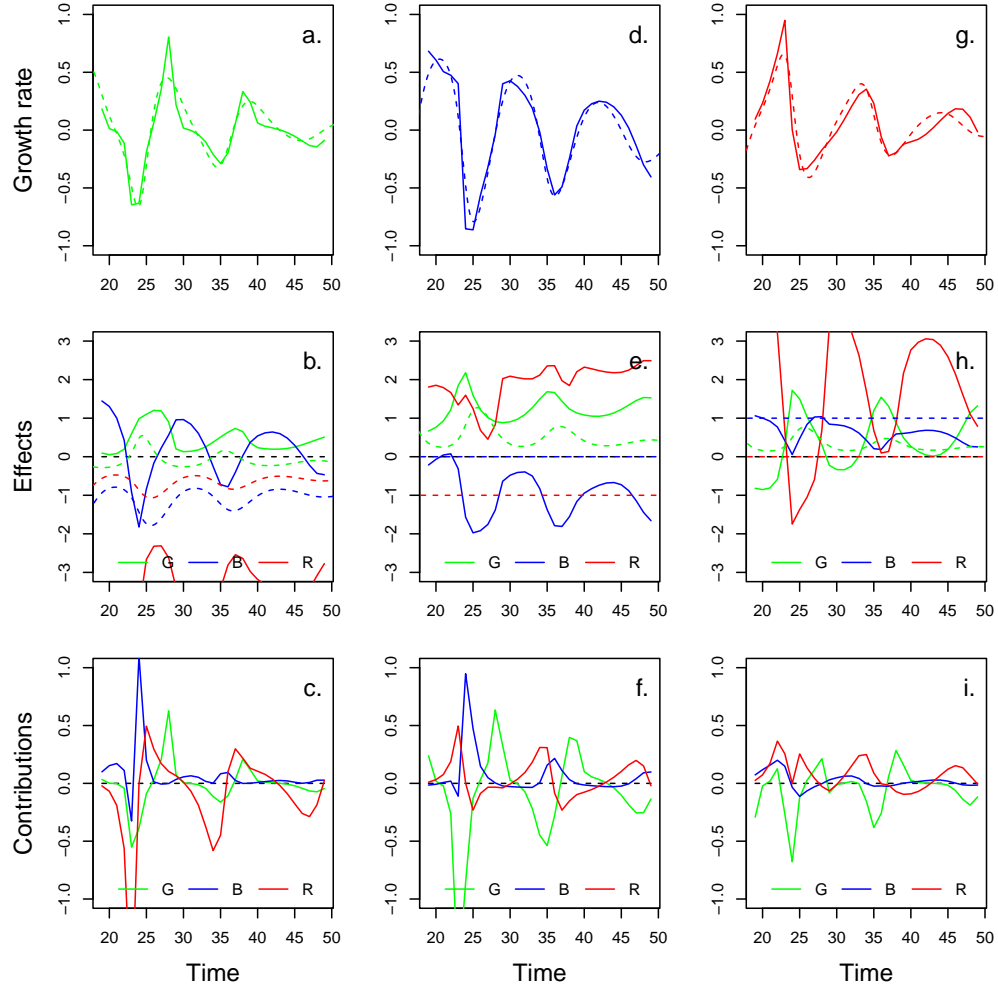


**Figure S4: Effects and contributions inferred by parametric ODE.** The ODE2 model parametrically approximates the per-capita growth rate of the 3 species with second order polynomial functions. 30 models are fitted to the two first third of the time series using BFGS and a runge-kutta ODE solver. The graphs present the predictions obtained for the model that maximises posterior density of the network parameters given the time series. We estimate the direction of ecological interactions (effects) by computing the derivative of the per-capita growth rate approximations with respect to each density. Finally, we compute the strength of ecological interactions (contributions) by multiplying the interpolated dynamics of each population with its effects.

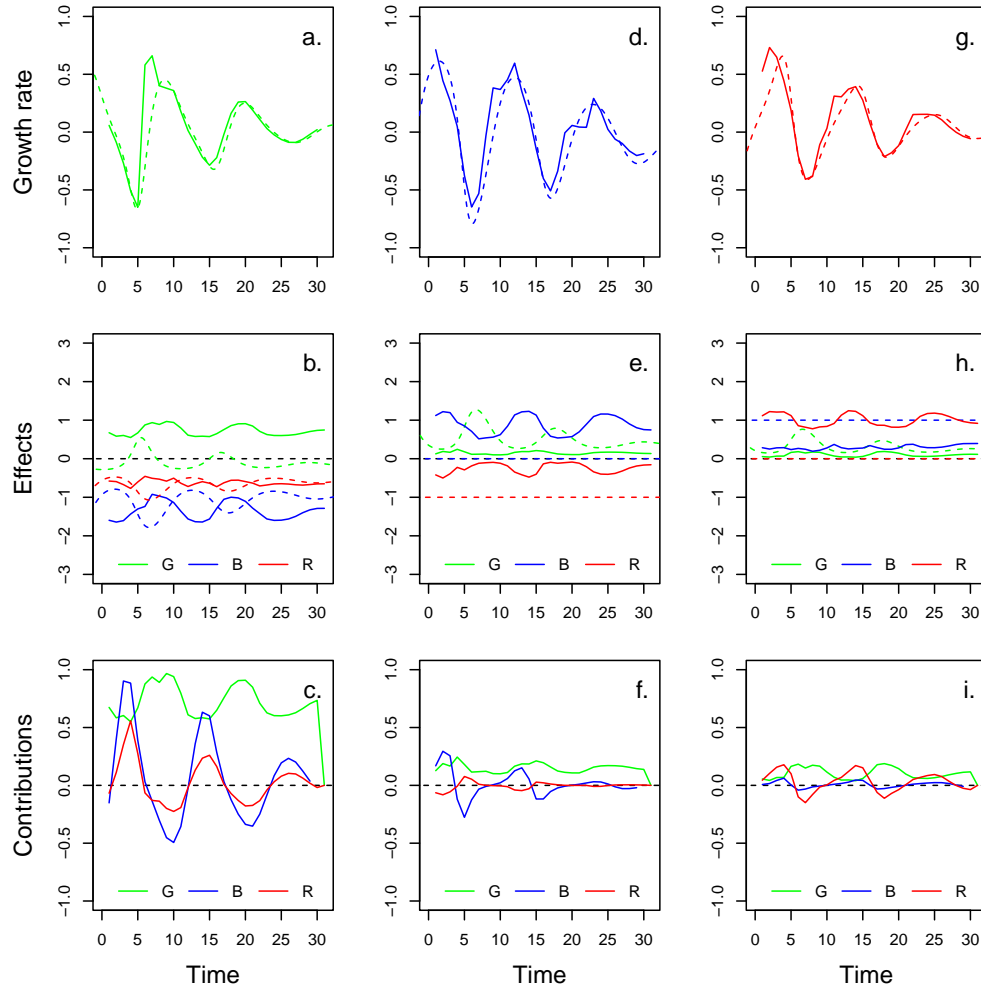


**Figure S5: Effects and contributions inferred by CCM.** The CCM method nonparametrically approximates the state space from which it derives the sensitivity of population dynamics to a change in the density of the species. We use the rEDM implementation and derived our code from the three species example provided in the package tutorial. We calculated the dynamics and per capita growth rate using finite differences, as the standard library does not readily provide estimates. The effects correspond to the s-map coefficients. Finally, we compute the strength of ecological interactions (contributions) by multiplying the interpolated dynamics of each population with its effects.



## C Complementary results case study 2 replicate A

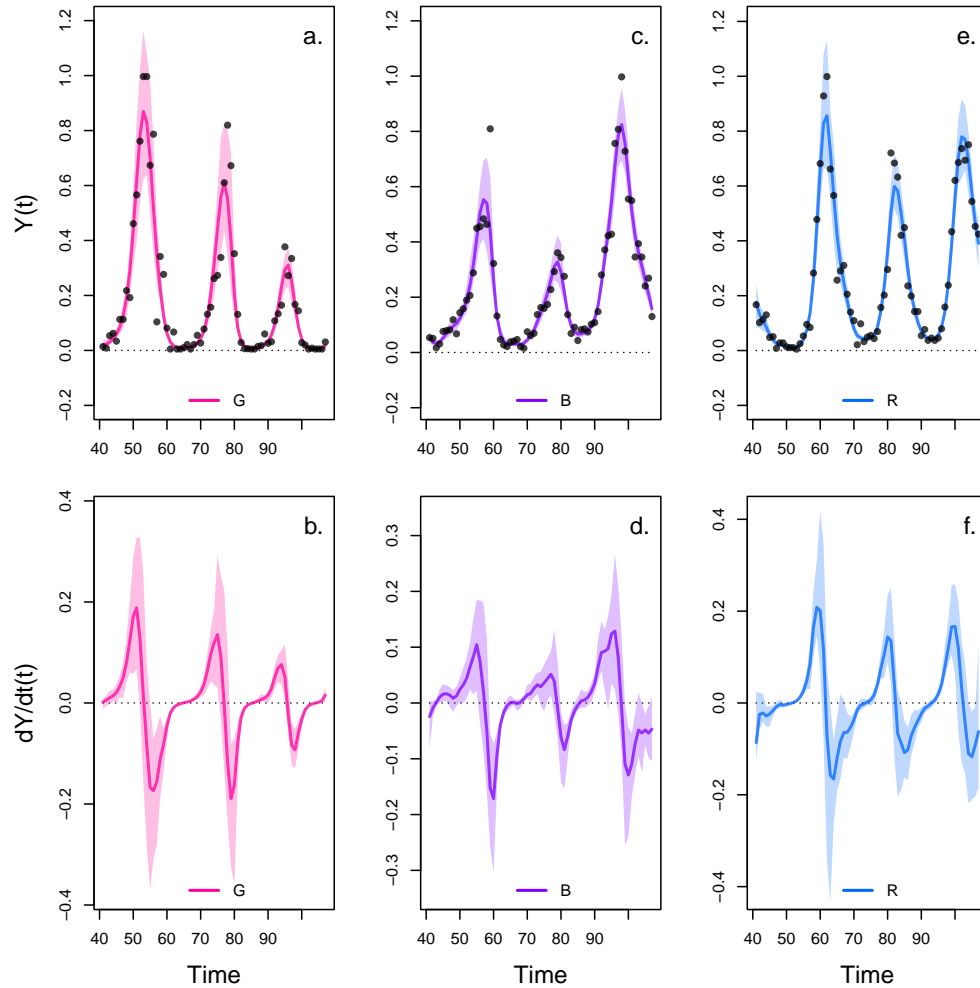


**Figure S6: Interpolation of state and dynamics of algae, flagellate, and rotifer density in replicate A.** Graph a., c., and e. display the neural interpolation of the population density of algae (G), flagellate (B), and rotifer (R), respectively (obtained with Eq. 7). Graph b., d., and f. show the corresponding interpolated dynamics, obtained by differentiating the interpolation of the states with respect to time (Eq. 5). The shaded areas represent the 90% confidence interval on estimates, obtained by anchored ensembling of the log marginal posterior distribution (Eq. 7) (Pearce et al. 2018). Time series are obtained from digitising the time series in Hiltunen et al. 2013.

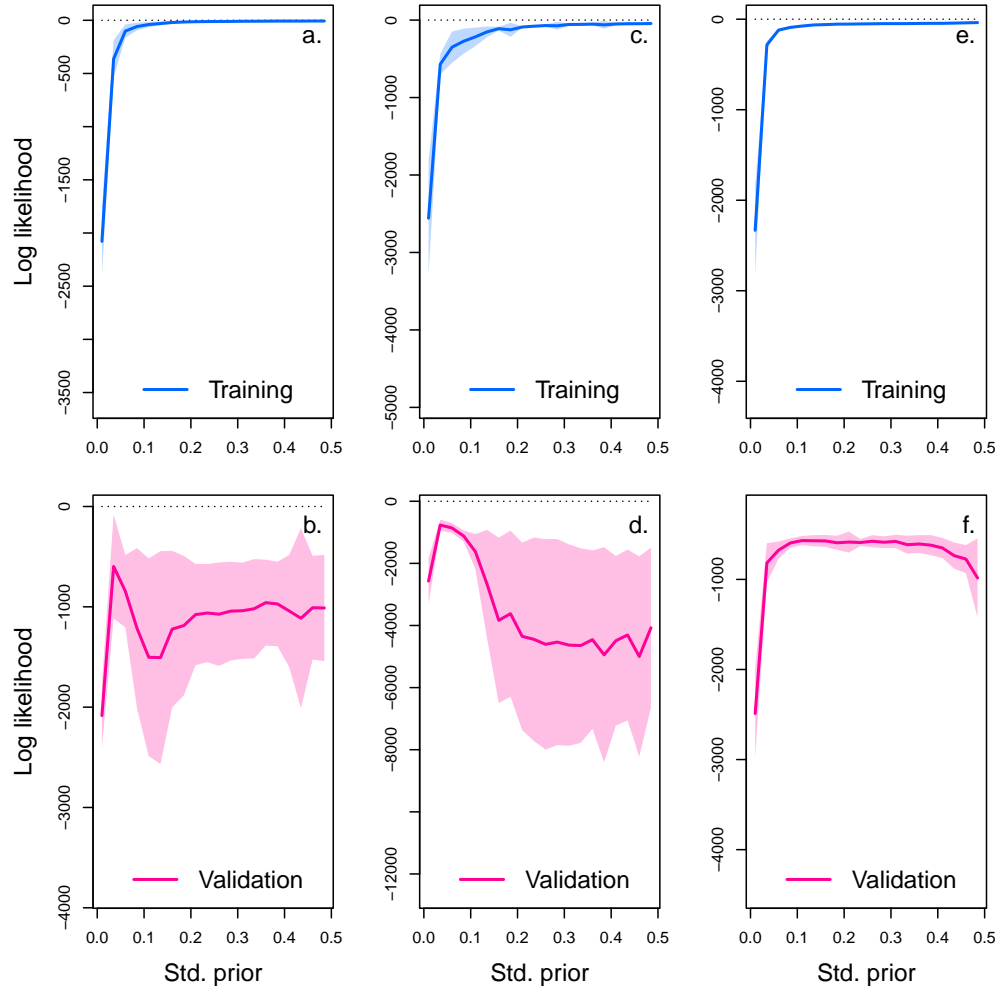


**Figure S7: Cross-validation plot of the NODE analysis of replicate A.** The x-axis of the graphs correspond to the standard deviation of the prior distribution of the NODE parameters, which constrains the nonlinearity of the nonparametric approximation of the NODEs. Small values of standard deviation correspond to a linear model, while higher values (towards 0.5) correspond to a highly nonlinear model. Time series of algae, flagellate, and rotifer are split in half to create a train set and a test set. The model is fitted to the train set for increasing value of standard deviation (from 0.05 to 0.5 by 0.05 increments), and evaluated on the test set. Graph a., c., and e. show the log likelihood of the NODE system fitted by BNGM to the train set of algae, flagellate, and rotifer, respectively. Graph b., d., and f. show the log likelihood of the fitted NODE, evaluated on the corresponding test set. The shaded areas represent the 90% confidence interval on estimates, obtained by anchored ensembling of the log marginal posterior distribution (Eq. 7) (Pearce et al. 2018).

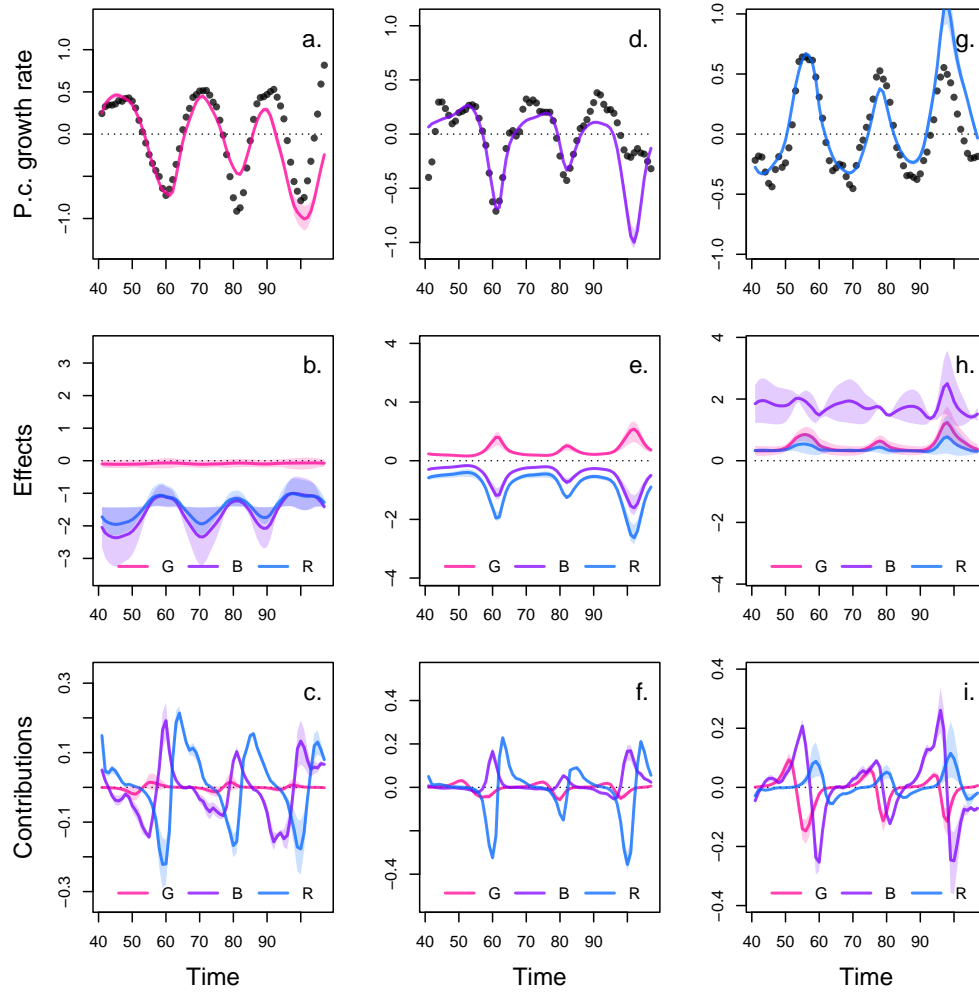


**Figure S8: Drivers of dynamics of algae, flagellate, and rotifer in replicate A.** This figure displays the NODE nonparametric approximations of the per-capita growth rate of algae (a., b., c.), flagellate (d., e., f.), and rotifer (g., h., i.). We obtain the NODE approximations (a., d., g., solid line) by fitting the interpolated per-capita growth rates (black dots) with ANNs that take population densities as input. We then estimate the direction of ecological interactions (effects, b., e., h.) by computing the derivative of the NODE approximations with respect to each density. Finally, we compute the strength of ecological interactions (contributions, c., f., i.) by multiplying the interpolated dynamics of each population with its effects. The shaded area shows the 90% confidence interval, obtained by approximately sampling the posterior distributions. The replicated time series were obtained by digitising the time series in Hiltunen et al. (2013).

## D Complementary results case study 2 replicate B

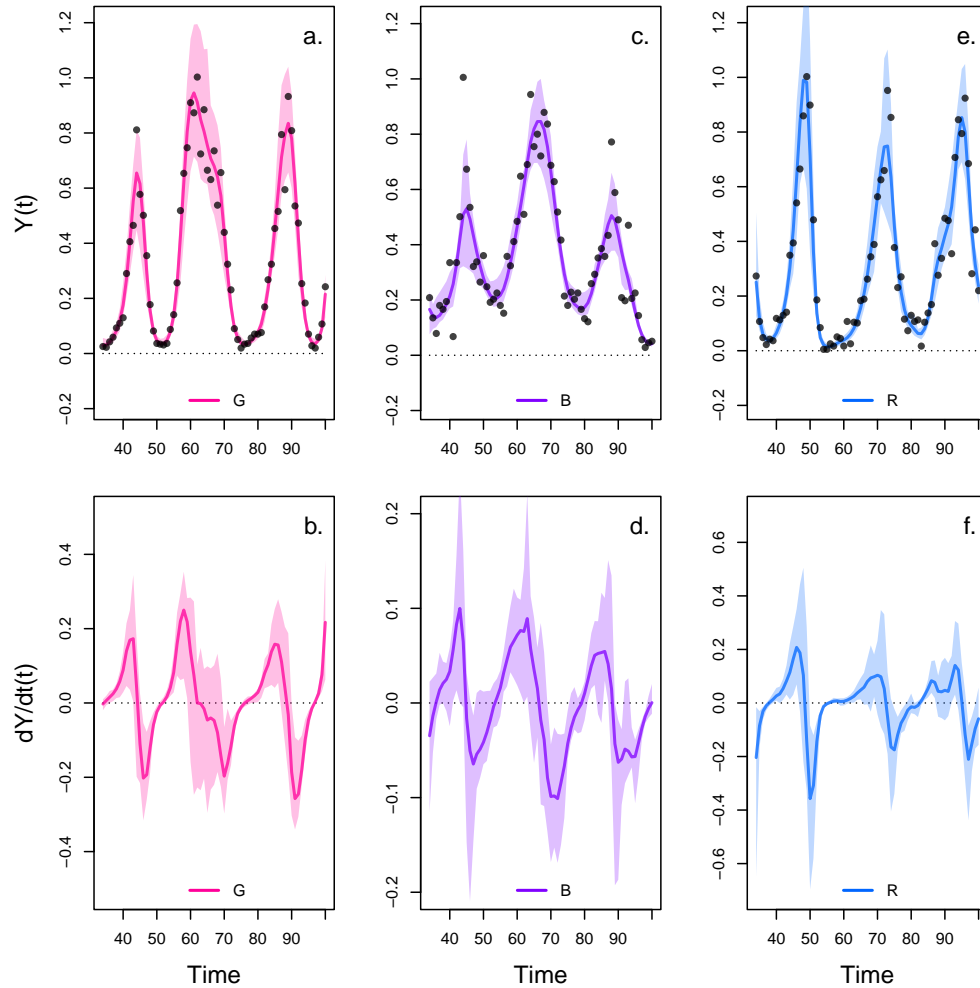


**Figure S9: Interpolation of state and dynamics of algae, flagellate, and rotifer density in replicate B.** Graph a., c., and e. display the neural interpolation of the population density of algae (G), flagellate (B), and rotifer (R), respectively (obtained with Eq. 7). Graph b., d., and f. show the corresponding interpolated dynamics, obtained by differentiating the interpolation of the states with respect to time (Eq. 5). The shaded areas represent the 90% confidence interval on estimates, obtained by anchored ensembling of the log marginal posterior distribution (Eq. 7) (Pearce et al. 2018). Time series are obtained from digitising the time series in Hiltunen et al. 2013.

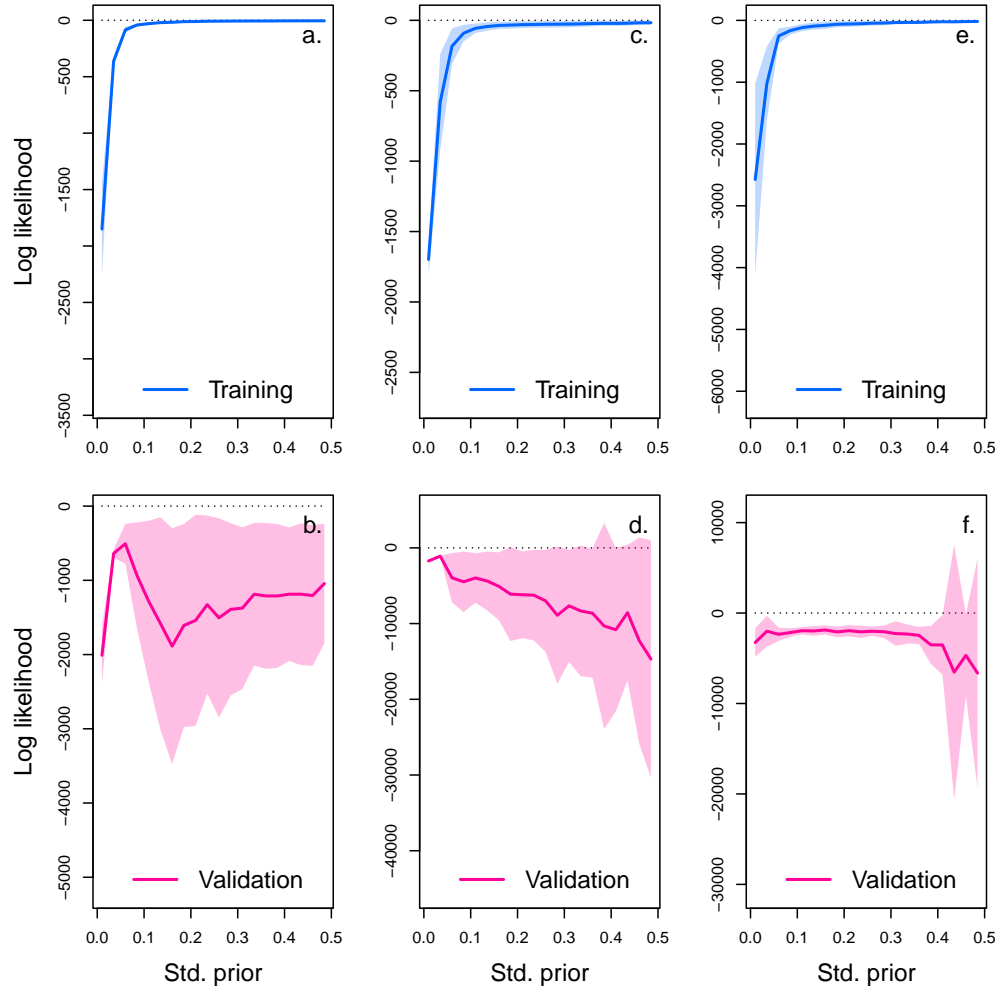


**Figure S10: Cross-validation plot of the NODE analysis of replicate B.** The x-axis of the graphs correspond to the standard deviation of the prior distribution of the NODE parameters, which constrains the nonlinearity of the nonparametric approximation of the NODEs. Small values of standard deviation correspond to a linear model, while higher values (towards 0.5) correspond to a highly nonlinear model. Time series of algae, flagellate, and rotifer are split in half to create a train set and a test set. The model is fitted to the train set for increasing value of standard deviation (from 0.05 to 0.5 by 0.05 increments), and evaluated on the test set. Graph a., c., and e. show the log likelihood of the NODE system fitted by BNGM to the train set of algae, flagellate, and rotifer, respectively. Graph b., d., and f. show the log likelihood of the fitted NODE, evaluated on the corresponding test set. The shaded areas represent the 90% confidence interval on estimates, obtained by anchored ensembling of the log marginal posterior distribution (Eq. 7) (Pearce et al. 2018).

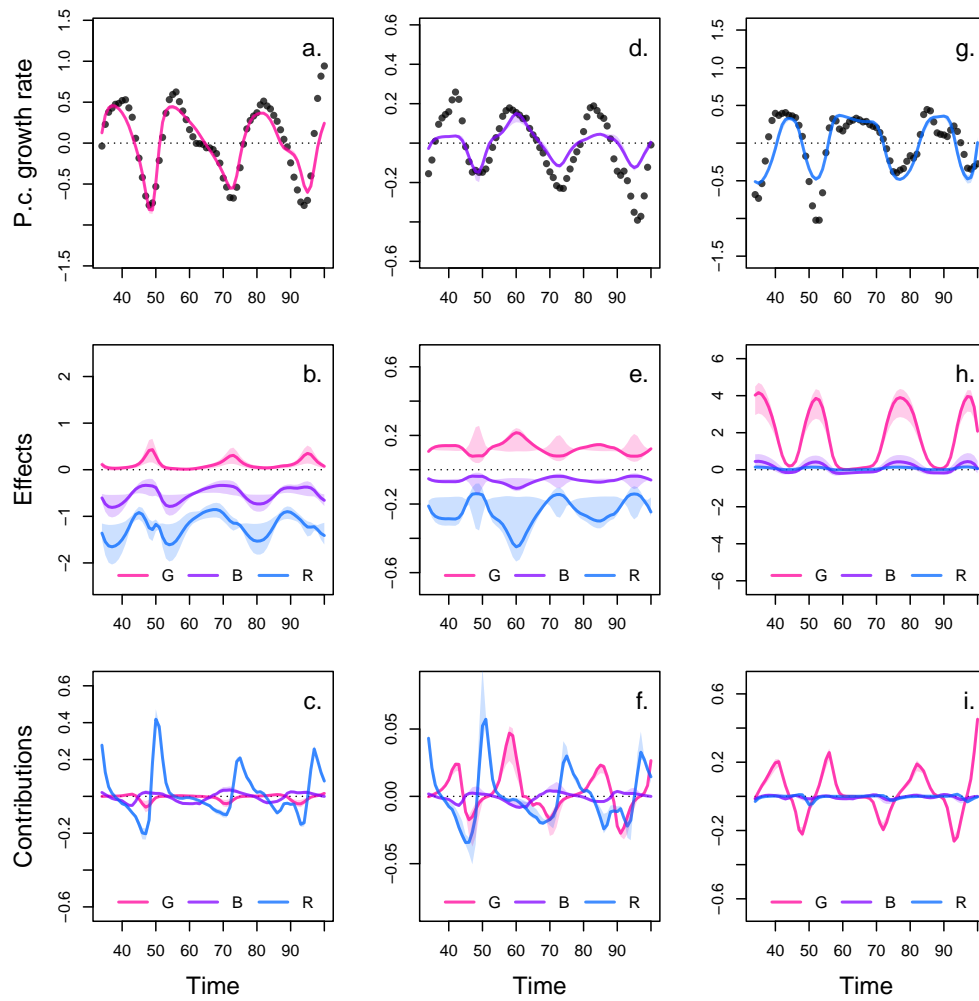


**Figure S11: Drivers of dynamics of algae, flagellate, and rotifer in replicate B.** This figure displays the NODE nonparametric approximations of the per-capita growth rate of algae (a., b., c.), flagellate (d., e., f.), and rotifer (g., h., i.). We obtain the NODE approximations (a., d., g., solid line) by fitting the interpolated per-capita growth rates (black dots) with ANNs that take population densities as input. We then estimate the direction of ecological interactions (effects, b., e., h.) by computing the derivative of the NODE approximations with respect to each density. Finally, we compute the strength of ecological interactions (contributions, c., f., i.) by multiplying the interpolated dynamics of each population with its effects. The shaded area shows the 90% confidence interval, obtained by approximately sampling the posterior distributions. The replicated time series were obtained by digitising the time series in Hiltunen et al. (2013).

## E Complementary results case study 2 replicate C

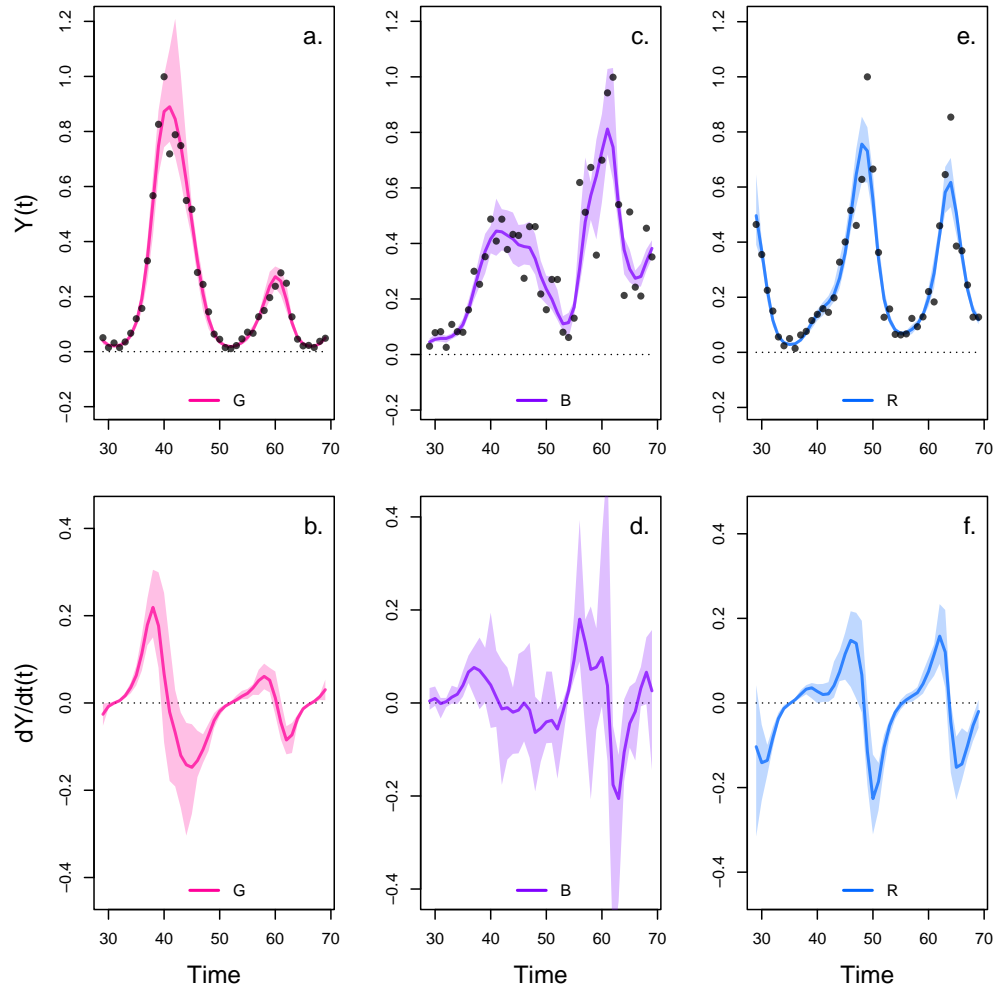


**Figure S12: Interpolation of state and dynamics of algae, flagellate, and rotifer density in replicate B.** Graph a., c., and e. display the neural interpolation of the population density of algae (G), flagellate (B), and rotifer (R), respectively (obtained with Eq. 7). Graph b., d., and f. show the corresponding interpolated dynamics, obtained by differentiating the interpolation of the states with respect to time (Eq. 5). The shaded areas represent the 90% confidence interval on estimates, obtained by anchored ensembling of the log marginal posterior distribution (Eq. 7) (Pearce et al. 2018). Time series are obtained from digitising the time series in Hiltunen et al. 2013.

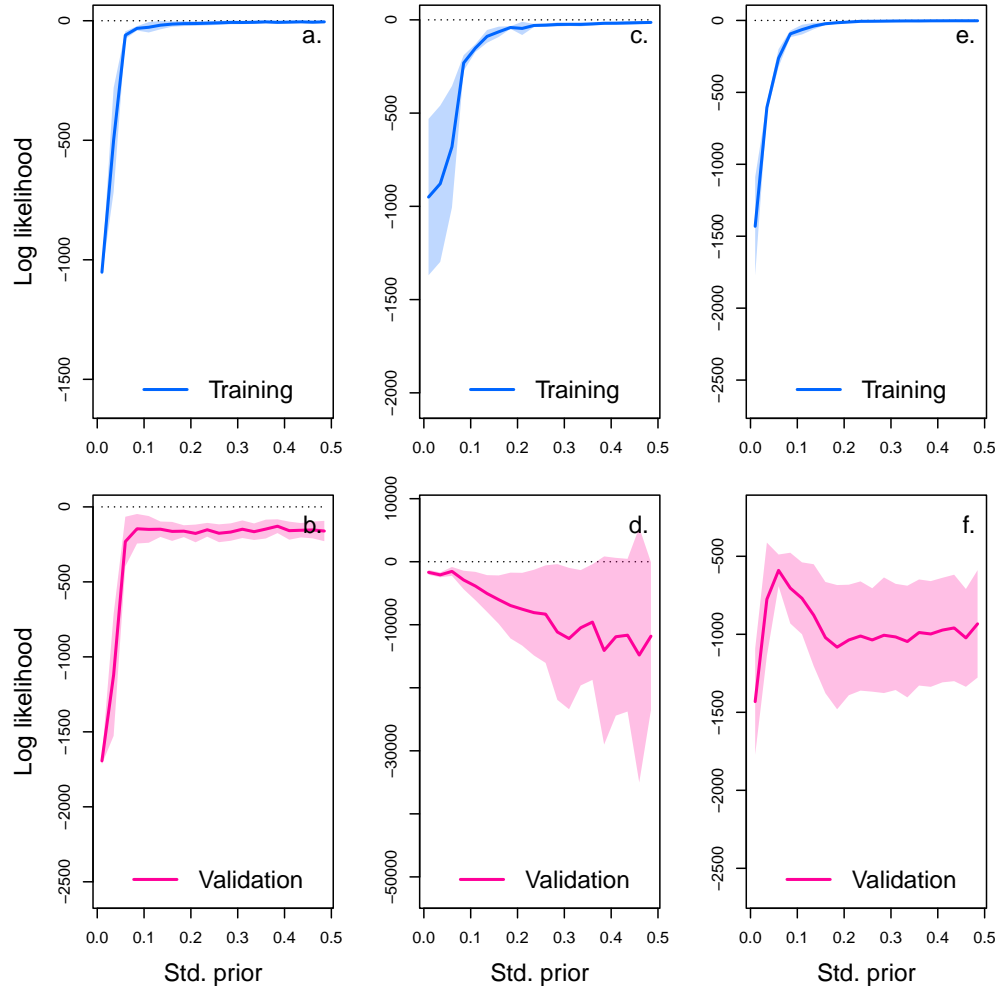


**Figure S13: Cross-validation plot of the NODE analysis of replicate C.** The x-axis of the graphs correspond to the standard deviation of the prior distribution of the NODE parameters, which constrains the nonlinearity of the nonparametric approximation of the NODEs. Small values of standard deviation correspond to a linear model, while higher values (towards 0.5) correspond to a highly nonlinear model. Time series of algae, flagellate, and rotifer are split in half to create a train set and a test set. The model is fitted to the train set for increasing value of standard deviation (from 0.05 to 0.5 by 0.05 increments), and evaluated on the test set. Graph a., c., and e. show the log likelihood of the NODE system fitted by BNGM to the train set of algae, flagellate, and rotifer, respectively. Graph b., d., and f. show the log likelihood of the fitted NODE, evaluated on the corresponding test set. The shaded areas represent the 90% confidence interval on estimates, obtained by anchored ensembling of the log marginal posterior distribution (Eq. 7) (Pearce et al. 2018).



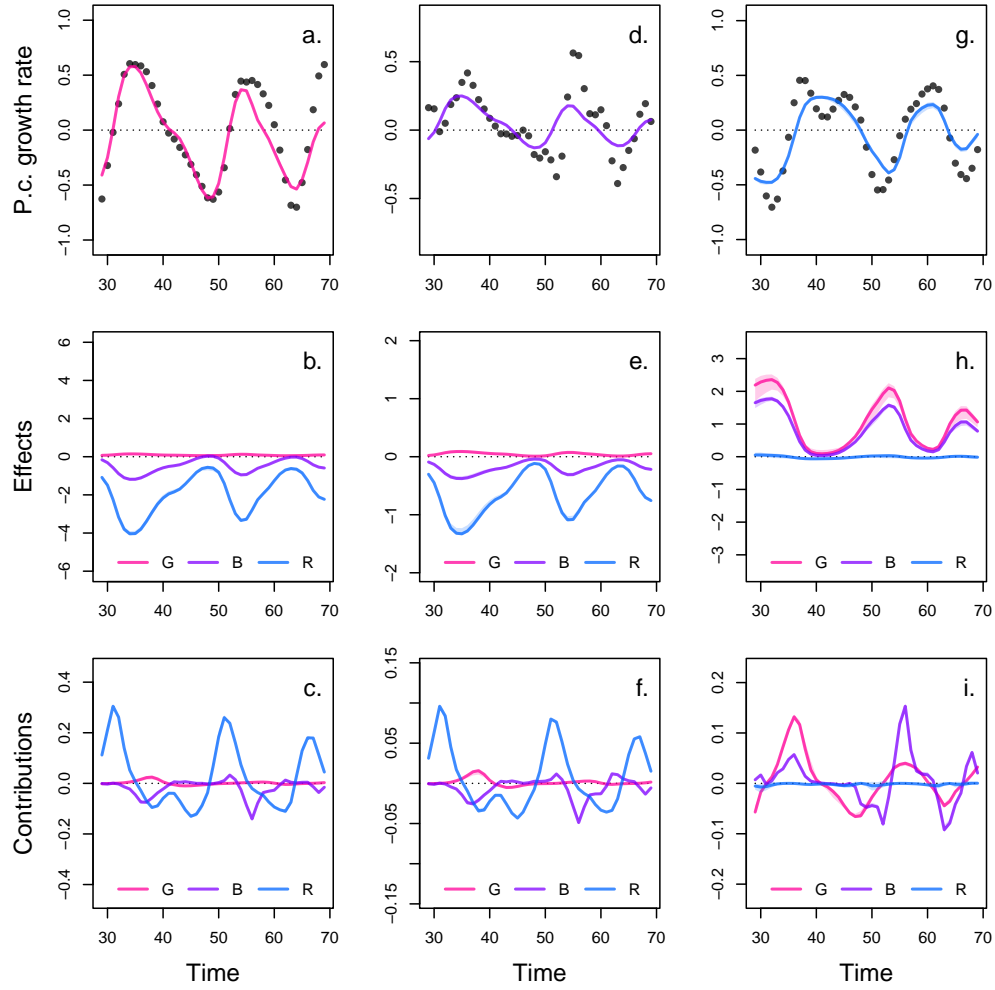


**Figure S14: Drivers of dynamics of algae, flagellate, and rotifer in replicate C.** This figure displays the NODE nonparametric approximations of the per-capita growth rate of algae (a., b., c.), flagellate (d., e., f.), and rotifer (g., h., i.). We obtain the NODE approximations (a., d., g., solid line) by fitting the interpolated per-capita growth rates (black dots) with ANNs that take population densities as input. We then estimate the direction of ecological interactions (effects, b., e., h.) by computing the derivative of the NODE approximations with respect to each density. Finally, we compute the strength of ecological interactions (contributions, c., f., i.) by multiplying the interpolated dynamics of each population with its effects. The shaded area shows the 90% confidence interval, obtained by approximately sampling the posterior distributions. The replicated time series were obtained by digitising the time series in Hiltunen et al. (2013).

## F Complementary results case study 3

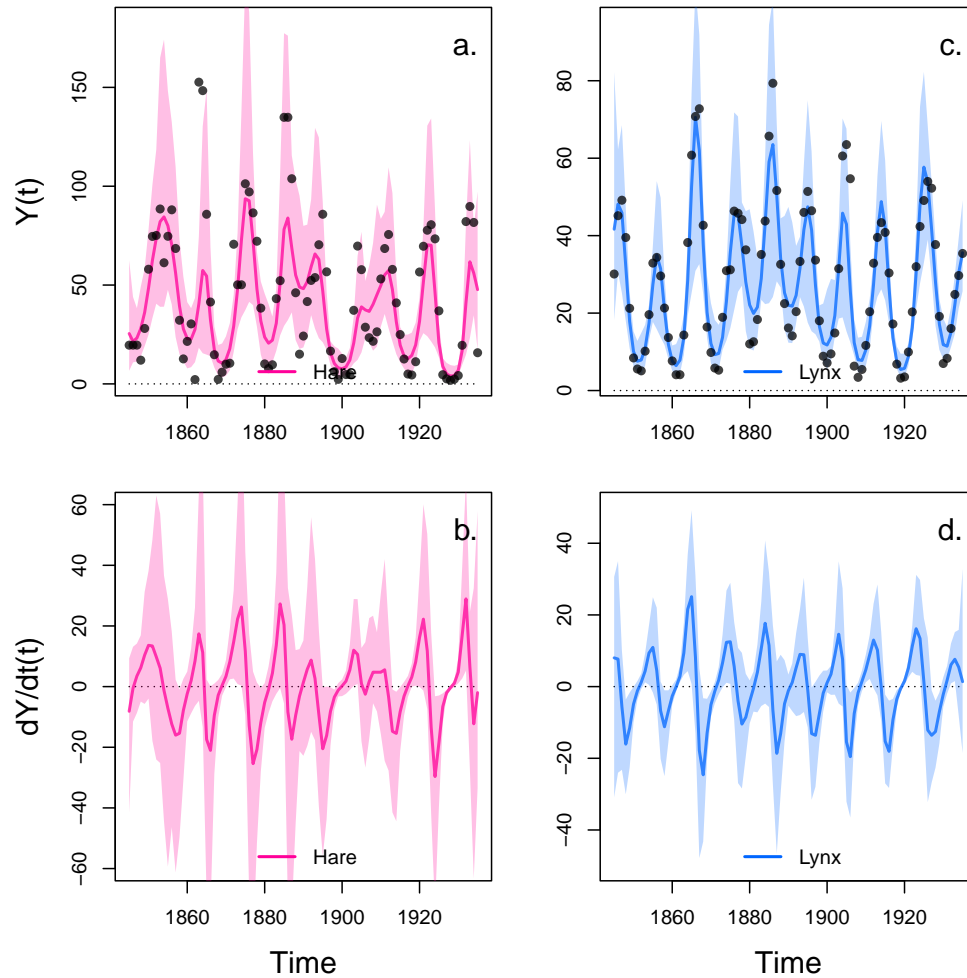


**Figure S15: Interpolation of state and dynamics of hare and lynx.** Graph a. and c. display the neural interpolation of the population density of hare and lynx respectively (obtained with Eq. 7). Graph b. and d. show the corresponding interpolated dynamics, obtained by differentiating the interpolation of the states with respect to time (Eq. 5). The shaded areas represent the 90% confidence interval on estimates, obtained by anchored ensembling of the log marginal posterior distribution (Eq. 7) (Pearce et al. 2018). Time series are obtained from Bonnaffé, Sheldon, and Coulson 2021, originally from Odum and Barrett 1972.

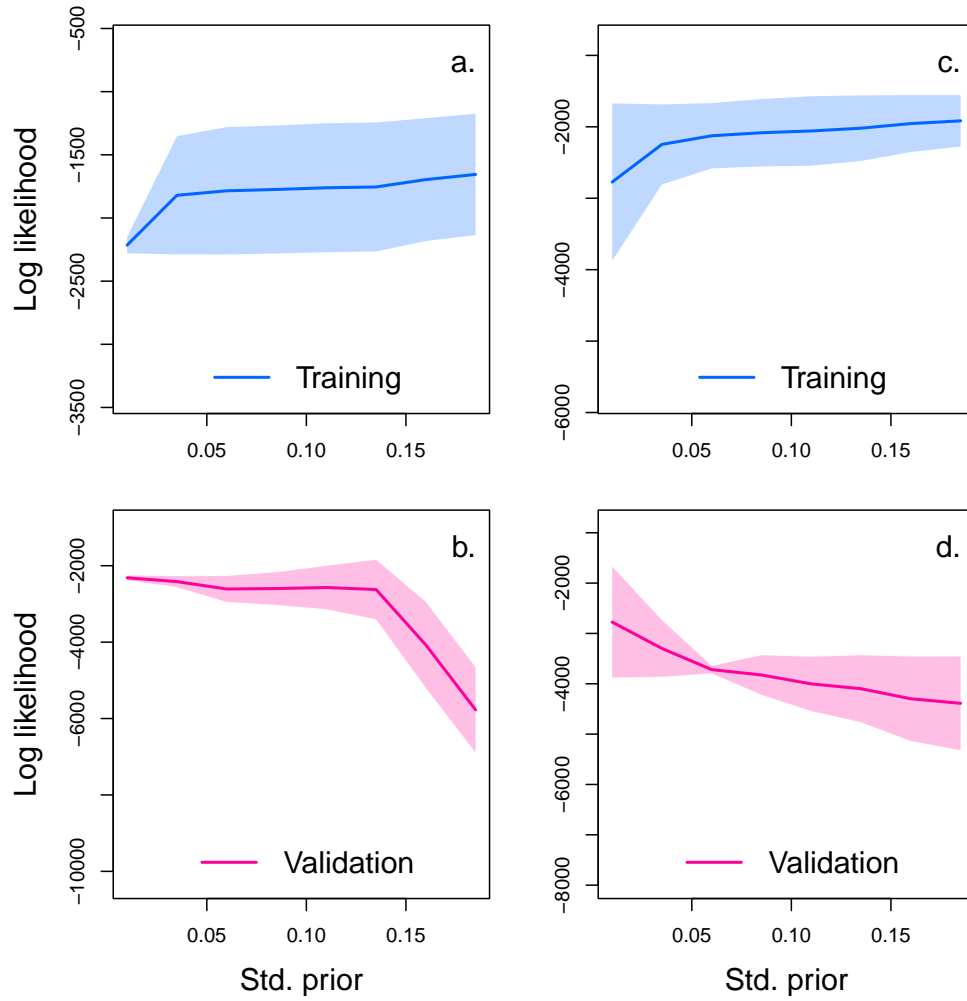


**Figure S16: Cross-validation plot of the NODE analysis of the hare-lynx system.** The x-axis of the graphs correspond to the standard deviation of the prior distribution of the NODE parameters, which constrains the nonlinearity of the nonparametric approximation of the NODEs. Small values of standard deviation correspond to a linear model, while higher values (towards 0.5) correspond to a highly nonlinear model. Time series of algae, flagellate, and rotifer are split in half to create a train set and a test set. The model is fitted to the train set for increasing value of standard deviation (from 0.05 to 0.5 by 0.05 increments), and evaluated on the test set. Graph a., c., and e. show the log likelihood of the NODE system fitted by BNGM to the train set of algae, flagellate, and rotifer, respectively. Graph b., d., and f. show the log likelihood of the fitted NODE, evaluated on the corresponding test set. The shaded areas represent the 90% confidence interval on estimates, obtained by anchored ensembling of the log marginal posterior distribution (Eq. 7) (Pearce et al. 2018).

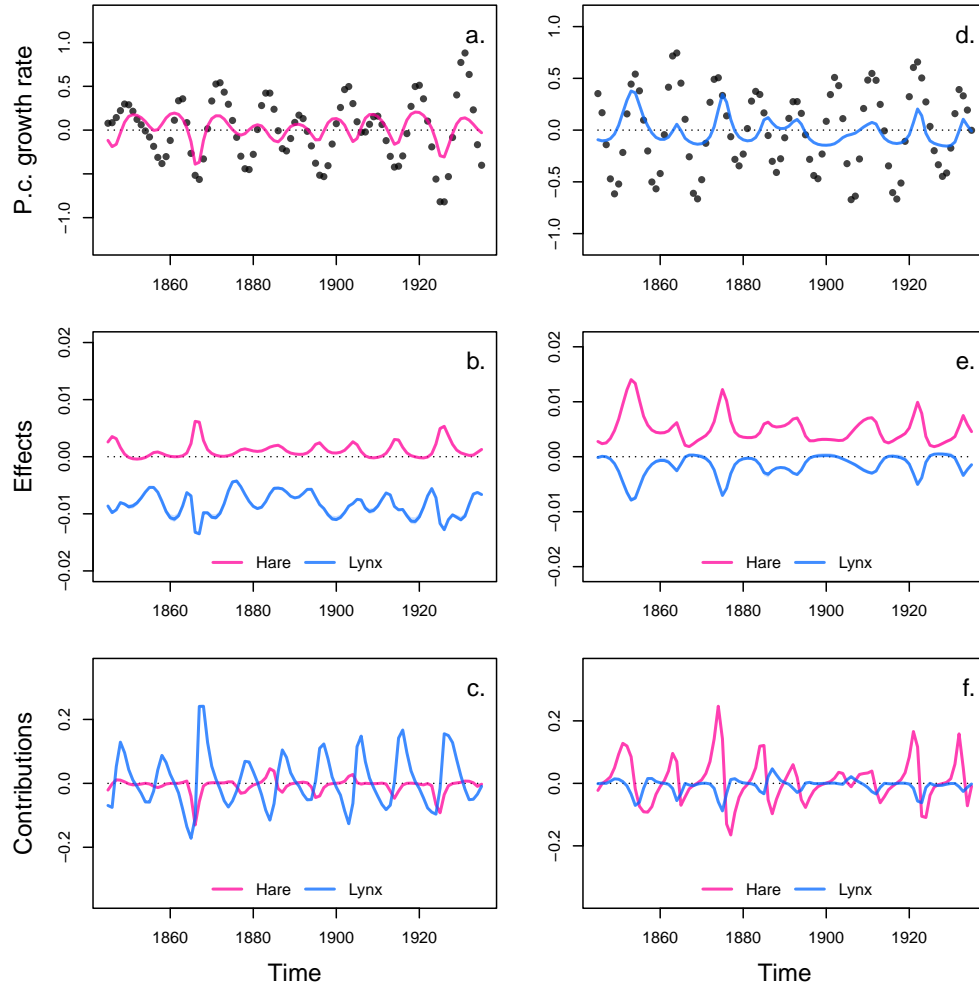


**Figure S17: Drivers of dynamics of hare and lynx in the Odum and Barrett pelt count time series.** This figure displays the NODE nonparametric approximations of the per-capita growth rate of hare (a., b., c.), and lynx (d., e., f.). We obtain the NODE approximations (a., d., solid line) by fitting the interpolated per-capita growth rates (black dots) with ANNs that take population densities as input. We then estimate the direction of ecological interactions (effects, b., e.) by computing the derivative of the NODE approximations with respect to each density. Finally, we compute the strength of ecological interactions (contributions, c., f.) by multiplying the interpolated dynamics of each population with its effects. The shaded area shows the 90% confidence interval, obtained by approximately sampling the posterior distributions.

## G Complementary results case study 4

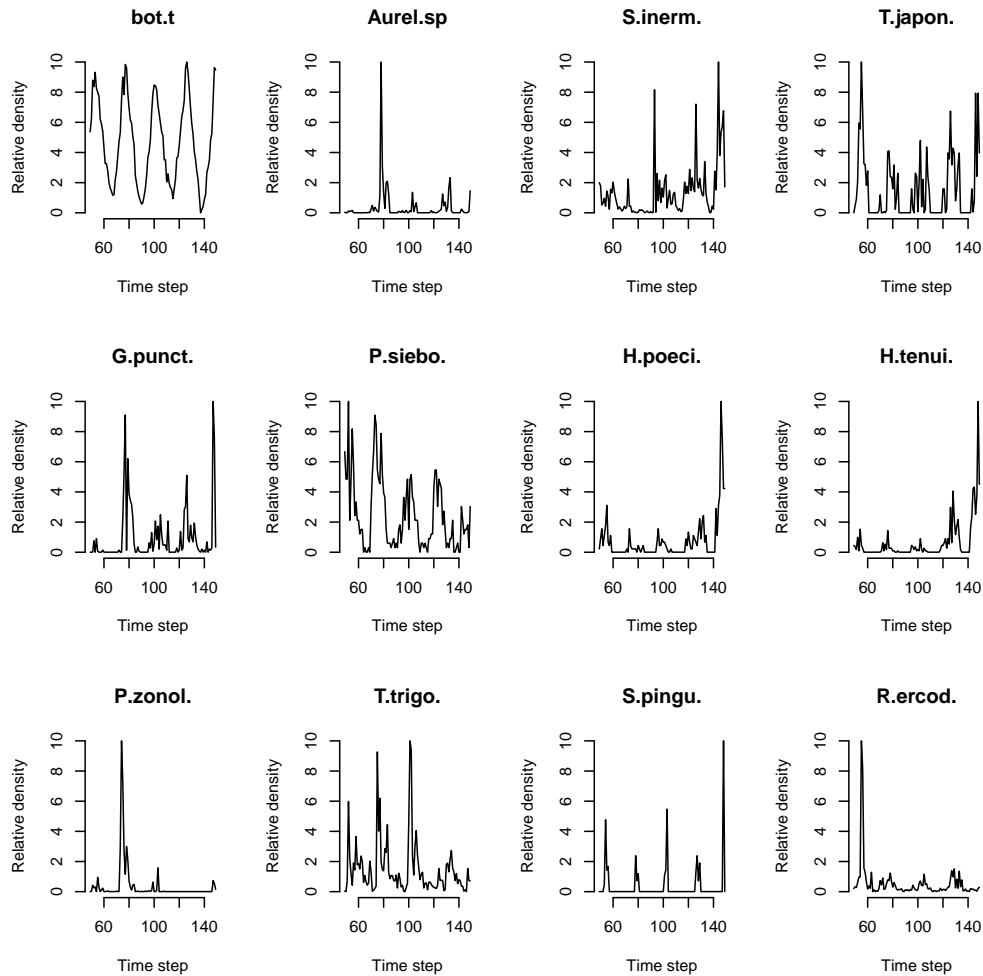


**Figure S18: Time series of the fish community in Ushio et al. 2018.** The time series was collected for 12-years on a fortnightly basis, for 15 dominant species in the Maizuru bay in Japan. We focus on the 11 species and the 100 time steps with the least sparse abundance records. Bot.t corresponds to water temperature near the bottom. The main species are *Aurelia sp.*, *Sebastes inermis*, *Trachurus japonicus*, *Girella punctata*, *Pseudolabrus sieboldi*, *Halichoeres poecilopterus*, *Halichoeres tenuispinnis*, *Pterogobius zonoleucus*, *Tridentiger trigonocephalus*, *Sphyrna pinniguis*, and *Rudarius ercodes*.

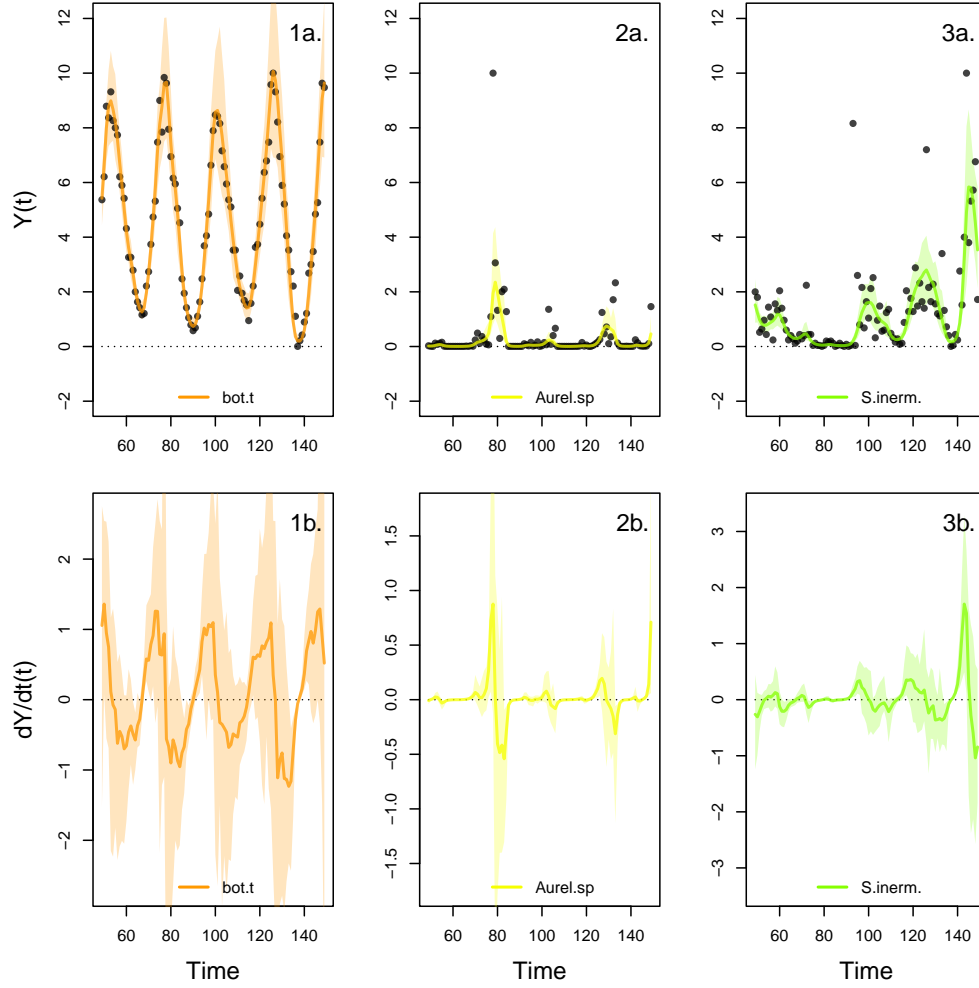


**Figure S19: Interpolation of state and dynamics of species abundance in the Maizuru bay community.** Graphs a. display the neural interpolations of the population density (obtained with Eq. 7). Graphs b. show the corresponding interpolated dynamics, obtained by differentiating the interpolation of the states with respect to time (Eq. 5). The shaded areas represent the 90% confidence interval on estimates, obtained by anchored ensembling of the log marginal posterior distribution (Eq. 7)

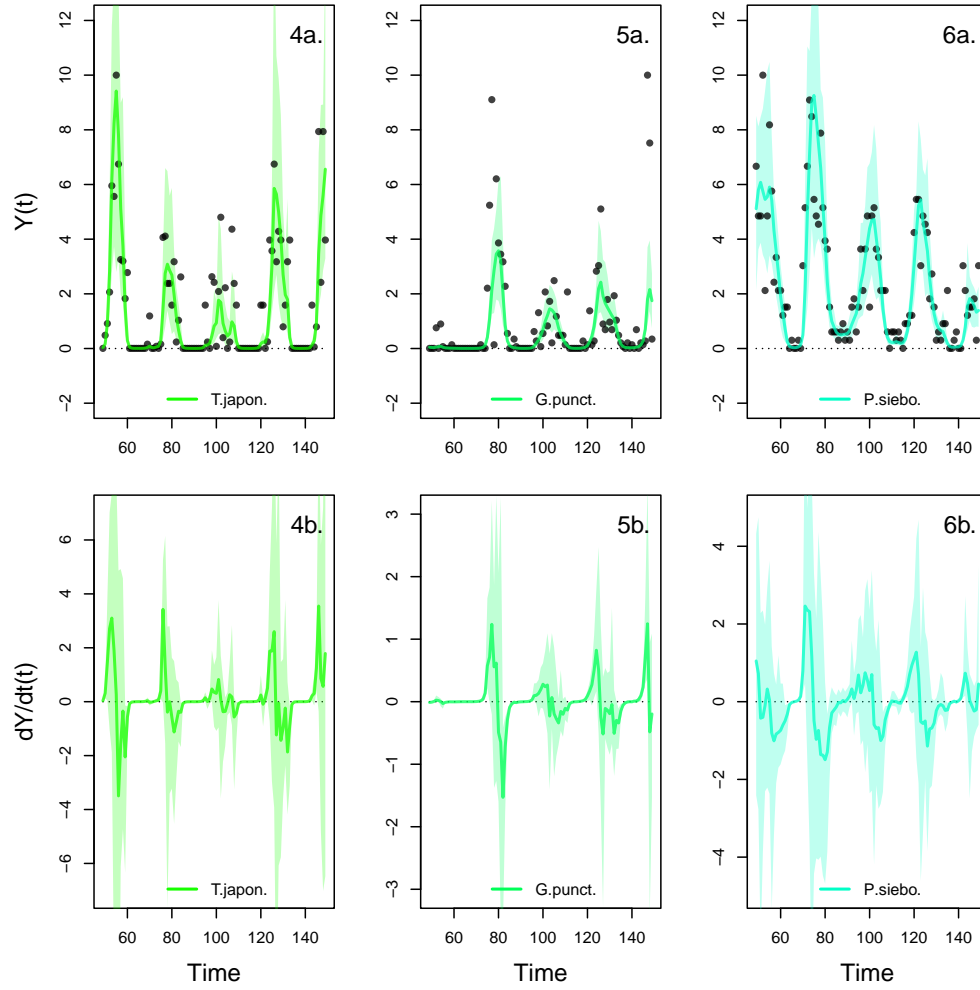


**Figure S20: Interpolation of state and dynamics of species abundance in the Maizuru bay community.** Graphs a. display the neural interpolations of the population density (obtained with Eq. 7). Graphs b. show the corresponding interpolated dynamics, obtained by differentiating the interpolation of the states with respect to time (Eq. 5). The shaded areas represent the 90% confidence interval on estimates, obtained by anchored ensembling of the log marginal posterior distribution (Eq. 7)

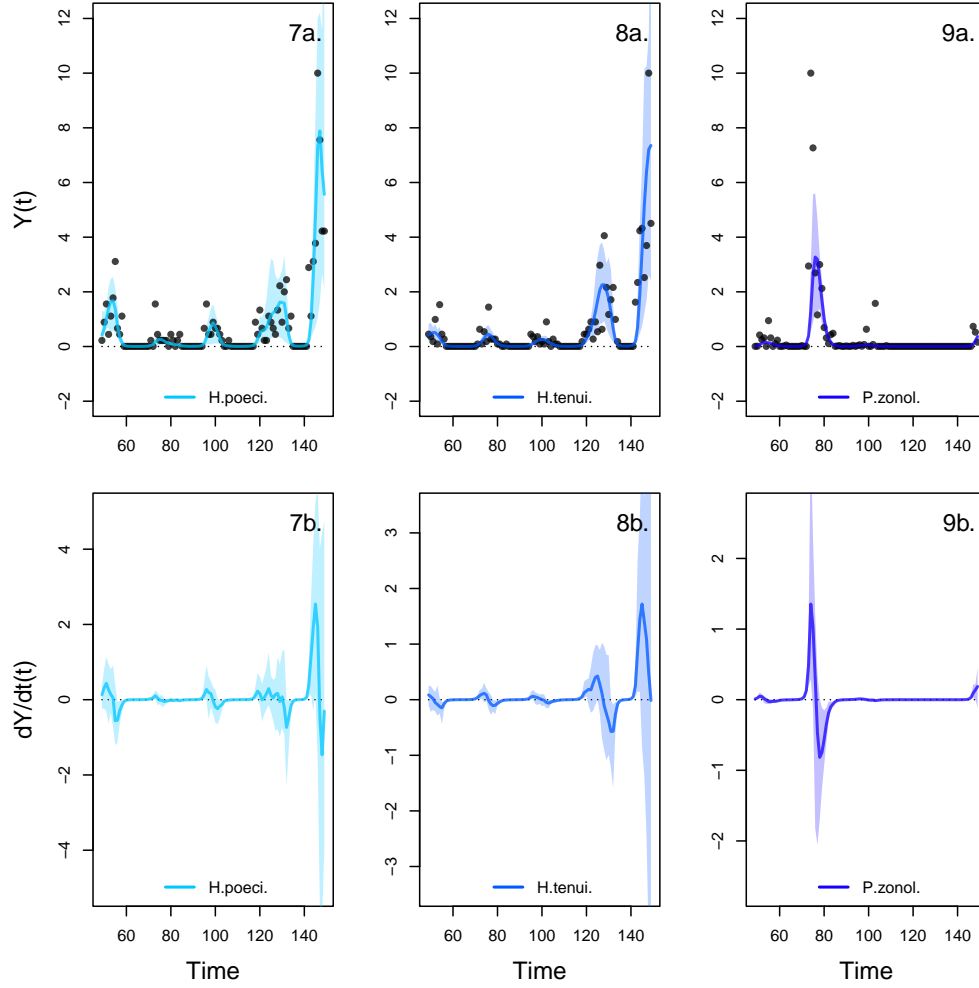


**Figure S21: Interpolation of state and dynamics of species abundance in the Maizuru bay community.** Graphs a. display the neural interpolations of the population density (obtained with Eq. 7). Graphs b. show the corresponding interpolated dynamics, obtained by differentiating the interpolation of the states with respect to time (Eq. 5). The shaded areas represent the 90% confidence interval on estimates, obtained by anchored ensembling of the log marginal posterior distribution (Eq. 7)



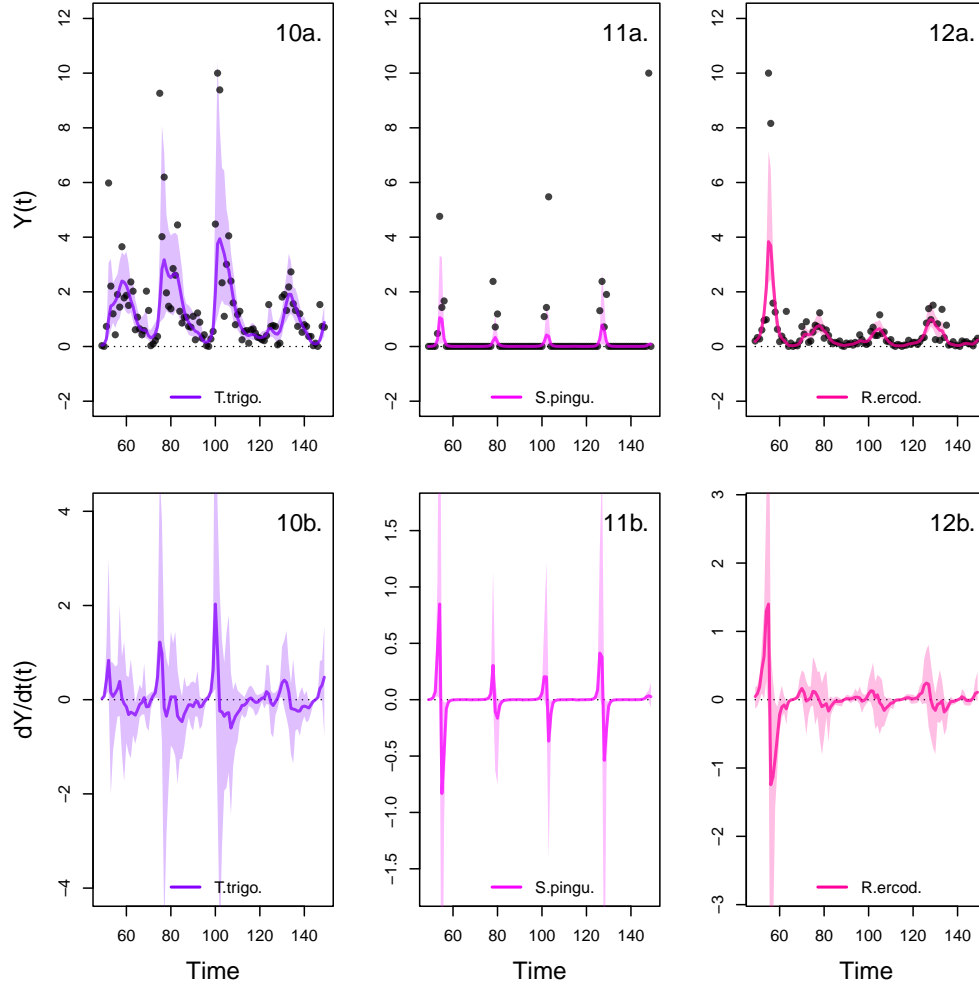


**Figure S22: Interpolation of state and dynamics of species abundance in the Maizuru bay community.** Graphs a. display the neural interpolations of the population density (obtained with Eq. 7). Graphs b. show the corresponding interpolated dynamics, obtained by differentiating the interpolation of the states with respect to time (Eq. 5). The shaded areas represent the 90% confidence interval on estimates, obtained by anchored ensembling of the log marginal posterior distribution (Eq. 7)

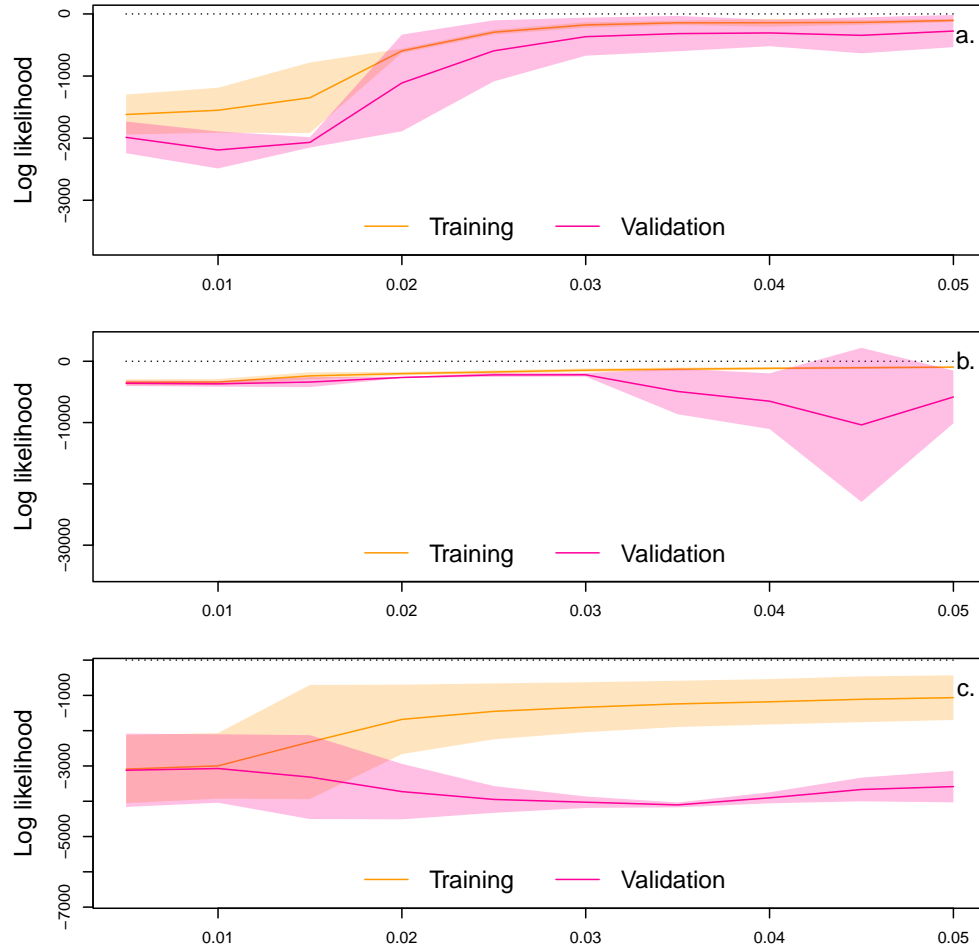


**Figure S23: Cross-validation plot of the NODE analysis of the Maizuru bay community.** The x-axis of the graphs correspond to the standard deviation of the prior distribution of the NODE parameters, which constrains the nonlinearity of the nonparametric approximation of the NODEs. Small values of standard deviation correspond to a linear model, while higher values (towards 0.5) correspond to a highly nonlinear model. Time series are split in three thirds to create a train, validation, and test set. The model is fitted to the train set (i.e. first third) for increasing value of standard deviation (from 0.05 to 0.5 by 0.05 increments), and evaluated on the validation set. The operation is repeated by swapping the training and validation set. The graphs show the log likelihood of the NODE system fitted by BNGM to the train set (in orange), and evaluated on the corresponding validation set (in red). The shaded areas represent the 90% confidence interval on estimates, obtained by anchored ensembling of the log marginal posterior distribution (Eq. 7) (Pearce et al. 2018).

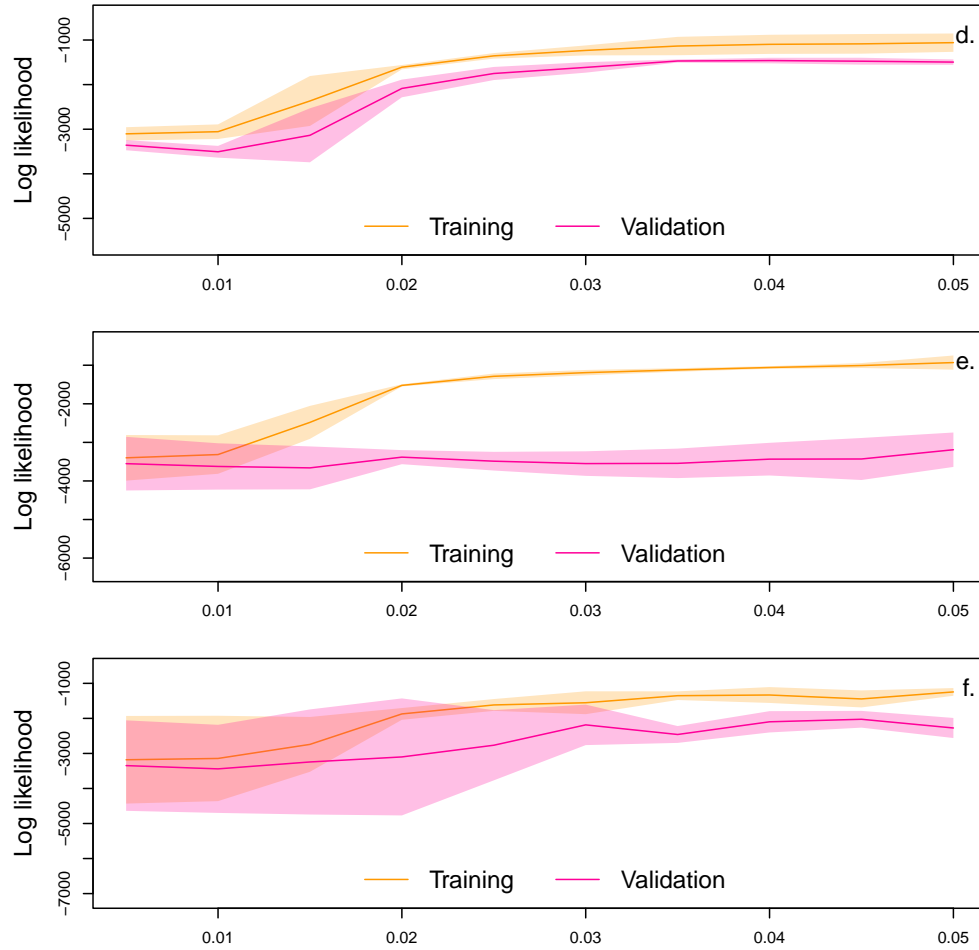


**Figure S24: Cross-validation plot of the NODE analysis of the Maizuru bay community.** The x-axis of the graphs correspond to the standard deviation of the prior distribution of the NODE parameters, which constrains the nonlinearity of the nonparametric approximation of the NODEs. Small values of standard deviation correspond to a linear model, while higher values (towards 0.5) correspond to a highly nonlinear model. Time series are split in three thirds to create a train, validation, and test set. The model is fitted to the train set (i.e. first third) for increasing value of standard deviation (from 0.05 to 0.5 by 0.05 increments), and evaluated on the validation set. The operation is repeated by swapping the training and validation set. The graphs show the log likelihood of the NODE system fitted by BNGM to the train set (in orange), and evaluated on the corresponding validation set (in red). The shaded areas represent the 90% confidence interval on estimates, obtained by anchored ensembling of the log marginal posterior distribution (Eq. 7) (Pearce et al. 2018).

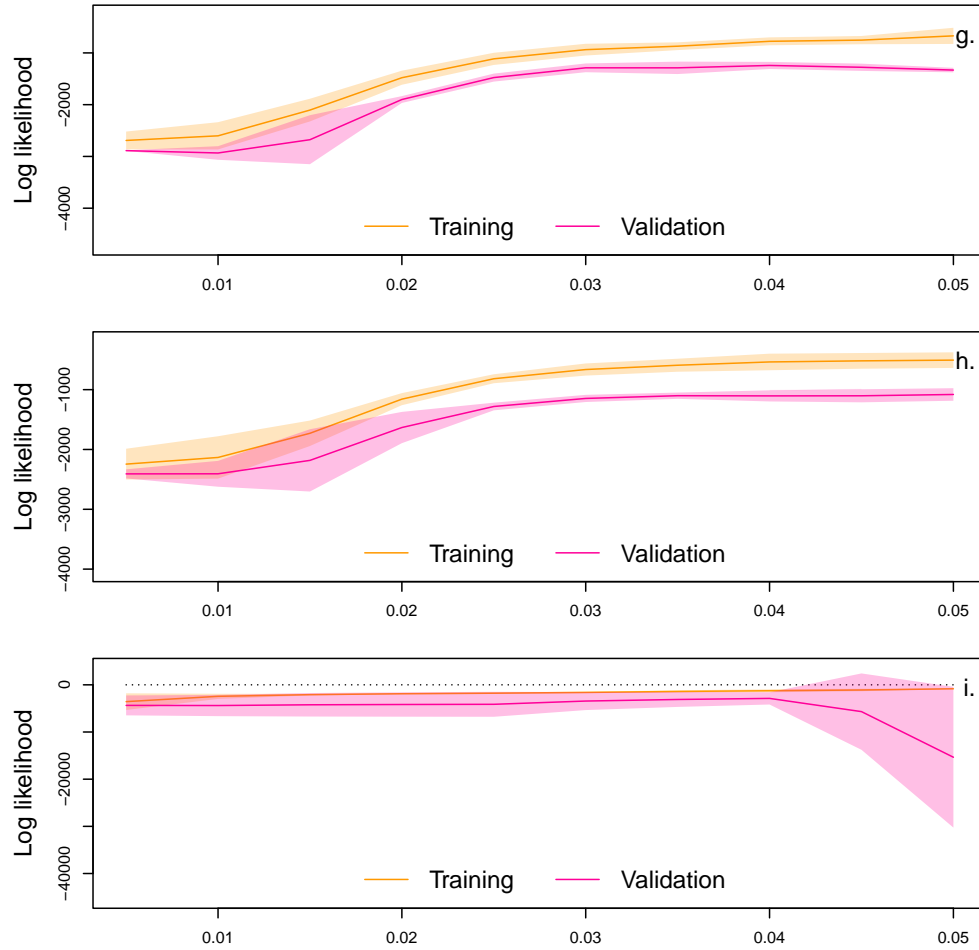


**Figure S25: Cross-validation plot of the NODE analysis of the Maizuru bay community.** The x-axis of the graphs correspond to the standard deviation of the prior distribution of the NODE parameters, which constrains the nonlinearity of the nonparametric approximation of the NODEs. Small values of standard deviation correspond to a linear model, while higher values (towards 0.5) correspond to a highly nonlinear model. Time series are split in three thirds to create a train, validation, and test set. The model is fitted to the train set (i.e. first third) for increasing value of standard deviation (from 0.05 to 0.5 by 0.05 increments), and evaluated on the validation set. The operation is repeated by swapping the training and validation set. The graphs show the log likelihood of the NODE system fitted by BNGM to the train set (in orange), and evaluated on the corresponding validation set (in red). The shaded areas represent the 90% confidence interval on estimates, obtained by anchored ensembling of the log marginal posterior distribution (Eq. 7) (Pearce et al. 2018).

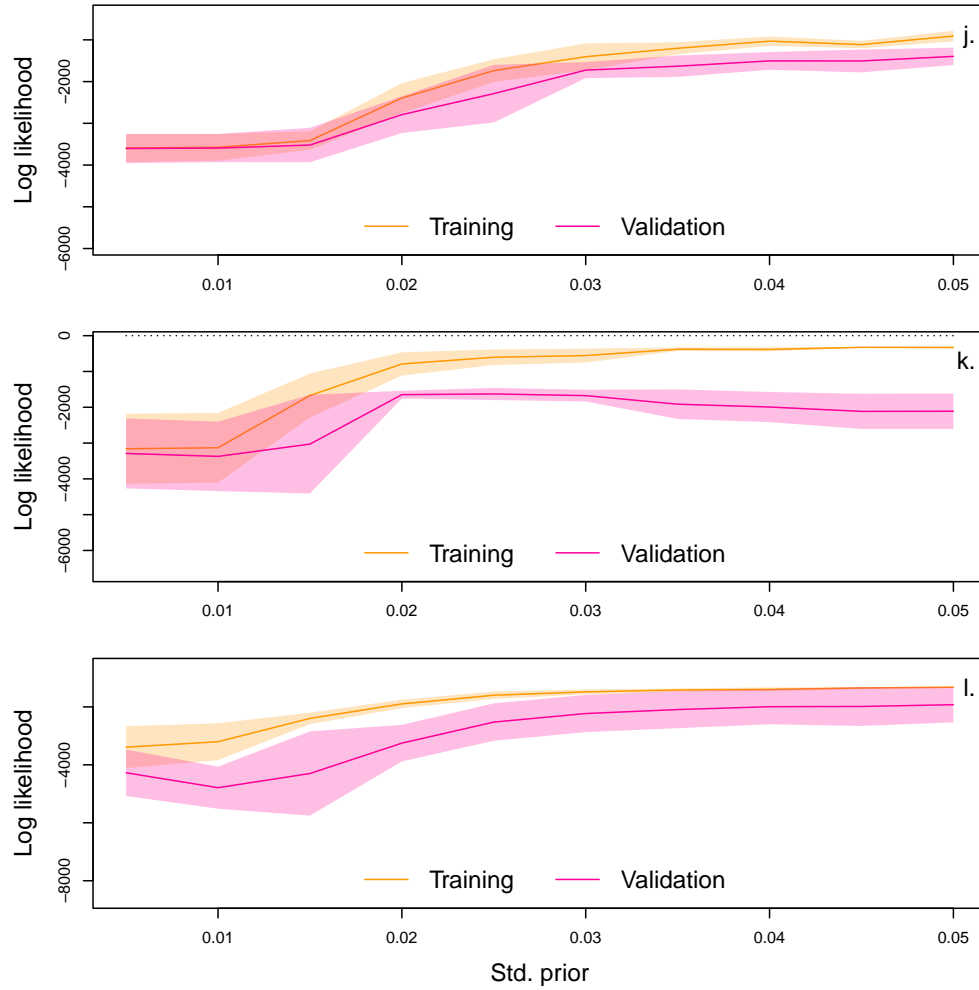


**Figure S26: Cross-validation plot of the NODE analysis of the Maizuru bay community.** The x-axis of the graphs correspond to the standard deviation of the prior distribution of the NODE parameters, which constrains the nonlinearity of the nonparametric approximation of the NODEs. Small values of standard deviation correspond to a linear model, while higher values (towards 0.5) correspond to a highly nonlinear model. Time series are split in three thirds to create a train, validation, and test set. The model is fitted to the train set (i.e. first third) for increasing value of standard deviation (from 0.05 to 0.5 by 0.05 increments), and evaluated on the validation set. The operation is repeated by swapping the training and validation set. The graphs show the log likelihood of the NODE system fitted by BNGM to the train set (in orange), and evaluated on the corresponding validation set (in red). The shaded areas represent the 90% confidence interval on estimates, obtained by anchored ensembling of the log marginal posterior distribution (Eq. 7) (Pearce et al. 2018).

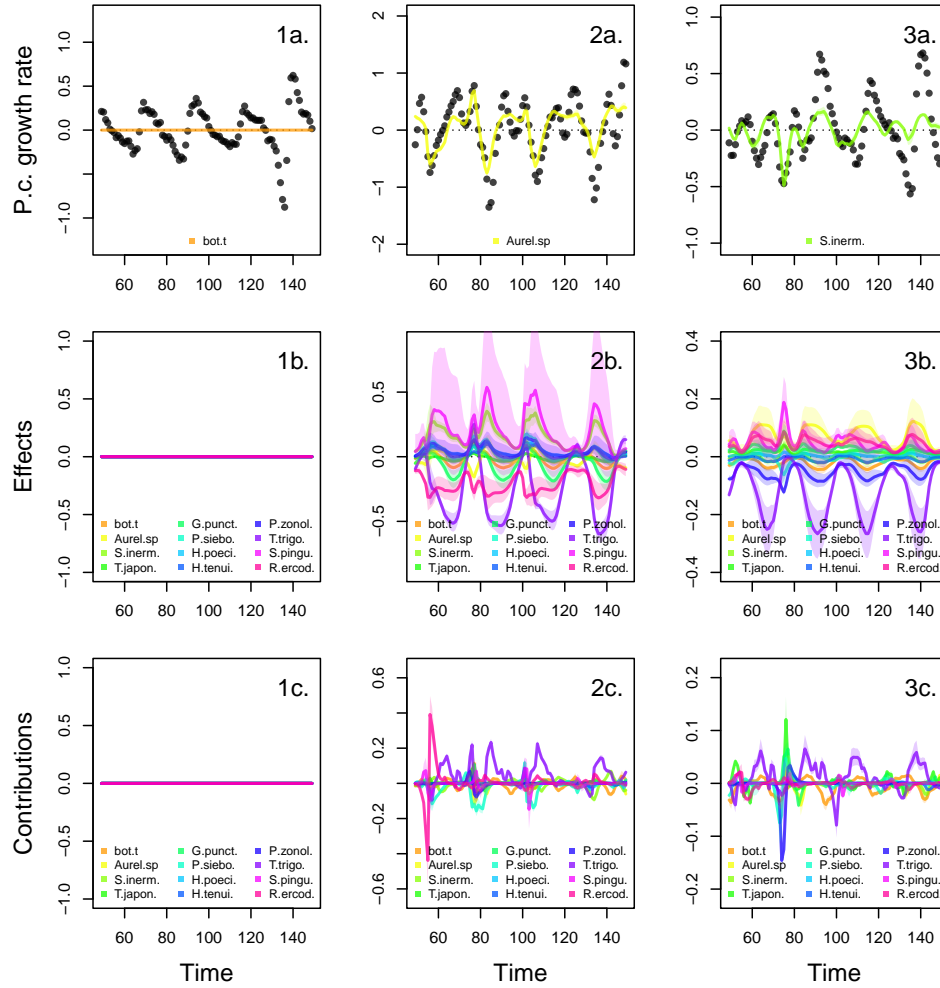


**Figure S27: Drivers of dynamics of species abundance in the Maizuru bay community.** This figure displays the NODE nonparametric approximations of the per-capita growth rates (2-3a.). We obtain the NODE approximations (2-3a., solid line) by fitting the interpolated per-capita growth rates (black dots) with ANNs that take population densities as input. We then estimate the direction of ecological interactions (effects, 2-3b.) by computing the derivative of the NODE approximations with respect to each density. Finally, we compute the strength of ecological interactions (contributions, 2-3c.) by multiplying the interpolated dynamics of each population with its effects. The shaded area shows the 90% confidence interval, obtained by approximately sampling the posterior distributions.

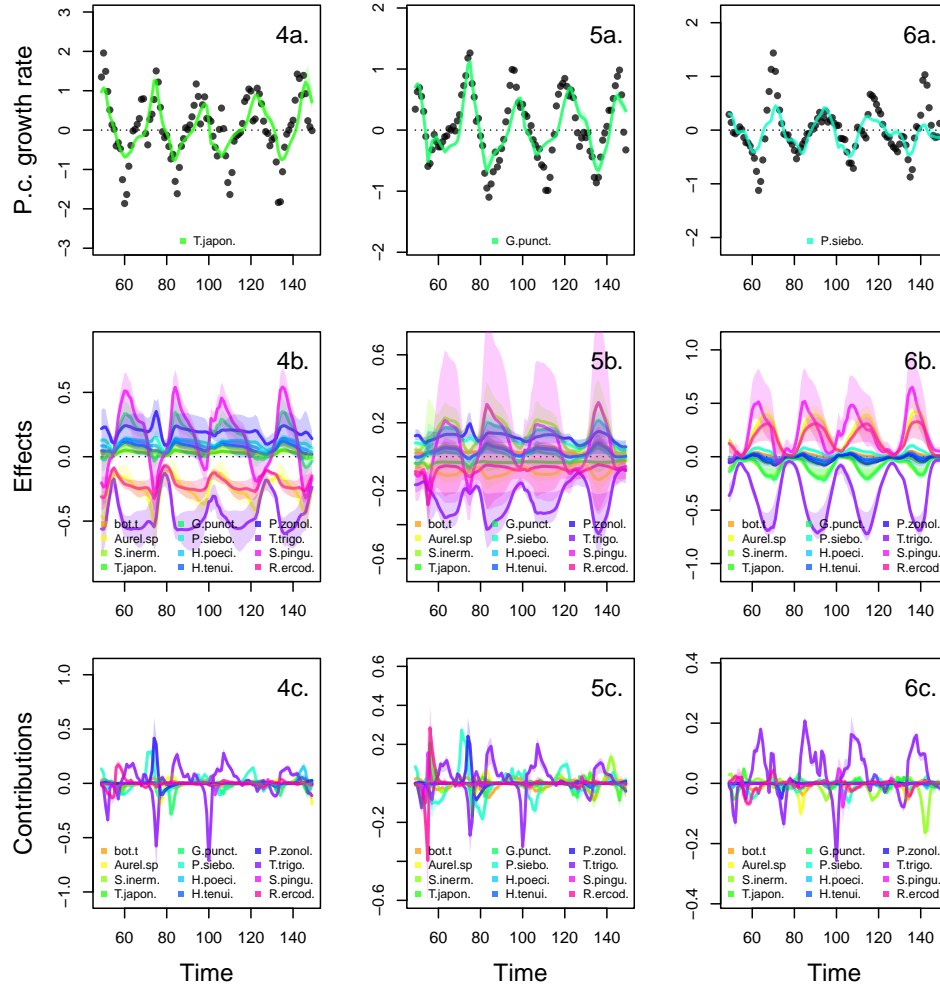


**Figure S28: Drivers of dynamics of species abundance in the Maizuru bay community.** This figure displays the NODE nonparametric approximations of the per-capita growth rates (4-6a.). We obtain the NODE approximations (4-6a., solid line) by fitting the interpolated per-capita growth rates (black dots) with ANNs that take population densities as input. We then estimate the direction of ecological interactions (effects, 2-6b.) by computing the derivative of the NODE approximations with respect to each density. Finally, we compute the strength of ecological interactions (contributions, 2-6c.) by multiplying the interpolated dynamics of each population with its effects. The shaded area shows the 90% confidence interval, obtained by approximately sampling the posterior distributions.

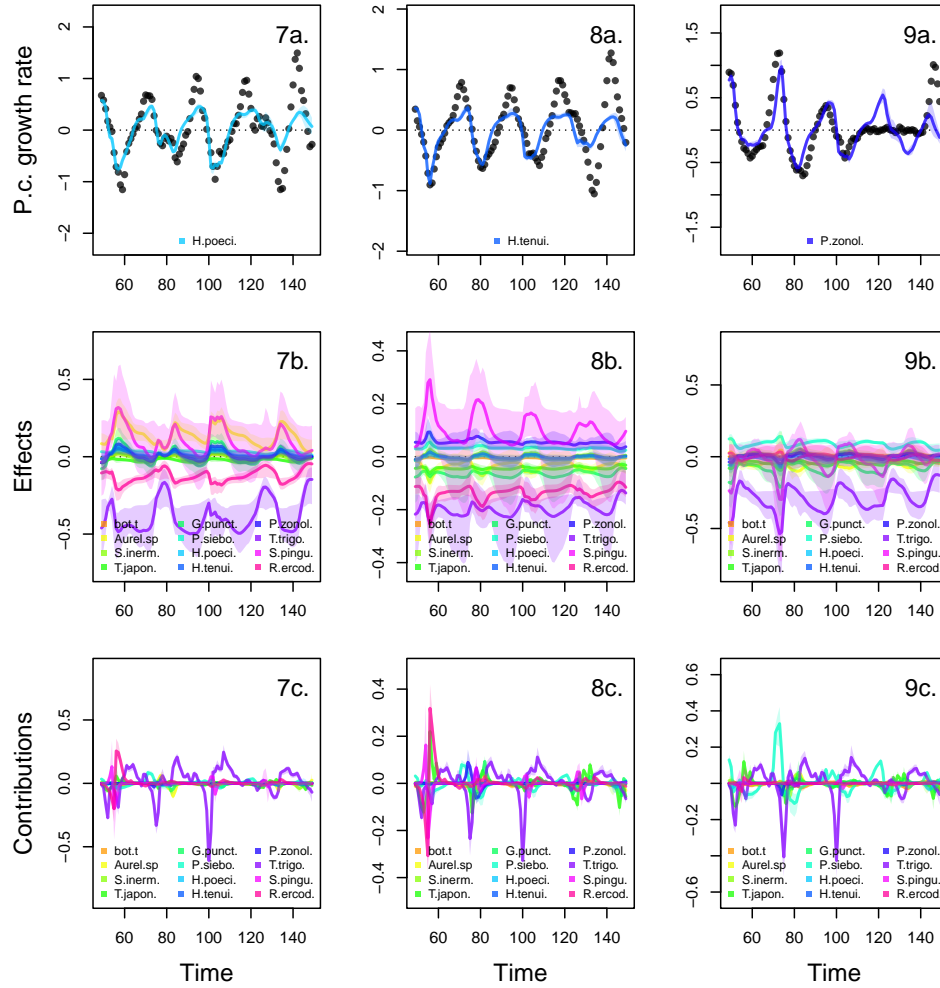


**Figure S29: Drivers of dynamics of species abundance in the Maizuru bay community.** This figure displays the NODE nonparametric approximations of the per-capita growth rates (7-9a.). We obtain the NODE approximations (7-9a., solid line) by fitting the interpolated per-capita growth rates (black dots) with ANNs that take population densities as input. We then estimate the direction of ecological interactions (effects, 7-9b.) by computing the derivative of the NODE approximations with respect to each density. Finally, we compute the strength of ecological interactions (contributions, 7-9c.) by multiplying the interpolated dynamics of each population with its effects. The shaded area shows the 90% confidence interval, obtained by approximately sampling the posterior distributions.



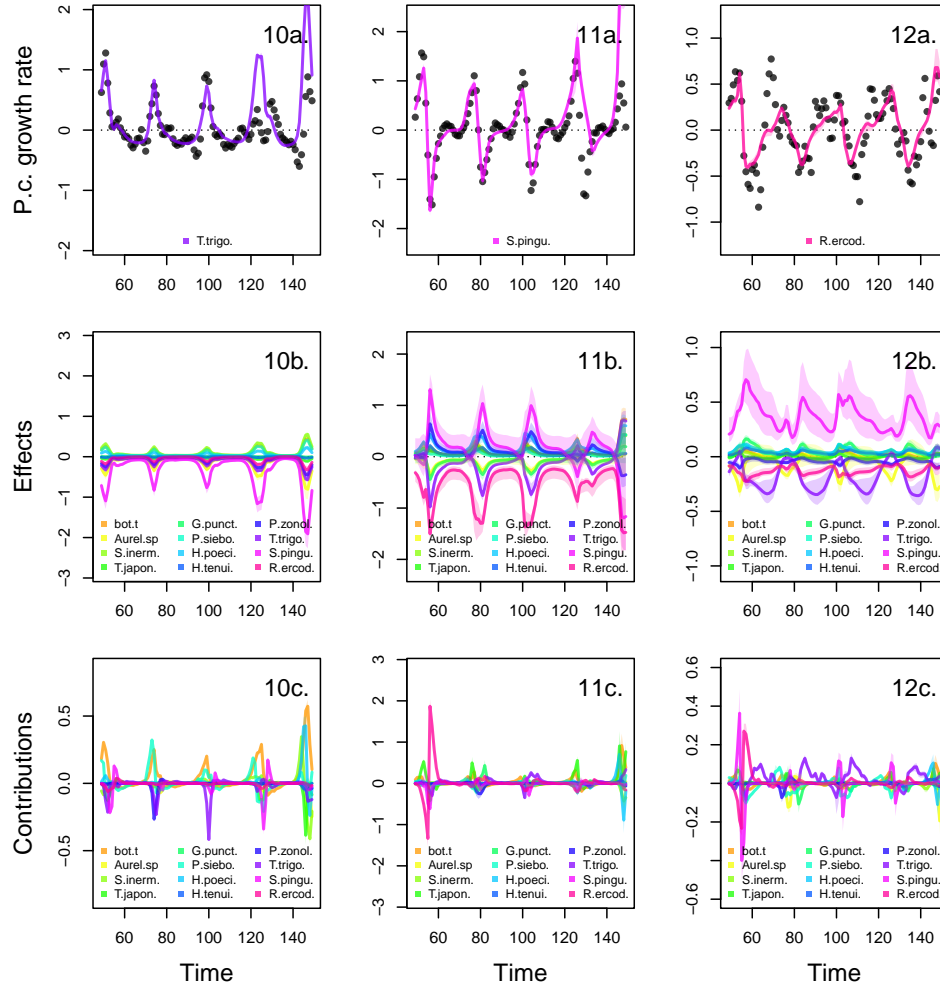


**Figure S30: Drivers of dynamics of species abundance in the Maizuru bay community.** This figure displays the NODE nonparametric approximations of the per-capita growth rates (10-12a.). We obtain the NODE approximations (10-12a., solid line) by fitting the interpolated per-capita growth rates (black dots) with ANNs that take population densities as input. We then estimate the direction of ecological interactions (effects, 10-12b.) by computing the derivative of the NODE approximations with respect to each density. Finally, we compute the strength of ecological interactions (contributions, 10-12c.) by multiplying the interpolated dynamics of each population with its effects. The shaded area shows the 90% confidence interval, obtained by approximately sampling the posterior distributions.